HYBRID FINITE ELEMENT/BOUNDARY ELEMENT SOLUTIONS OF GENERAL TWO DIMENSIONAL ELECTRO-MAGNETIC SCATTERING PROBLEMS

by

Frans J.C. Meyer

February 1991

This thesis is presented in partial fulfillment of the requirements for the degree
of
MASTER
of Engineering (Electronic)
at the
University of Stellenbosch

Supervisor: D.B. Davidson

DECLARATION

I, the undersigned, hereby declare that the work contained in this thesis is, unless stated otherwise, my own. It has not previously been submitted for a degree at any University.

F.J.C. Meyer Date

ABSTRACT

A two-dimensional Coupled Element Method (CEM) for solving electromagnetic scattering problems involving lossy, inhomogeneous, arbitrarily shaped cylinders, was investigated and implemented. The CEM uses the Finite Element Method (FEM) to approximate the fields in and around the scatterer and the Boundary Element Method (BEM) to approximate the far-field values. The basic CEM theory is explained using the special, static electric field problem involving the solution of Laplace's equation. This theory is expanded to incorporate scattering problems, involving the solution of the Helmholtz equation. This is done for linear as well as quadratic elements. Some of the important algorithms used to implement the CEM theory are discussed.

Analytical solutions for a round, homogeneous- and one layer coated PC cylinder are discussed and obtained. The materials used in these analytical solutions can be lossy as well as chiral. The CEM is validated by comparing near- and far-field results to the analytical solution. A comparison between linear and quadratic elements is also made. The theory of the CEM is further expanded to incorporate scattering from chiral media.

OPSOMMING

'n Gekoppelde Element Metode (GEM) wat elektromagnetiese weerkaatsingsprobleme, van verlieserige, nie-homogene, arbitrêre voorwerpe kan oplos, is ondersoek en geïmplimenteer. Die GEM gebruik die Eindige Element Metode (EEM) om die velde in en om die voorwerp te benader. 'n Grenselementmetode word gebruik om die vervelde te benader. Die basiese teorie van die GEM word verduidelik deur die toepassing daarvan op die spesiale geval van 'n statiese elektriese veld- probleem. Hierdie probleem verlang die oplossing van Laplace se vergelyking. Die teorie word uitgebrei om weerkaatsingsprobleme te kan hanteer. Die weerkaatsingsprobleme verlang die oplossing van 'n Helmholtz-vergelyking. Hierdie teorie word ontwikkel vir lineêre sowel as kwadratiese elemente. Van die belangrike algoritmes wat gebruik is om die GEM-teorie te implimenteer, word bespreek.

Analietise oplossings vir ronde, homogene en eenlaag bedekte perfek geleidende silinders word bespreek en verkry. Die material wat in die oplossings gebruik word, kan verlieserig of kiraal wees. Die GEM word bekragtig deur naby- en verveld resultate te vergelyk met ooreenkomstige analitiese oplossings. Die lineêre en kwadratiese element- resultate word ook met mekaar vergelyk. Die GEM-teorie is verder uitgebrei sodat weerkaatsing vanaf kirale materiale ook hanteer kan word.

To my mother

ACKNOWLEDGEMENTS

I would like to acknowledge the following people who inspired the development of this thesis.

During my first post-graduate year my supervisor, David Davidson, lectured a subject which caught my attention. His lectures were always very clear and motivated and very interesting. I would like to thank him for this inspiration which lead me into choosing this specific subject to work on for my Masters degree. I would also like to thank him for his help and encouraging comments throughout the year.

My family and all my friends have played a great part in inspiring me throughout the year. I would like to thank each one of them for supporting me in their own special way.

My sister, Rina, has gone to a lot of trouble in helping me with the grammatical upgrading of my written thesis. I would like to express my appreciation to her.

Gronum Smith and Danie Le Roux helped me with the construction of one of the graphical presentations. I would like to thank them for their work on that.

During the past year I had to interrupt my work for two months. I would like to thank Prof. J.H. Cloete and my supervisor, David Davidson, for their understanding and help in that situation.

I would like to thank James C. Maxwell for developing his field equations and Oliver Heaviside for transforming these equations to their current comprehensible form.

I would also like to acknowledge the Tao.

TABLE OF CONTENTS

1 INTRODUCTION

Electromagnetic scattering problems have always been a subject of great interest. Although a lot of work has already been done on it, more speed and accuracy is still in great demand in especially numerical analyses of these electromagnetic field problems. Apart from the theoretical interest in such problems, increasing interest in the practical usage of solutions of these scattering problems has developed. One of the main applications is in the field of radar detection. A consequence of solving a scattering problem from a certain object is that the result can be used to define the radar cross section (σ) of the object. This is a measure of the visibility of an object, by a radar system. These practical problems are spatially three-dimensional, and usually quite difficult to solve. If the object under consideration is cylindrical, with long but finite length, the radar cross section can be written as [18]

$$\sigma = \tau\left(\frac{2b^2}{\lambda}\right) \qquad (1.01)$$

with b the length of the cylindrical object, and τ the two-dimensional radar width. The radar width can be obtained by solving two-dimensional scattering problems, which is much less complicated than three-dimensional problems.

Various numerical as well as a few analytical methods for solving two-dimensional scattering problems have been developed [9],[19]. The analytical solutions exist only for a few specially shaped objects, such as round cylinders. When the scatterer is an arbitrarily shaped, inhomogeneous object, numerical approximation methods are the only means for solving these problems. By combining some of the existing numerical methods, the complexity of obtaining a solution for general scattering problems can be greatly reduced [2],[3],[20]. A method combining a differential equation method, the finite element method (FEM), with an integral equation method, the boundary element method (BEM) will be examined, implemented and verified in this thesis. The method is known as the coupled element method (CEM) and utilizes the characteristics of the FEM and BEM where it is most efficient. The CEM seems to be the most accurate, efficient and feasible numerical method to solve general (arbitrarily shaped, lossy and inhomogeneous) two-dimensional scattering problems. Different numerical methods are briefly discussed in chapter 2.

Both the FEM and BEM can be applied to the elementary, static electric field problem [2]. This requires a solution of Laplace's equation in a specified region. Although this is a special and simplified electric field problem, the CEM theory, for solving such problems, will be discussed in detail in chapter 3. This will serve as a basis for the general scattering problem and its numerical solution using the CEM, addressed in chapter 4.

The efficiency of a numerical method is greatly dependent on the types of algorithms chosen to implement them. Optimum algorithms differ from method to method and their feasibility and utilization of the characteristics of a method should be examined before implementation. Algorithms chosen and developed for implementing the CEM are discussed in chapter 5. These algorithms seem to be the most efficient, considering the characteristics of the CEM. It is possible that refined coding would result in a considerable improvement of the speed and accuracy of the CEM.

The validation of an implemented numerical method is of utmost importance. This enables one to get an idea of the accuracy of the method itself and the correctness of its implementation. Validation can be performed by comparing results generated with the numerical method to either measured results or results obtained for a canonical problem (for which an analytical solution exists). Care should be taken that the formulation of the method does not involve simplifications which might not affect the numerical solution of these special canonical problems, but do affect general problems. This could be validated by comparing some numerical results to experimental results.

Analytical solution methods for scattering from right circular cylindrical two-dimensional objects are discussed in chapter 7. These methods were implemented and serve as validation for the CEM. It should be noted that no experimental validation was performed.

2 NUMERICAL METHODS

2.1 Introduction

In the past 30 years or so, the memory and speed capabilities of computers have increased rapidly, and are still increasing. This has brought into being a new field in science and mathematics, namely computational problem solving. Numerical methods, of which some were derived in the previous century, can now be implemented to solve problems using digital computers. The fields of experimentation and analytical developments have been complemented with the third field of computational numerical approximations. Many large, complex problems in a variety of fields, which are unsolvable analytically, have already been solved using computational problem solvers. In electromagnetics a variety of numerical methods have been developed to solve problems, arising from Maxwell's equations. The methods developed to solve scattering problems can broadly be divided into integral equation methods (IEM) and differential equation methods (DEM). An investigation of the different numerical methods available for solving scattering problems was performed [8],[19],[20]. They will be discussed briefly in this chapter.

2.2 Integral Equation Methods (IEM)

Integral equation numerical methods for solving electromagnetic scattering problems, involve writing the fields inside a surface region for a two-dimensional problem, in terms of integrals over the boundaries surrounding the region. These integrals are obtained by using Green's theorem and a Green's function appropriate to the specific region and problem. The boundary conditions at the various boundaries must be satisfied. This leads to an integral operator which acts on the unknown fields. The boundaries can be discretised (the first approximation) into a finite set of elements. The fields or their equivalences (for example surface currents) on the boundaries interact with one another through the integral equation. Because of the discretisation, this integral equation can be used to set up a set of linear independent equations containing the unknown fields or equivalences on the boundaries. Written in matrix form, these equations can be solved to obtain an approximated field (or current) value on each element. The fields inside the surface region can now be written in terms of these approximated boundary field values.

The IEM can be formulated in a variety of ways, depending on the specific problem under consideration. The well-known method of moments is an example of an IEM. The characteristics of the IEM, enabling one to write the fields inside a region in terms of the boundary fields, make it suitable for problems with a region extending to infinity, of which a scattering problem is an example.

The matrix equation one needs to solve to obtain the boundary fields has the form:

$$[A][u] = [B] \qquad (2.01)$$

with u the unknown field values at nodes (element connection points) on the boundary and [A], a square matrix of size n (number of nodes or unknown fields). Solving equation (2.01) is one of the main time consuming procedures of an IEM. The solving time increases with an order close to three, with respect to the number of unknowns. The size and characteristics of [A] are thus crucial to the efficiency of the numerical method. The formulation of an IEM causes [A] to be a fully populated, possibly asymmetric matrix.

The boundaries surrounding the surface region(s), are one-dimensional and the number of nodes required on the boundary is dependent of the size of the boundary and the wavelength of the electromagnetic field. This one-dimensional characteristic leads to a much smaller size for [A] than in the case of the DEM where nodes over the whole two-dimensional region must be defined (sec 2.3). If an inhomogeneous region is encountered, the IEM loses its advantage of only nodes on a one-dimensional boundary. The inhomogeneous region requires that the unknown fields on two-dimensional node patches be incorporated into the integral equations. This usually leads to quite a large number of nodes and thus a large, fully populated, asymmetric matrix [A]. This fully populated matrix, with globally interacting elements, leads to another possible time consuming procedure namely the filling of [A]. The interaction of the field on each node with all the fields on other nodes has to be calculated to obtain the elements of [A]. For a large number of nodes, this matrix filling procedure can decrease the efficiency of the IEM considerably.

2.3 Differential Equation Methods (DEM)

The starting point of a differential equation method is directly from Maxwell's curl equations. The fields, on which the differential operator in the curl equations acts, are approximated over the whole two-dimensional region. The differential operator itself is also approximated. The errors made by these approximations are weighted

and distributed over the entire region. This region can now be divided into sub-elements. The differential operator has a local nature, thus acting upon the fields in every sub-region individually. This makes it suitable for problems with inhomogeneous regions. From the formulation described above, a set of linear equations can again be obtained and written in matrix form. The matrix equation has a similar form as equation (2.01). A solution of this matrix equation yields the fields in all the sub-regions.

Different approximating methods can be used, yielding a number of these differential equation methods. The well-known finite element method and the finite difference time domain methods are examples of DEM. The fact that the entire two-dimensional region has to be divided into sub-region rules out any direct use of these methods where infinite regions are present. Another consequence is that quite a large number of sub-regions have to be defined to cover the two-dimensional region. This leads to a large number of unknown field values to be calculated. The [A] matrix encountered with a DEM is usually much larger than with an IEM. The formulation of differential equation methods usually ensures a symmetric matrix [A]. Due to only local interactions between the fields, which is a consequence of the local nature of the differential operator, [A] is very sparse. This is advantageous to both the memory requirements and computational time of the DEM. Another consequence of the local nature of the differential operator is that inhomogeneous regions can be handled without any increase in the size of the matrix [A]. It should be noted that the time it takes to fill the sparse matrix [A] of a DEM, is almost negligible.

2.4 Combining a DEM with an IEM

Two-dimensional scattering from lossy, inhomogeneous, arbitrarily shaped objects is a very general problem. Most of the numerical methods in use are quite efficient and accurate for specific kinds of problems. For general problems, however, all the methods seem to fail to produce acceptable results at some stage or another. The finite spatial requirements of the differential equation methods, rule out their use when far-field information is required. The complexity and inefficient computing time make the integral equation methods undesirable when severely inhomogeneous objects are present. A combination of these two kinds of numerical methods seems to provide the answer to the difficulties encountered when these general scattering problems are considered [3]. Any finite, possibly lossy, inhomogeneous

regions can be solved using a DEM. An infinite homogeneous, free-space region can be solved using an IEM. The finite element differential equation method and the boundary element integral equation method will be used in the different regions. The combination of these two methods is not very complex and enables one to apply each method where it is most efficient and accurate. The combination of the finite element method (FEM) and the boundary element method (BEM) is known as the combined element method (CEM), and will be investigated and implemented in this thesis.

Another coupled method which could have been used is the so-called transfinite element method (TEM) [20]. This method also uses the FEM in any inhomogeneous regions, but an analytical (Hankel function expansion) solution is used in the region extending to infinity. The analytical solution requires a circular boundary around any scatterer. This requirement might increase the number of finite elements to an unacceptably high value, if the scatterer is ill-shaped (sec 4.8.7).

3 COUPLED ELEMENT METHOD

3.1 Introduction

The coupled element method (CEM) [2],[3] is a numerical method which combines the Boundary Element Method (BEM) [4],[5] with the Finite Element Method (FEM) [6]. The BEM is suitable for problems in a region which consists of free space and extends to infinity. The FEM is suitable for problems in a finite region consisting of inhomogeneous, lossy media. The two methods are mathematically easy to combine. In this chapter the basic theory of both the BEM and FEM will be discussed. Two-dimensional structures will be considered, thus the z-axis in the Cartesian coordinate system extends to infinity. First order elements will be used in both methods, applied in a charge free region where Laplace's equation holds. An extension of these methods will be done in later chapters.

3.2 Finite Element Method (FEM)

Consider a region such as indicated in fig-3.1 . The equation governing in a region can be derived from Maxwell's equations. If the fields in such a region are static and the region is charge free, Laplace's equation

$$\nabla(\epsilon\nabla\Phi) = 0 \qquad (3.01)$$

can be derived as the governing equation. This follows from Maxwell's equations using a potential function representation [1,p157].

Figure-3.1 Two-dimensional region where Laplace's equation holds.

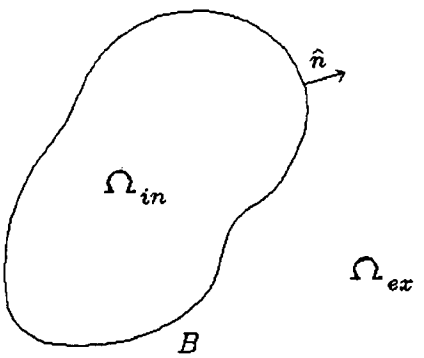

3.2.1 Approximating potentials

If the interior region (Ω_{in}) is divided into triangular elements (fig-3.2), the scalar potential Φ can be approximated in each triangle. A first order (linear) approximation can be used in each triangle (fig-3.3), with the linear approximation function given by

$$U = a + bx + cy \qquad (3.02)$$

where U is the approximation for Φ and a , b and c (different in every triangle) are local constants to be obtained. The variables x and y are the coordinates in the two-dimensional cartesian coordinate system.

Figure-3.2 Partial triangulation of the inside region.

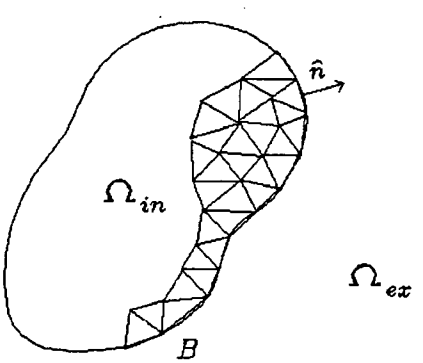

Figure-3.3 Linear approximation function in a finite element.

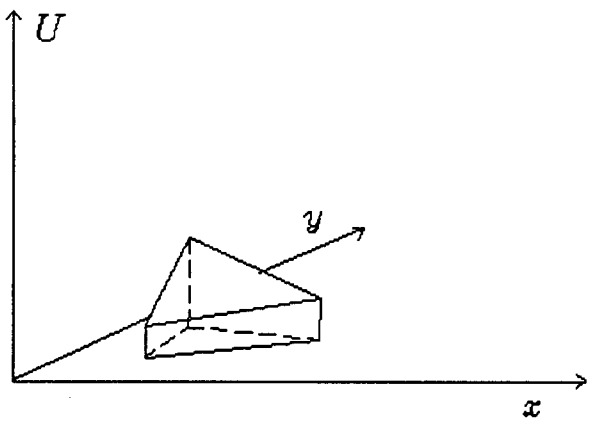

3.2.2 Simplex coordinates

Instead of using the global two-dimensional coordinate system for the variables in the approximation function (3.02), a local coordinate system called simplex coordinates can be used [6,p102]. The approximation function can be given in terms of coordinates, valid only in the triangular element under consideration. The advantage of these local simplex coordinates is that the mathematical formulation for the FEM can be done for one triangle and applied to all other triangles, using easy coordinate transformation rules. For first order triangles, the simplex coordinates are given as

$$2A\begin{bmatrix}\xi_1\\ \xi_2\\ \xi_3\end{bmatrix}=\begin{bmatrix}x_2y_3-x_3y_2 & y_2-y_3 & x_3-x_2\\ x_3y_1-x_1y_1 & y_3-y_1 & x_1-x_3\\ x_1y_2-x_2y_1 & y_1-y_2 & x_2-x_1\end{bmatrix}\begin{bmatrix}1\\ x\\ y\end{bmatrix} \qquad (3.03)$$

[6,p105]. In this matrix equation, (x_1, y_1), (x_2, y_2) and (x_3, y_3) are the global cartesian coordinates of the corner points of the triangular element under consideration. ξ_1, ξ_2 and ξ_3 are the three simplex coordinates. The approximation function (3.02) in terms of these simplex coordinates is then given by

$$U=\sum_{i=1}^{3}u_i\xi_i \qquad (3.04)$$

as shown in [6,p108].

3.2.3 Weak formulation

With U approximating Φ, the governing equation in Ω_{in} becomes

$$\nabla(\epsilon\nabla U) \neq 0 = error \tag{3.05}$$

The error can be distributed over the region and minimized in an average sense by weighting it and setting it equal to zero [2],

$$\int_{\Omega_{in}} \nabla(\epsilon\nabla U) W \, d\Omega_{in} = 0 \tag{3.06}$$

Different weighting functions can be chosen to give different results [4],[5]. The Galerkin method, where the weighting function has the same form as the approximating function, will be used here [4,p7]:

$$W = \sum_{i=1}^{3} \xi_i \tag{3.07}$$

The error will thus be distributed in accordance with the function W. W is a sub-domain weighting function, acting independently in every triangular element. This characteristic provides flexibility in the weighting function over the global region, advantageous especially with inhomogeneous regions. One disadvantage of this first order weighting function is the discontinuity present at the sub-domain or triangular element boundaries. Although the potential itself is continuous, its first derivative is not. The smoothness of the approximated potentials, and thus the accuracy, is affected.

By integrating once by parts [6,p335], the so-called weak formulation [3],[4,p10] is obtained:

$$\int_{\Omega_{in}} \epsilon\nabla U \cdot \nabla W \, d\Omega_{in} - \oint_{B} W \frac{dU}{dn} dB = 0 \tag{3.08}$$

This is called the weak formulation because a second order differential equation (Laplace's equation) is approximated by functions having only one derivative. The integral over B is a line integral over the boundary enclosing Ω_{in}. The normal derivatives of the potentials at the boundary can be approximated by the linear, one dimensional approximation function

$$\frac{dU}{dn} = \sum_{i=1}^{2} \xi_i \left(\frac{du}{dn}\right)_i \tag{3.09}$$

3.2.4 Matrix formulation

Equation (3.08) is the approximated governing equation in Ω_{in}, and can be discretised [3] to apply in each triangular element. This gives

$$\sum_{j=1}^{o} \epsilon_j \int_{\Omega_{in_j}} \nabla U \cdot \nabla W \, d\Omega_{in_j} - \sum_{j=1}^{p} \int_{B_j} W \frac{du}{dn} dB_j = 0 \qquad (3.10)$$

where o is the number of triangular elements and p the number of boundary elements. From this discretisation a set of matrix equations can be obtained (appendix A 3.1):

$$[S][u] - [T]\left[\frac{du}{dn}\right] = 0 \qquad (3.11)$$

3.2.4.1 The S-matrix

The S-matrix is a square matrix with the size n, n being the number of nodes (intersections points of triangles) in Ω_{in}. The elements of [S] can be obtained by first obtaining the local 3x3 [S_e] matrices of every triangular element. By substituting (3.04) and (3.07) into (3.10), [S_e] is given by

$$S_e^{ij} = \epsilon_e \sum_{i=1}^{3} \sum_{j=1}^{3} \int_{\Omega_{in_e}} \nabla \xi_i . \nabla \xi_j \, d\Omega_{in_e} \qquad (3.12)$$

If one adds an element of the 3x3 [S_e] matrices to [S], whenever a local node coincides with a global node, [S] is obtained [6,p31].
(3.12) can also be written as

$$S_e^{ij} = \epsilon_e \sum_{k=1}^{3} Q_{ij}^{k} \cot \Theta_k \qquad (3.13)$$

[6,p111]. This is where the local simplex coordinates come in handy. The 3x3 matrices Q^1, Q^2 and Q^3 have to be calculated and tabulated [6,p112] only once, because it stays the same irrespective of the size, shape or position of the triangular element under consideration. Θ_1, Θ_2 and Θ_3 are the enclosed angles of the triangular element under consideration [6,p332]. It is evident that the local [S_e] matrices differ only because of the different enclosed angles the triangular elements might have.

3.2.4.2 The T-matrix

The T-matrix is a square matrix with the size m, m being the number of boundary nodes on B. The components of [T] are again the sum of the local matrices [T_e] whenever the a local node coincides with the global node under consideration. [T_e] is a 2x2 matrix, one dimension less than [S_e], because the boundary elements consist of only one side of a triangular element. [T_e] can be calculated from (3.07),(3.09) in (3.10) as

$$T_e^{ij} = \sum_{i=1}^{2} \sum_{j=1}^{2} \int_{B_e} \xi_i \xi_j dB_e \qquad (3.14)$$

and the integral can be written as

$$T_e^{ij} = L \int_{B_e} \xi_i \xi_j \frac{dB_e}{L} \qquad (3.15)$$

[6,p10]. L is the length of the boundary element and the integral can be calculated and tabulated in 2x2 matrix form [6,p10] as was done with the Q matrices in the previous section. The different local matrices ([T_e]) will thus only differ because of the different lengths the elements might have.

3.2.4.3 Unknown potentials and its derivatives

From equation (3.11) it can be seen that the approximated potentials at each node as well as the approximated normal derivatives at each boundary node are unknowns. There is thus a need for another matrix equation to solve all the unknowns. The BEM, which will be discussed in sec 3.3, will provide another matrix equation with two unknowns, which will enable one to obtain a solution.

3.2.5 Prescribed potentials

To excite a region where Laplace's equation governs, some of the nodes in the region (not on the boundary) must have prescribed potential values. The global [S] matrix must be altered to accommodate these prescribed values. The part of the matrix equation (3.11) associated with the internal nodes have the form

$$[S_{in}][u_{in}] = 0 \qquad (3.16)$$

or

$$\begin{bmatrix} S_{ff} & S_{fp} \\ S_{pf} & S_{pp} \end{bmatrix} \begin{bmatrix} u_f \\ u_p \end{bmatrix} = 0 \qquad (3.17)$$

where the subscript f stands for free- and p for prescribed potentials [6,p34]. Incorporating the prescribed potentials (Φ_p) in equation (3.17) yields

$$\begin{bmatrix} S_{ff} & 0 \\ 0 & 1 \end{bmatrix} \begin{bmatrix} u_f \\ u_p \end{bmatrix} = \begin{bmatrix} 0 \\ \Phi_p \end{bmatrix} \qquad (3.18)$$

In this matrix equation, it is clear that the approximated potentials (u_p) at each node will obtain the exact value of the prescribed potential at that node. The part of [S] associated with internal nodes, thus takes on the form of (3.18).

3.3 Boundary Element Method (BEM)

Consider a region as indicated in fig-3.4 , with Ω_{ex} a source free, free space region extending to infinity. Laplace's equation is again the governing equation. The BEM is a variation of the well known method of moments [8]. The method is a numerical approximation of Huygens' principle [9,p377], expressing the potential at a given observation point in a region in terms of known potentials and its normal derivatives at an enclosed boundary. The basic theory and set-up of the BEM will now be discussed.

Figure-3.4 Two-dimensional region where Laplace's equation governs. The region (Ω_{ex}) extends to infinity.

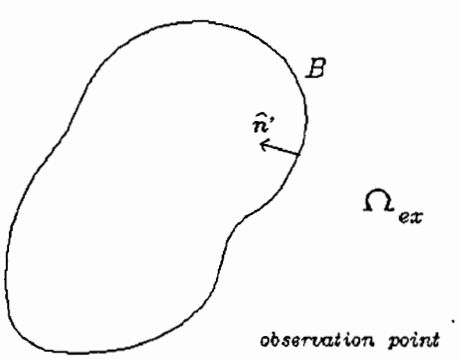

3.3.1 Homogeneous coordinates

The boundary region is divided into boundary elements as seen in fig-3.5 . The potentials and its normal derivatives are approximated linearly over each element.

Figure-3.5 Division of boundary (B) into boundary elements with boundary nodes at the intersection of two boundary elements.

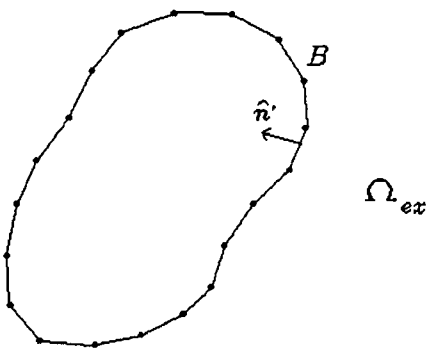

As with the FEM a local coordinate system is chosen to represent the approximations. The homogeneous coordinate system [4,p56] used here is a one dimensional system with coordinate ξ varying from -1 to 1 along the boundary element under consideration (see fig-3.6). This particular form of homogeneous coordinates is chosen to simplify the numerical integration that will be performed over the boundary element (sec 3.3.4.1).

Figure-3.6 Homogeneous coordinate system on a boundary element.

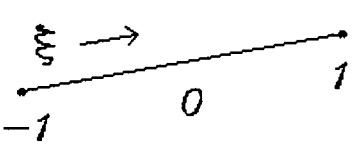

The linear approximated potential on a given element is given in homogeneous coordinates as

$$U = \sum_{i=1}^{2} \phi_i u_i \tag{3.19}$$

with

$$\phi_1 = \frac{1}{2}(1 - \xi) \tag{3.20}$$

and

$$\phi_2 = \frac{1}{2}(\xi + 1) \tag{3.21}$$

Fig-3.7 shows a typical representation of ϕ_1,ϕ_2 and U over an element.

Figure-3.7 Typical linear potential approximation on a boundary element. The approximated potential (U) is the sum of the approximation functions ϕ_1 and ϕ_2

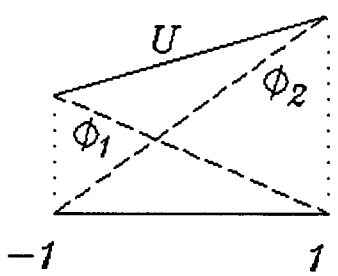

The necessary mathematical manipulation can be done on each element in the global x-y coordinate system using this local coordinate system. It should be noted that a coordinate transformation is necessary between the global and local coordinate systems [4,p64]. The two transformation rules are

$$x = \phi_1 x_1 + \phi_2 x_2 \tag{3.22}$$

$$y = \phi_1 y_1 + \phi_2 y_2 \tag{3.23}$$

where (x_1, y_1) and (x_2, y_2) are the x-y coordinates of the two ends of the boundary

element.

3.3.2 Deriving the boundary equation

With Laplace's equation governing in the region, an approximation of the potential Φ is used again, namely U. This yields

$$\nabla^2 U \neq 0 = error \tag{3.24}$$

The error which occurs because of the approximation is now distributed over the region by weighting the Laplacian [3], [4,p3]

$$\int_{\Omega_{ex}} \nabla^2 U W \, d\Omega_{ex} = 0 \tag{3.25}$$

The Laplacian of the approximating function is thus set equal to zero in an average sense. The choice of weighting function will be discussed in sec 3.3.3.

To obtain the boundary equations, (3.25) must be integrated twice by parts [2,p8] (Green's second theorem is applied). This yields

$$\int_{\Omega_{ex}} \nabla^2 W U \, d\Omega_{ex} - \int_B U \frac{dW}{dn} dB + \int_B \frac{dU}{dn} W \, dB = 0 \tag{3.26}$$

3.3.3 The weighting function

The region (Ω_{ex}) in which the weighting function must be applied is an infinite region. An entire domain weighting function is thus chosen to accommodate the infinity of the region. The region is also homogeneous and source free, making the use of sub-domain weighting functions unnecessary.

Consider the following equation

$$\nabla^2 W = \delta(\vec{r}_o - \vec{r}_s) \tag{3.27}$$

This is Laplace's equation in an infinite region with a unit applied potential at a given source point s. The fundamental solution [3],[4,p29] of (3.27) is

$$W = \frac{1}{2\pi} \ln\left(\frac{1}{|\vec{r}_o - \vec{r}_s|}\right) \tag{3.28}$$

This is the source free, two-dimensional Green's function in an infinite, free space region. In these equations, r_o is the observation point and r_s is the source point. Choosing the weighting function as this source free Green's function and thus substituting equations (3.27) into (3.26) (appendix A 3.2) yields

$$U_o = -\int_B U\frac{dW}{dn}dB + \int_B \frac{dU}{dn}W\,dB \tag{3.29}$$

Taking the observation point r_o to the boundary B [4] gives

$$\frac{1}{2}U_o = -\int_B U\frac{dW}{dn}dB + \int_B \frac{dU}{dn}W\,dB \tag{3.30}$$

(appendix A3.3).

3.3.4 Matrix formulation

Equation (3.30) can be discretised (division of boundary into elements as discussed before) to give

$$\frac{1}{2}U_o = -\sum_{j=1}^{n}\int_{B_j} U\frac{dW}{dn}dB_j + \sum_{j=1}^{n}\int_{B_j}\frac{dU}{dn}W\,dB_j \tag{3.31}$$

This can be written in matrix form (appendix A3.4) as

$$[H][u_b] - [G]\left[\frac{du_b}{dn}\right] = 0 \tag{3.32}$$

3.3.4.1 The H-matrix

[H] is a square matrix with size n (the total number of boundary nodes). The components of [H] not on the diagonal, can be obtained as follows. Beginning with node one through to n, integration is performed over each element on the boundary, with the location of the node under consideration (say i) the observation point. A local value for the integral is defined as H'^{j}_{i} with

$$H'^{j}_{i} = \int_{-1}^{1}\phi_k\frac{dW}{dn}J\,d\xi \qquad j = a, b \tag{3.33}$$

and a and b the boundary node numbers at the ends of the element which is integrated over, k=1 when j=a and k=2 when j=b and

$$J = \sqrt{\frac{1}{4}(x_b - x_a)^2 + \frac{1}{4}(y_b - y_a)^2} \tag{3.34}$$

A coordinate transformation from the global format in equation (3.31) to the local format in equation (3.33) was done (appendix A3.5). The components of the first row of [H] is obtained by adding H'^{a}_{1} or H'^{b}_{1} to H_{1j} whenever a or b coincides with the column of [H] under consideration (column j). This procedure is performed for all nodes, thus filling all the rows of [H].

The elements on the diagonal is equal to $\frac{1}{2}$. This is because the term on the left hand side of equation (3.31) is incorporated into the [H] matrix. The integral part of any H_{ii} term is always zero because the term $\frac{dW}{dn}$ is zero when the observation point is on the element which is integrated over. This can be seen from equation (3.35) with $\hat{n}$ orthogonal to $\hat{r}$.

The normal derivative of the Green's function as used in equation (3.33) is

$$\frac{dW}{dn} = -\frac{\hat{n}.\hat{r}}{2\pi|r|} \tag{3.35}$$

(appendix A3.6). The integration of equation (3.33) is done numerically using four point Gaussian integration [5,p185] summed up as

$$\int_{-1}^{1} f(\xi)d\xi \approx \sum_{i=1}^{4} f(\xi_i)w_i \tag{3.36}$$

The homogeneous coordinate system for the boundary elements was chosen to coincide with this Gaussian integration format.

3.3.4.2 The G-matrix

The global G-matrix is also a square matrix with size n (number of nodes on boundary). The components of [G] can again be obtained by integrating over each element using node one through to node n as observation points. Just as described in sec 3.3.4.1 with [H], the local value for the integral is defined as G'_i with

$$G'^{j}_{i} = \int_{-1}^{1} \phi_j W J \, d\xi \qquad j = a, b \tag{3.37}$$

Again, whenever column j coincides with nodes a and b (the nodes at each end of the element under consideration) G'^{a}_{i} or G'^{b}_{i} is added to G'_{ij}, a component of [G].

Four point Gaussian integration is used again to obtain the integral value of (3.37) but with an important alteration. Whenever the observation point (node i) lies on the element to be integrated over, a singularity occurs in the Green's function because the argument of the natural logarithmic function becomes zero (see equation 3.28). To avoid this singularity a logarithmic Gaussian integration [5,p187] is performed to obtain the integral. This integration formula is given as

$$\int_{0}^{1} \ln\left(\frac{1}{\xi}\right) f(\xi) d\xi \approx \sum_{i=1}^{4} w_i f(\xi_i) \tag{3.38}$$

Equation (3.37) must thus be altered to obtain the format of the left hand side of (3.38) whenever the observation point lies on the element (appendix A3.7).

3.3.5 Potential values in the free space region

Matrix equation (3.32) can be solved if either the potential values on the boundary or the normal derivatives are known. The solution then yields an approximation of the potentials as well as normal derivatives on each element on the boundary. This information, combined with equation (3.29) can be used to determine the potential at any point in Ω_{ex}. If the potential at a point p is required, integration is performed over each element as required by equation (3.29), with p as the observation point. It is evident that this method is a numerical approximation of Huygens' principle defined before.

3.4 Combining FEM and BEM

The two methods described above are different numerical methods used most efficiently for different applications. If, however, a problem arises which requires the application of both methods it can be seen that equations (3.11) and (3.32) are compatible. The so-called coupled element method (CEM) takes advantage of the characteristics of both the FEM and BEM. The CEM uses FEM characteristics to handle that part of a problem containing inhomogeneous materials. BEM char-

acteristics are used to determine potentials at relative long distances from the prescribed potentials where too many finite elements would have been required. A discussion on the theory for combining these methods will now follow.

3.4.1 Choosing a boundary

When combining the FEM and BEM the region under consideration is divided into two regions (see fig-3.1). The boundary dividing these two regions is chosen in such a way that all inhomogeneous and non-free space materials are enclosed. This is the interior region (Ω_{in}) where the FEM will be applied. The BEM will be applied in the exterior region (Ω_{ex}). Because the boundary is chosen in free space, one ensures that the boundary conditions requiring continuity in the potentials and their normal derivatives over the boundary, are satisfied. Thus

$$u_b^{FEM} = u_b^{BEM} \tag{3.39}$$

and

$$\frac{du_b^{FEM}}{dn} = -\frac{du_b^{BEM}}{dn'} \tag{3.40}$$

3.4.2 Equilibrium conditions

The continuity of potentials over the boundary is one condition for combining the BEM and FEM. The second condition is the equilibrium condition [2]. This requires that the approximation functions used for the FEM on the boundary must match those used for the boundary elements of the BEM. Although different local coordinate systems were used for the two methods (as described in previous sections), the approximation functions were both linear. By choosing the boundary elements of the BEM as the sides of the triangles in the FEM which touches the boundary B, the equilibrium condition will be met.

3.4.3 Obtaining a solution

With the above mentioned conditions met, the two equations (3.11) and (3.32) can be joined to obtain a solution of the potentials on the nodes in Ω_{in}. These values together with (3.04) enable one to obtain an approximated potential value in any triangular element. The solution of potentials in Ω_{ex} can be obtained using equation

(3.29) because the potentials and their normal derivatives on each boundary element are known. Methods used for numerical matrix solutions will be discussed in chapter 5.

3.4.4 Numerical examples

Computer code was written to apply the CEM discussed above. Two examples will be considered. The results will be compared with analytical solutions where possible.

3.4.4.1 Perfectly conducting parallel plates

Fig-3.8 shows two parallel plates with three dielectrics between the two plates. The top plate has a fixed potential of 1 Volt and the bottom plate a fixed potential of -1 Volt. The region was divided into finite elements and boundary elements as shown in fig-3.9.

Figure-3.8 Conducting parallel plates with dielectrics in between. The length of the plates is 0.4 m and the distance between them 0.2 m. Line a is 1 m long.

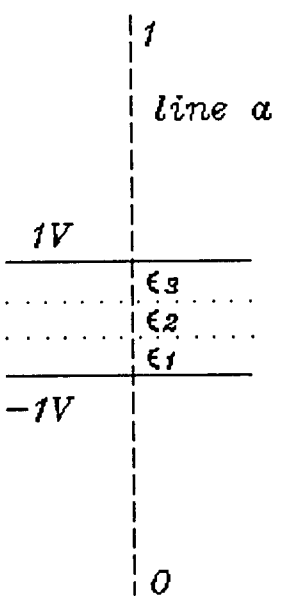

Figure-3.9 Triangulated region around and between parallel plates used for ϵ_1, ϵ_2 and $\epsilon_3 = 0$. The triangulated region consists of 61 total nodes, 16 boundary nodes and 104 finite elements.

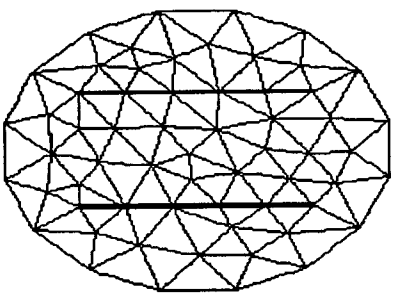

With ϵ_1, ϵ_2 and $\epsilon_3 = 0$, the potential along line a is shown in graph-3.1. The potential between the two plates as seen in graph-3.1 can be verified analytically (appendix A3.8). Graph-3.2 shows the equi-potential lines in- and outside Ω_{in}. The fringing potentials outside the space between the two plates are clearly visible. Graph-3.3 shows the potentials along line a with $\epsilon_1 = 6, \epsilon_2 = 4$ and $\epsilon_3 = 2$. The different gradients of the potentials in the different dielectrics is noticeable.

Graph-3.1 The potential along line a (fig-3.8), calculated in the finite element and boundary element regions.

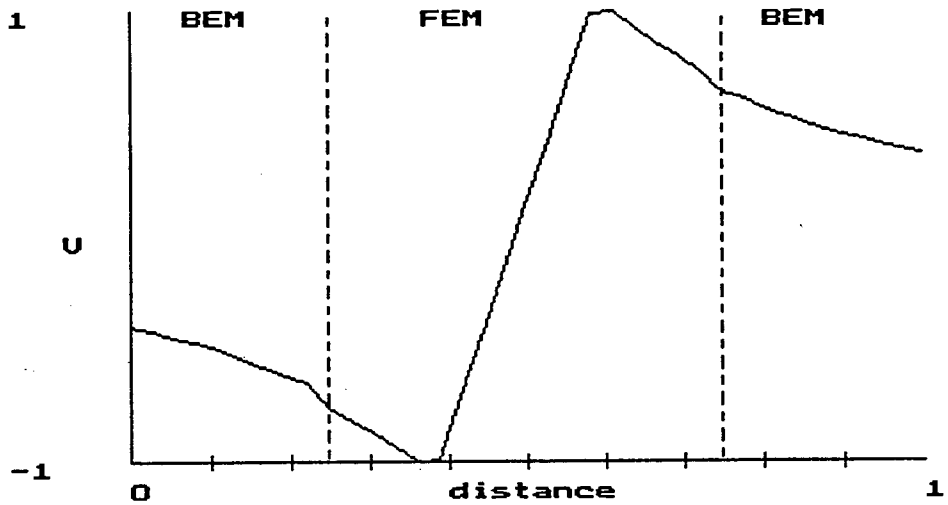

Graph-3.2 Equo-potential lines in between and around the parallel plates of fig-3.8.

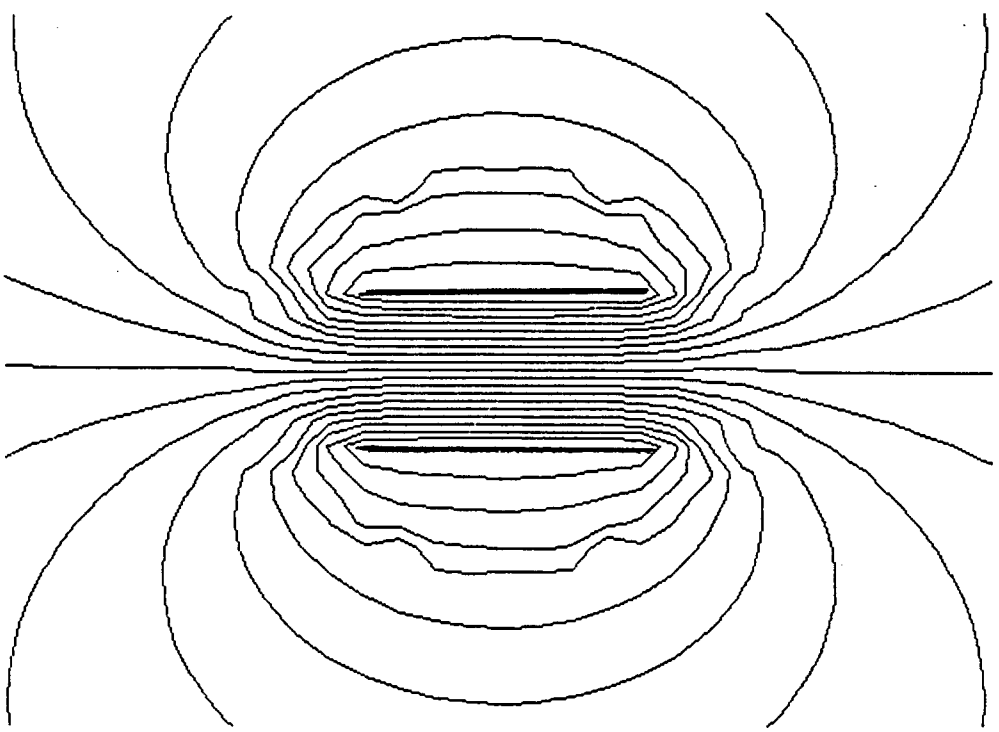

Graph-3.3 The potential along line a (fig-3.8), with varying dielectrics between the plate.

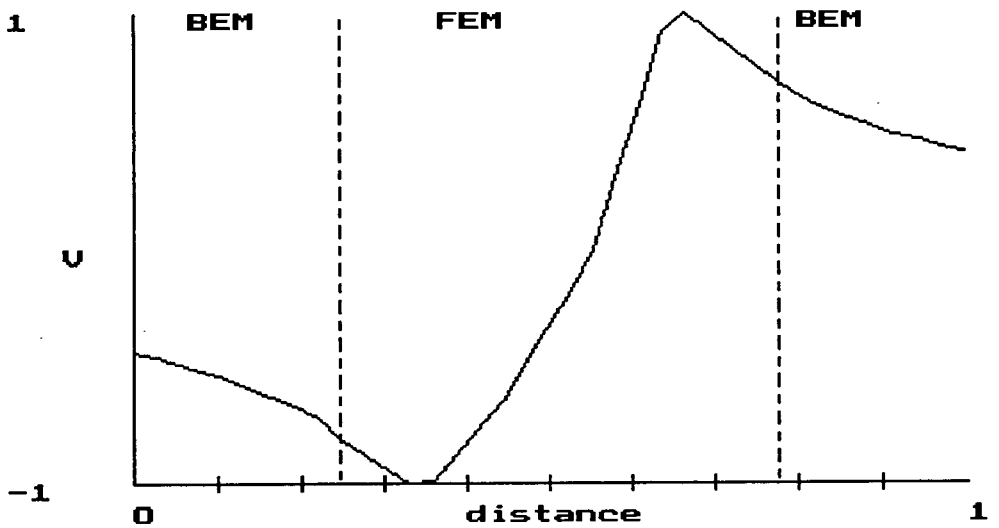

3.4.4.2 Perfectly conducting cylinders

The region shown in fig-3.10 was divided into finite elements around the two round, perfectly conducting cylinders. The cylinder on the right and left were given prescribed potential values of 1 Volt and -1 Volt respectively. Graph-3.4 shows the potential along line a in fig-3.10.

Figure-3.10 Perfectly conducting round cylinders with a boundary around them separating the finite element region from the boundary element region. The radii of the cylinders are both 0.1 m. The length of line a is 1 m.

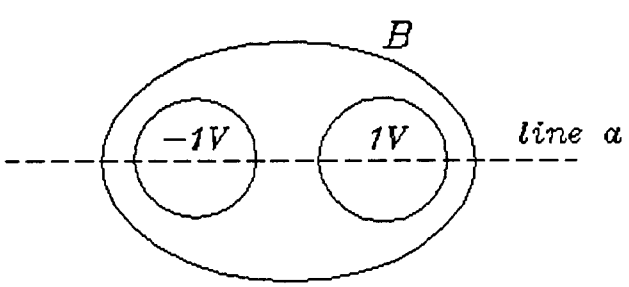

Graph-3.4 The potential along line a (fig-3.9), calculated in the finite element and boundary element regions.

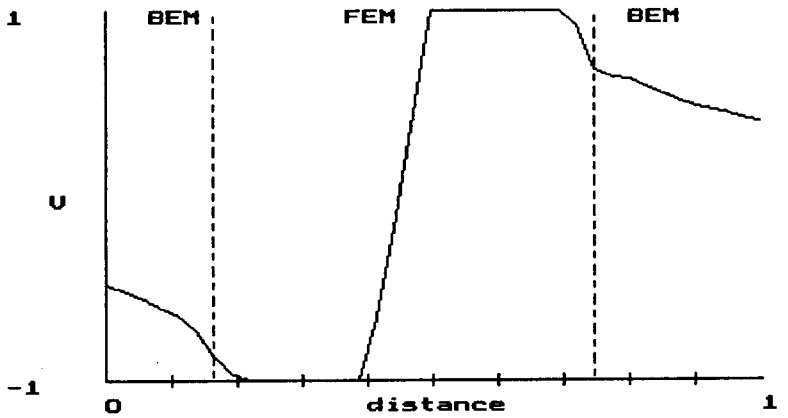

3.4.5 Conclusion

The basic theory for the CEM was discussed in this chapter. The compatibility of the FEM and BEM was shown to be quite trivial. Extending this theory to accommodate more difficult problems than the static Laplace's governing equation will be done in the following chapters. The basic theory stays the same but a few extra details, associated with the specific governing equations, have to be considered. The static case, as described in this chapter, provides a good basis for developing the more complicated CEM associated with electromagnetic scattering problems.

4 HELMHOLTZ EQUATION SOLUTION

4.1 Introduction

The CEM theory discussed in chapter 3 can be expanded to incorporate electromagnetic scattering problems. The governing equation associated with scattering problems is the Helmholtz equation. The basic theory, however, stays the same. The fields inside a region, divided into finite elements, will again be approximated using the FEM. The fields outside this region will be approximated in terms of fields on the boundary of the finite element region using the BEM. The CEM's application to scattering problems [2],[3] will be discussed in detail in this chapter. The FEM method is very useful in the handling of problems where the fields inside inhomogeneous, lossy objects have to be obtained. The BEM is suitable for handling scattering problems. The CEM is thus a very good method to use in connection with problems concerning scattering from inhomogeneous, lossy objects because it again uses the characteristics of both the FEM and BEM where it is most efficient. The theory will be developed from Maxwell's equations and most of the methods discussed in chapter 3 will be used again.

4.2 Problem set-up

Consider a region as indicated in fig-4.1. The region consists of a two dimensional scatterer enclosed by a boundary (B) separating the inside region (Ω_{in}) from the outside region (Ω_{ex}). Ω_{ex} extends to infinity. An incident plane wave is exciting the scatterer.

Figure-4.1 Two-dimensional finite region (Ω_{in}) excited by an incident plane wave. The inside region contains a possibly inhomogeneous, lossy scatterer and the exterior free-space region (Ω_{ex}) is homogeneous and extends to infinity.

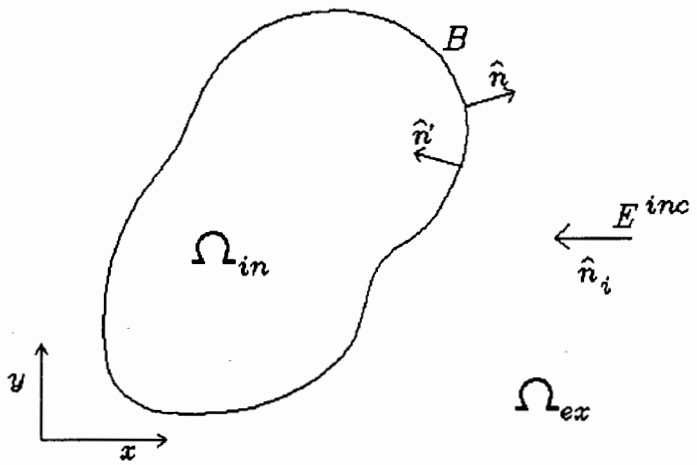

4.2.1 Polarization

The field incident on a two dimensional scatterer (fig-4.1) can be divided into its Transverse Magnetic (TM) and Transverse Electric (TE) components. The same convention as in [1] will be used, with the transversity of the fields being with respect to the x-y plane. A TE polarized wave has an electric field component only in the z direction. The z direction is orthogonal to the x-y directions (fig-4.1) and extends to infinity. A TM polarized wave has a magnetic field component only in the z direction. FEM will be applied to the TM and TE-cases separately. Two different inhomogeneous Helmholtz equations will be used (appendix A4.1) for the two different polarizations. These equations can be derived from Maxwell's phasor equation notation ($e^{-j\omega t}$ time convention) in a source-free region [9,p60]. The governing equation for the TE case is

$$\nabla \frac{1}{\mu_r} \nabla E_z + \epsilon_r k_o^2 E_z = 0 \qquad (4.01)$$

and for the TM case it is

$$\nabla \frac{1}{\epsilon_r} \nabla H_z + \mu_r k_o^2 H_z = 0 \qquad (4.02)$$

In these equations E_z and H_z are the electric and magnetic fields respectively, k_o is the free-space wave number, μ_r the relative permeability and ϵ_r the relative permittivity.

4.2.2 Incident field

The field incident on a scatterer at any point (say p) in the interior or exterior regions is [9,p490]

$$U_{inc} = U_o e^{-jk(r\hat{r}\cdot\hat{n}_{inc})} \tag{4.03}$$

The unit vector $\hat{n}_{inc}$ is in the direction the incident field is travelling and $\hat{r}$ in the direction of point p from the origin of the x-y coordinate system. The field U_{inc} can be either the electric or magnetic field value depending on the polarization under consideration with U_o the amplitude of the wave. The value r , is the distance to point p from the origin. The normal derivative of the field at point p on the boundary (B) will be required when the FEM and BEM are coupled and can be calculated as

$$\frac{dU_{inc}}{dn} = -jk\hat{n}\cdot\hat{n}_{inc}U_{inc} \tag{4.04}$$

(appendix A4.2).

4.3 Finite Element Method

With the scatterer being a potentially inhomogeneous, lossy object, the FEM will be used to obtain the fields in Ω_{in}. The equation governing in Ω_{in} is the inhomogeneous Helmholtz equation (4.01) or (4.02) . The variable U_z will be used for the fields wherever either the electric or magnetic field is referred to. Linear approximation functions will be used throughout this chapter. The detail of the FEM applied to the inhomogeneous Helmholtz equation will now be discussed.

4.3.1 Approximating the fields

The fields in Ω_{in} can be approximated by dividing Ω_{in} into triangular elements as discussed in sec 3.2.1. The governing equation is then approximately satisfied in Ω_{in} and the result is a linear approximation of the total field value (incident plus scattered) in each triangular element.

4.3.2 Weak formulation for the Helmholtz equation

An approximated field value E'_z (TE case will be considered first) can be defined in Ω_{in} resulting in an approximated governing equation

$$\nabla \frac{1}{\mu_r} \nabla E'_z + \epsilon_r k_o^2 E'_z \neq 0 = error \tag{4.05}$$

The error can be distributed and minimized in an average sense by weighting it and setting the weighted error equal to zero

$$\int_{\Omega_{in}} \left(\nabla \frac{1}{\mu_r} \nabla E'_z + \epsilon_r k_o^2 E'_z \right) W \, d\Omega_{in} = 0 \tag{4.06}$$

The Galerkin method, with the weighting function equal to the approximated field function will be used again (sec 3.2.3). By integrating the left most term in (4.06) by parts (appendix A4.3), the weak formulation is obtained

$$\int_{\Omega_{in}} \nabla W \frac{1}{\mu_r} \nabla E'_z \, d\Omega_{in} - \int_{\Omega_{in}} \epsilon_r k_o^2 E'_z W \, d\Omega_{in} - \oint_B W \frac{1}{\mu_r} \frac{dE'_z}{dn} dB = 0 \tag{4.07}$$

4.3.3 Discretizing the weak formulation

Equation (4.07) can be discretised to apply in each triangular element separately giving

$$\sum_{j=1}^{o} \int_{\Omega_{in_j}} \nabla W \frac{1}{\mu_{r_j}} \nabla E'_z \, d\Omega_{in_j} - \sum_{j=1}^{o} \int_{\Omega_{in_j}} \epsilon_{r_j} k_o^2 E'_z W \, d\Omega_{in_j}$$

$$- \sum_{j=1}^{p} \int_{B_j} W \frac{1}{\mu_{r_j}} \frac{dE'_z}{dn} dB_j = 0 \tag{4.08}$$

Using simplex coordinates and the same approximation functions as in sec 3.2.2 and 3.2.3, E'_z in each triangular element is given by

$$E'_z = \sum_{i=1}^{3} E'_{zi} \xi_i \tag{4.09}$$

and its normal derivative by

$$\frac{dE'_z}{dn} = \sum_{i=1}^{3} \left(\frac{dE'_z}{dn} \right)_i \xi_i \tag{4.10}$$

With ϵ_r and μ_r constant within each element and substituting (4.09) and (4.10) into (4.08) yields

$$\sum_{j=1}^{o} \frac{1}{\mu_{r_j}} \int_{\Omega_{in_j}} \sum_{i=1}^{3} \nabla\xi_i \sum_{k=1}^{3} \nabla\xi_k E'_{z_k} d\Omega_{in_j} - \sum_{j=1}^{o} \epsilon_{r_j} k_o^2 \int_{\Omega_{in_j}} \sum_{i=1}^{3} \xi_i \sum_{k=1}^{3} \xi_k E'_{z_k} d\Omega_{in_j}$$

$$- \sum_{j=1}^{p} \frac{1}{\mu_{r_j}} \int_{B_j} \sum_{i=1}^{2} \xi_i \sum_{k=1}^{2} \xi_k \frac{dE'_{z_k}}{dn} dB_j = 0 \qquad (4.11)$$

Equation (4.11) can be written in matrix form as

$$[S][E'_z] - [T]\left[\frac{dE'_z}{dn}\right] = 0 \qquad (4.12)$$

For a TM polarized field, (4.02) can be developed in exactly the same way as (4.01) to yield the matrix equation

$$[S][H'_z] - [T]\left[\frac{dH'_z}{dn}\right] = 0 \qquad (4.13)$$

4.3.4 Matrix elements

The elements of the global [S] matrix can again be obtained by adding up the 3x3 local [S_e] matrices (see sec 3.2.4.1). The elements of [S_e] are now given from (4.11) as

$$S_e^{ij} = \frac{1}{\mu_{r_e}} \sum_{i=1}^{3} \sum_{k=1}^{3} \int_{\Omega_e} \nabla\xi_i \cdot \nabla\xi_j d\Omega_e - \epsilon_{r_e} k_o^2 \sum_{i=1}^{3} \sum_{k=1}^{3} \int_{\Omega_e} \xi_i \xi_j d\Omega_e \qquad (4.14)$$

The first term in (4.14) has the same form as (3.12) and it can thus be obtained from tabulated values. The second term can be written as

$$S'^{ij}_e = \epsilon_{r_e} k_o^2 A \sum_{i=1}^{3} \sum_{j=1}^{3} \int_{\Omega_e} \xi_i \xi_j \frac{d\Omega_e}{A} \qquad (4.15)$$

A is the area of the element under consideration. The integrals in (4.15) have to be calculated [6,p11] only once and can be tabulated [6,p112]. The local matrices only differ because of the different areas the elements might have.

The global [T] matrix has the same form as the [T] matrix in (3.11) and its elements can be obtained as described in sec 3.2.4.2.

The equations giving the elements of the [S] and [T] matrices for the TM-case stay the same as for the TE-case but with ϵ_r taking the place of μ_r and vica versa.

4.3.5 Prescribed or known field values

If a perfect conductor is present in Ω_{in} it does not have to be divided into triangular elements. The boundary conditions on a perfect conductor requires that the tangential electrical field has to be zero. If some of the nodes lie on a perfect conductor, their field values are thus known to be zero. The [S] matrix has to be altered accordingly as was done with the known potentials in sec 3.2.5. If the TM-case is considered, the transverse magnetic fields on the perfect conductor have to satisfy the Neumann (or natural) boundary conditions [6,p74]. H_z can thus be left as an unknown field value to be approximated.

4.3.6 Lossy media

The FEM provides a way to handle inhomogeneous regions by dividing the region into homogeneous triangles. If the region is lossy (ϵ_r and μ_r have complex values), the method can be applied exactly as described above. The only difference is that the elements of the matrices will have complex values. It should be noted that the imaginary parts of ϵ_r and μ_r must be positive because of the time convention chosen with the phasor notation (sec 4.2.1).

4.3.7 Conclusion

The FEM described above is a numerical method approximating the fields in a potentially inhomogeneous, lossy region. The matrix equation (4.12) is a set of linear independent equations with two sets of unknowns (the fields inside Ω_{in} and on B, and their normal derivatives on B). The BEM will again enable one to obtain another set of linear equations with the same two sets of unknowns.

4.4 Boundary Element Method

The fields in the exterior region (Ω_{ex}) of fig-4.1 will be obtained using the BEM in a similar manner as discussed in sec 3.3, but with the Helmholtz equation as the

governing equation. The fields on the boundary (B) will again be approximated and the fields in Ω_{ex} can then be expressed in terms of these boundary fields. The theory of the BEM applied to scattering problems will be discussed in this section.

4.4.1 The boundary equation

The boundary (B) enclosing the scatterer is chosen to ensure that any non-free space material lies in the finite element region. The governing equation in Ω_{ex} is thus the homogeneous Helmholtz equation, given by (4.01) and (4.02) with $\epsilon_r = 1$ and $\mu_r = 1$:

$$\nabla^2 E_z + k_o^2 E_z = 0 \tag{4.16}$$

for TE polarization and

$$\nabla^2 H_z + k_o^2 H_z = 0 \tag{4.17}$$

for TM polarization.
Consider the TE-case. Approximating E_z by E'_z and weighting and minimizing the approximated Helmholtz equation yields

$$\int_{\Omega_{ex}} (\nabla^2 E'_z + k_o^2 E'_z) W \, d\Omega_{ex} = 0 \tag{4.18}$$

Applying Green's second theorem (as was done in sec 3.3.2) to the first term in the integral of (4.18) gives

$$\int_{\Omega_{ex}} (\nabla^2 W + k_o^2) E'_z \, d\Omega_{ex} - \int_B \frac{dW}{dn'} E'_z \, dB + \int_B \frac{dE'_z}{dn'} W \, dB = 0 \tag{4.19}$$

4.4.2 Weighting function

The weighting function will again be chosen as the Green's function satisfying the governing equation with a unit applied field at a source point (sec 3.3.3). The equation that has to be satisfied is thus

$$\nabla^2 W + k_o^2 = \delta(r_o - r_s) \tag{4.20}$$

The two-dimensional Green's function satisfying this equation is given by [9,p376] as

$$W = \frac{j}{4} H_o^{(1)}(k_o | r_o - r_s |) \tag{4.21}$$

with $H_o^{(1)}$ the Hankel function of the first kind order zero [10,p138]. Substituting (4.20) into (4.19) and following the same procedure as in appendix A3.4 yields

$$E'_{z_o} = -\int_B \frac{dW}{dn'} E'_z dB + \int_B \frac{dE'_z}{dn'} W dB \tag{4.22}$$

E'_{z_o} is the field at an observation point r_o in Ω_{ex}. Taking this observation point to the boundary (B) [3,p119]) yields

$$\frac{1}{2} E'_{zb_o} = -\int_B \frac{dW}{dn'} E'_z dB + \int_B \frac{dE'_z}{dn'} W dB \tag{4.23}$$

4.4.3 Matrix formulation

Equation (4.23) can be discretised in a similar manner as in sec 3.3.4 to give

$$\frac{1}{2} E'_{zb_o} = -\sum_{j=1}^{n} \int_{B_j} \frac{dW}{dn'} E'_z dB_j + \sum_{j=1}^{n} \int_{B_j} \frac{dE'_z}{dn'} W dB_j \tag{4.24}$$

which can be written in matrix form as

$$[H][E'_{zb}] - [G]\left[\frac{dE'_{zb}}{dn'}\right] = 0 \tag{4.25}$$

A similar equation applies for the TM polarization case giving

$$[H][H'_{zb}] - [G]\left[\frac{dH'_{zb}}{dn'}\right] = 0 \tag{4.26}$$

4.4.3.1 The H-matrix

The elements of [H] can be obtained in a similar manner as described in sec 3.3.4.1. Homogeneous coordinates are again used on each boundary element and four point Gaussian integration is used to calculate the integral over each element. The only difference is the function $\frac{dW}{dn'}$. The normal derivative of (4.21) can be calculated as

(appendix A4.4)

$$\frac{dW}{dn'} = \hat{r} \cdot \hat{n} \frac{jk_o}{4} H_1^{(1)}(k_o | r_o - r_s |) \tag{4.27}$$

with $\hat{r}$ the unit vector in the direction of the vector $\vec{r}_o - \vec{r}_s$ and $H_1^{(1)}$ the Hankel function of the first kind and first order.

The Hankel function of the first kind is given in terms of the Bessel functions of the first and second kind [10,p137]. Both the Bessel functions of the first and second kind consist of a term involving an infinite summation [10,p166]. With very small arguments both kinds of Bessel functions for zeroth and first order can be accurately calculated using the small argument approximation [12,p176]. With large arguments the asymptotic expansions [10,p143] can be used. With arguments where both these approximations fail to provide an acceptable accuracy, the infinite sum can be approximated by only adding the first n terms . The n'th term is the first term in the series with a value small enough to be neglected. This method is applicable because all four functions discussed above are converging functions [12,p177].

4.4.3.2 The G-matrix

The elements of [G] can be obtained in a similar manner as described in sec 3.3.4.2, the only difference being the difference in the weighting function W. A problem arises if the observation point lies on the element integrated over. The argument of the Hankel function becomes zero and the imaginary part of the Hankel function becomes infinite when the argument becomes zero. This singularity can be avoided by an analytical integration over the element (appendix A4.5).

4.4.4 Field values in the outside region

The field values in Ω_{ex} can be calculated using a discretised form of (4.22)

$$E^{'}_{z_0} = -\sum_{j=1}^{n} \int_{B_j} \frac{dW}{dn'} E^{'}_{z} dB_j + \sum_{j=1}^{n} \int_{B_j} \frac{dE^{'}_{z}}{dn'} W dB_j \qquad (4.28)$$

It is clear that the exact or approximated field values on the boundary have to be known to obtain the field value at the observation point using (4.28). The boundary field values can be obtained by solving the matrix equation (4.25). Equation (4.25) has two sets of unknowns and can be solved if one of the sets of unknowns is given. An example is when the boundary (B) is on a perfect conductor and the transverse electric field values are known to be zero on the boundary (TE polarization).

4.5 Coupled Element Method

Similar as in sec 3.4 the FEM matrix equation (4.12) can be coupled with the BEM matrix equation (4.25). Both equations have two sets of unknown values which can be related using boundary conditions. By combining the matrix equations of these two methods the fields in the finite, potentially inhomogeneous region (Ω_{in}) and the infinite, outside region (Ω_{ex}) can be obtained.

4.5.1 Conditions for compatibility

If the equilibrium conditions for compatibility are satisfied on the boundary (B) as described in sec 3.4.2, the continuity of fields [1,p143] over the boundary is the only other condition required. The fields approximated on the boundary by the BEM are just the scattered fields and not the total fields as with the case of the FEM. This means that the FEM approximates the sum of the known incident and unknown scattered fields in the finite interior region. The BEM extends to infinity and the radiation condition requiring that the fields at infinity be zero is met [3,p199]. The boundary conditions thus require that

$$E_z^{'FEM} = E_z^{'BEM} + E_z^{inc} \tag{4.29}$$

and

$$\frac{dE_z^{'FEM}}{dn} = -\frac{dE_z^{'BEM}}{dn'} - \frac{dE_z^{inc}}{dn'} \tag{4.30}$$

These conditions provide a link between the FEM and BEM described above.

4.6 Field values

4.6.1 Near fields

The solution of the coupled matrix equations of the FEM and the BEM provides the approximated field values at all the nodes in Ω_{in} and on B. Equation (4.09) can be used to obtain the field values in each triangular element and (4.28) can be used to obtain the field value at any point in Ω_{ex}.

4.6.2 Far-fields

The echo width or radar width of the scatterer defined as

$$\sigma(\phi) = 2\pi r \left| \frac{U_z^{sca}(\phi)}{U_z^{inc}} \right|^2 \tag{4.31}$$

can also be obtained. The scattered field ($U_z^{sca}(\phi)$) in (4.31) is the field at an observation point r_o in Ω_{ex} where the point r_o is at an angle ϕ relative to the direction of the incident wave. The point r_o is also a large distance (r) from the scatterer. $U_z^{sca}(\phi)$ can be obtained using (4.28) or a similar equation for the TM-case. The asymptotic expressions of the Hankel functions are used in the integrals. These asymptotic expressions can be used because the argument of the Hankel functions ($k_o r$) is large. The function W (equation 4.21) becomes (appendix A4.6)

$$W = \frac{j}{4}\sqrt{\frac{2}{\pi k_o r}} e^{jk_o r''} \tag{4.32}$$

with r'' the distance from the origin of the coordinate system to the point on the boundary under consideration in (4.28). The normal derivative of W becomes (appendix A4.6)

$$\frac{dW}{dn'} = (\hat{n}' \cdot \hat{r}) jk_o W \tag{4.33}$$

When determining the radar width, the $\sqrt{\frac{1}{r}}$ term present in W and $\frac{dW}{dn'}$ can be withdrawn from (4.28). If this term is squared as required by (4.31), it is evident that the variable r, present in (4.31), is cancelled out. The radar width can thus be determined without defining a specific distance to the observation point.

4.7 Chirality

Except for the usual macroscopic quantities (permittivity and permeability) materials might have, another quantity called chirality [11] exists. A chiral material has the property that it splits a linear polarized incident wave up into left-circular and right-circular polarized waves. The chirality factor β is a measurement of the chirality of a material. In this section the CEM developed for inhomogeneous scattering problems will be extended to handle chiral materials.

4.7.1 Constitutive relations

The chirality of materials can be described mathematically by defining new constitutive relations to incorporate chirality. The constitutive relations are given by [11,p4] as

$$D = \epsilon E + \epsilon\beta \nabla \times E \tag{4.34}$$

and

$$B = \mu H + \mu\beta \nabla \times H \tag{4.35}$$

with D the electric flux density and B the magnetic flux density. It is evident that the electric flux density (D) is not only dependent on the electric field (E) but also on the curl of the electric field via the chirality factor. The same applies for the magnetic flux density and its dependency on the magnetic field (H). If the chirality factor is made zero, the material has no chirality characteristics and (4.34) and (4.35) becomes the usual constitutive relations given by [1,p127] as

$$D = \epsilon E \tag{4.36}$$

and

$$B = \mu H \tag{4.37}$$

4.7.2 A chiral Helmholtz equation

By using (4.34) and (4.35) together with Maxwell's equations, two inhomogeneous chiral Helmholtz equations can be derived (appendix A4.7):

$$\nabla \frac{(1 - \epsilon_r \mu_r k_o^2 \beta^2)}{\mu_r} \nabla E_z + \epsilon_r k_o^2 \frac{(1 + \epsilon_r \mu_r k_o^2 \beta^2)}{(1 - \epsilon_r \mu_r k_o^2 \beta^2)} E_z + \frac{j2\epsilon_r \mu k_o^2 \omega\beta}{(1 - \epsilon_r \mu_r k_o^2 \beta^2)} H_z = 0 \tag{4.38}$$

and

$$\nabla \frac{(1 - \epsilon_r \mu_r k_o^2 \beta^2)}{\epsilon_r} \nabla H_z + \mu_r k_o^2 \frac{(1 + \epsilon_r \mu_r k_o^2 \beta^2)}{(1 - \epsilon_r \mu_r k_o^2 \beta^2)} H_z - \frac{j2\epsilon \mu_r k_o^2 \omega\beta}{(1 - \epsilon_r \mu_r k_o^2 \beta^2)} E_z = 0 \tag{4.39}$$

It should be noted that any one of the two governing equations has to be written in terms of both the electric and magnetic field values. The reason is that the chiral medium circulates the electromagnetic wave, and any TE or TM polarized incident wave changes its polarization as it travels through the medium. If, for instance, a TE polarized wave is incident on a chiral medium, the incident electric field will thus have only a component in the $\hat{z}$ direction. As the field enters the chiral medium, the wave is broken up into two opposite circulating waves. The electric field thus obtains

a component in the direction perpendicular to the $\hat{z}$ direction. This component is equivalent to the magnetic field in the $\hat{z}$ direction and H_z in (4.38) is thus representative of this non-TE component.

Equations (4.38) and (4.39) become the governing equations in a potentially inhomogeneous, chiral region. The FEM can be applied in this region.

4.7.3 The CEM applied to the chiral Helmholtz equation

Equations (4.38) and (4.39) can both be weighted, minimized, integrated by parts and discretised in finite elements using similar procedures as described in sec 4.3. This yields the following two matrix equations:

$$[S][E_z'] - [R][H_z'] - [T]\left[\frac{\delta E_{z_b}'}{\delta n}\right] = 0 \qquad (4.40)$$

and

$$[S'][H_z'] + [R'][E_z'] - [T']\left[\frac{\delta H_{z_b}'}{\delta n}\right] = 0 \qquad (4.41)$$

(appendix A4.8).
Four sets of unknowns are present in these two equations and combining them with the BEM equations (4.25) and (4.26) (TE and TM polarization) is sufficient to obtain a solution. The same equilibrium and boundary conditions as discussed in sec 4.5 have to be satisfied to combine the four equations above. It is evident from (4.40) and (4.41) that E_z' and H_z' is interdependent and this is why both the electric and magnetic field equations have to be solved simultaneously.

4.8 Numerical examples

Code was developed to implement the CEM discussed in this chapter. Implementation techniques are discussed in chapter 5. The memory restrictions of the personal computer used to execute the code, allow the solution of problems using only a few hundred unknowns. This restricts one to accurately solving problems with sizes not larger than the wavelength of the incident field. In this section, a validation of the CEM will be performed, using a few examples. The examples chosen are canonical

problems for which analytical solutions exist. This will enable one to get an idea of the accuracy of the CEM. The results obtained will be compared to the analytical solutions (chapter 7).

4.8.1 Round, perfectly conducting (PC) cylinder

The triangulated region around a round, PC cylinder is shown in fig-4.2. In this example, the frequency of the incident wave was chosen as 500 MHz resulting in a free-space wavelength (λ_o) of 0.6 m. The relative permeability and the relative permittivity of all the finite elements are one. The radius of the PC cylinder is 0.25 m ($0.4167\lambda_o$).

Figure-4.2 Triangulation of the region around a round, PC cylinder. The region consists of 191 total nodes, 57 boundary nodes and 268 triangular elements.

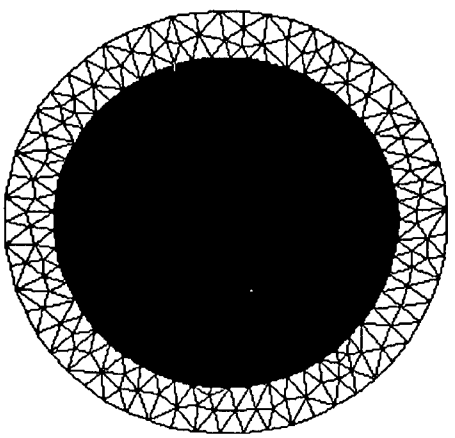

The CEM and analytical solution of the radar width for the PC cylinder, TE and TM polarization, is shown in graph-4.1 and graph-4.2 respectively.

Graph-4.1 Radar width of a round, PC cylinder for TE polarization. Frequency: 500 MHz, radius: 0.25 m.

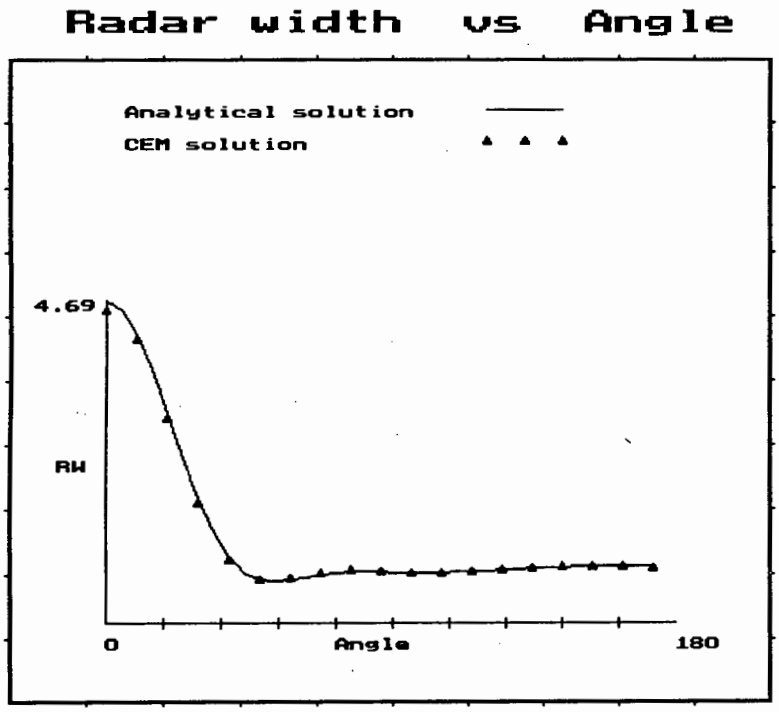

Analytical

	RW (m)	RW dB
0	4.69	6.71
180	0.83	-0.80

CEM

	RW (m)	RW dB
0	4.55	6.58
180	0.78	-1.11

Average normalized error 2.64%

The difference in radar width between the CEM and analytical solution was calculated at angular intervals of 3° over the entire 180°. This difference was normalized with respect to the analytical solution at each specific angle and the average error was calculated. This error is given in graph-4.1 and 4.2. The numerical values of the radar width at 0° and 180°, together with their corresponding dB values, are also given in graph-4.1 and 4.2. Back scattering is at 180°. The average higher accuracy of the TE-case is due to the fact that the transverse electric field on the PC cylinder is known to be, and set to, zero. In the TM-case, the magnetic fields on the PC cylinder are, similar to all other nodes, approximated.

Graph-4.2 Radar width of a PC cylinder for TM polarization. Frequency: 500 MHz, radius: 0.25 m.

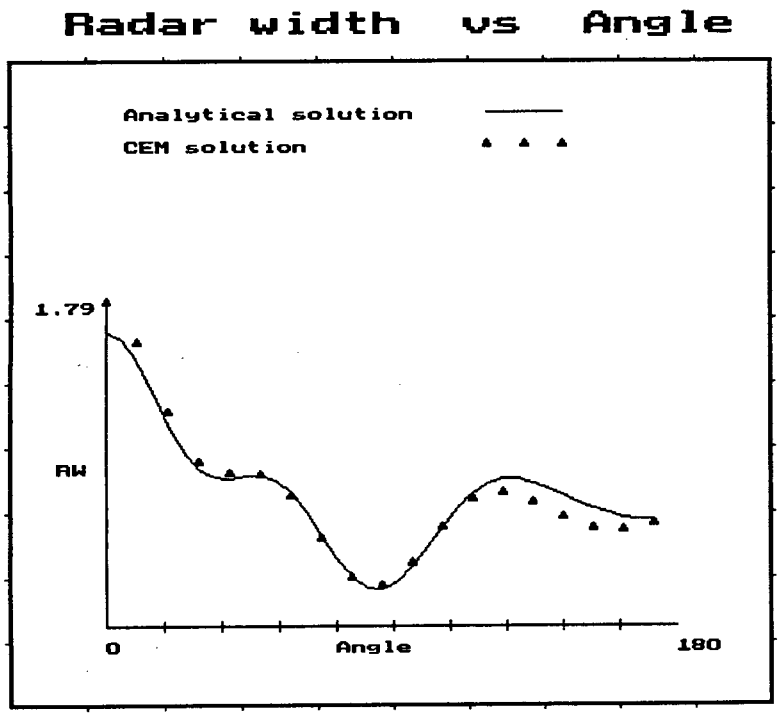

Analytical

	RW (m)	RW dB
0	1.64	2.14
180	0.59	-2.28

CEM

	RW (m)	RW dB
0	1.79	2.53
180	0.56	-2.48

Average normalized error
6.86%

4.8.2 Round, coated PC cylinder

Triangulation of the region in and around the coating on a round, PC cylinder is shown in fig-4.3. The frequency of the incident wave is again chosen as 500 MHz. The radius of the PC cylinder is 0.2 m and of the coating is 0.3 m. The radar width of the coated PC cylinder (TM polarization) is shown in graph-4.3. The relative permittivity of the coating is 3 and the relative permeability is 1. This corresponds to a wavelength in the coated material of $0.346\lambda_r$. The average normalized error is a bit higher than with the round, PC cylinder in the previous example. One reason for this is that the shorter wavelength in the coated material requires a higher number of triangles per meter to obtain the same accuracy. It should be noted that, at the angles where the radar width is close to zero, the normalized difference increases quite drastically although the difference stays quite small. This is due to the division with a very small number when the normalized error is calculated.

Figure-4.3 Triangulation in and around the coating on a PC cylinder. The region consists of 348 total nodes, 58 boundary nodes and 576 triangular elements. The line shown starts on the PC cylinder (x=0.2 with the centre of the cylinder as the origin) and is 0.6 meters long.

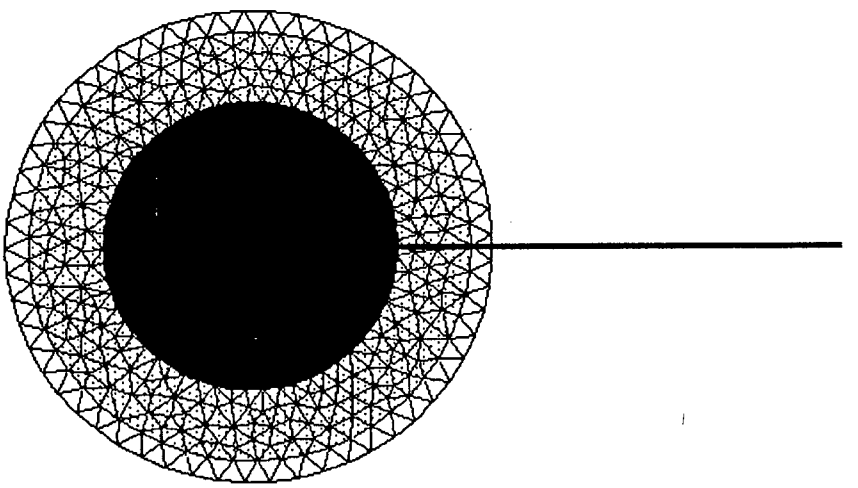

Graph-4.3 Radar width of round coated PC cylinder for TM polarization. Frequency: 500 MHz, PC radius: 0.2 m, coating radius: 0.3 m, ϵ_r: 3, μ_r: 1.

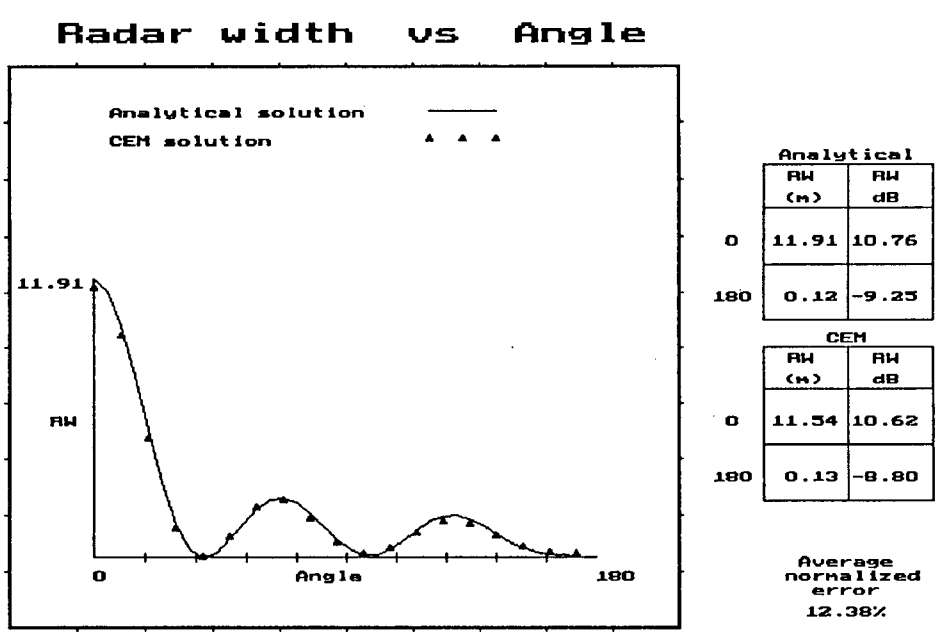

Analytical

	RW (m)	RW dB
0	11.91	10.76
180	0.12	-9.25

CEM

	RW (m)	RW dB
0	11.54	10.62
180	0.13	-8.80

Average normalized error
12.38%

4.8.3 Accuracy vs. number of nodes

Table-4.1 shows the decrease in normalized error of the radar width as the number of unknowns increases. These values were calculated for a round, coated PC cylinder with the same specifications as given in graph-4.3. TE polarization was used. Although a decreasing tendency is evident, convergence to an exact solution as the number of unknowns is increased, has not been formally proven in this thesis.

Table-4.1 Decreasing tendency of the average radar width error, as the number of unknowns increases. Different triangulation densities were used in and around the coating on a PC cylinder (specifications as in graph-4.3). A TE polarized incident field was used.

Total number of nodes	Number of boundary nodes	Number of finite elements	Average normalized error (%)
57	19	76	30.9
105	26	158	22.1
169	35	266	10.5
212	45	334	12.8
348	58	576	8.45

4.8.4 Accuracy vs. frequency

The round, coated PC cylinder used in sec.4.8.2 and sec.4.8.3, will again be used as the scatterer in this section. The specifications of the triangulation are the same (348 total nodes) as in fig-4.3. The radar width was calculated, using the CEM and analytical solution, at different frequencies. Table-4.2 and table-4.3 show the back scattering radar width for TE and TM polarization, respectively. The same number of nodes was used at all frequencies. It is evident that the accuracy tends to decrease as the frequency increases. This is mainly because of the shorter wavelength associated with higher frequencies. These shorter wavelengths require a higher density of unknowns to approximate the fields accurately. Although the results in table-4.2 and 4.3 seem to indicate a higher accuracy for the TM-case. This is not true when the average normalized error is considered.

Table-4.2 Back scattered radar width error at different frequencies of a round, coated PC cylinder with specifications as given in graph-4.3. TE polarized incident field.

Frequency (MHz)	Coating radius (λ_r)	Backscattering radar width (CEM)	Backscattering radar width (analytical)	Normalized difference (%)
50	0.087	1.51	1.55	2.58
100	0.173	1.01	1.03	1.94
200	0.346	0.73	0.75	2.67
500	0.867	0.57	0.57	0.02
1000	1.732	0.32	0.42	23.81

Table-4.3 Back scattered radar width error at different frequencies of a round, coated PC cylinder with specifications as given in graph-4.3. TM polarized incident field.

Frequency (MHz)	Coating radius (λ_r)	Backscattering radar width (CEM)	Backscattering radar width (analytical)	Normalized difference (%)
50	0.087	0.0925	0.0916	0.98
100	0.173	0.6115	0.6112	0.05
200	0.346	1.0662	1.0159	4.95
500	0.867	0.1682	0.1887	10.86
1000	1.732	1.3349	1.5148	11.88

4.8.5 Lossy media

The code developed is able to handle scattering from lossy media. For realizable materials, the imaginary parts of the relative permittivity and permeability have to be positive due to the time convention chosen. With the coating on the same round PC cylinder used in the previous sections being lossy, the radar width at a frequency of 200 MHz was calculated (graph-4.4). It is evident from graph-4.4 that the CEM is also acceptably accurate for scattering from lossy media. The results obtained when higher frequencies or higher relative permittivity values were use, were less accurate.

Graph-4.4 Radar width of a round, coated PC cylinder. The coating material is lossy with $\epsilon_r = 3 + j3$ and $\mu_r = 2 + j2$. A TE polarized incident field with a frequency of 200 MHz was used. Other specifications are the same as given in graph-4.3.

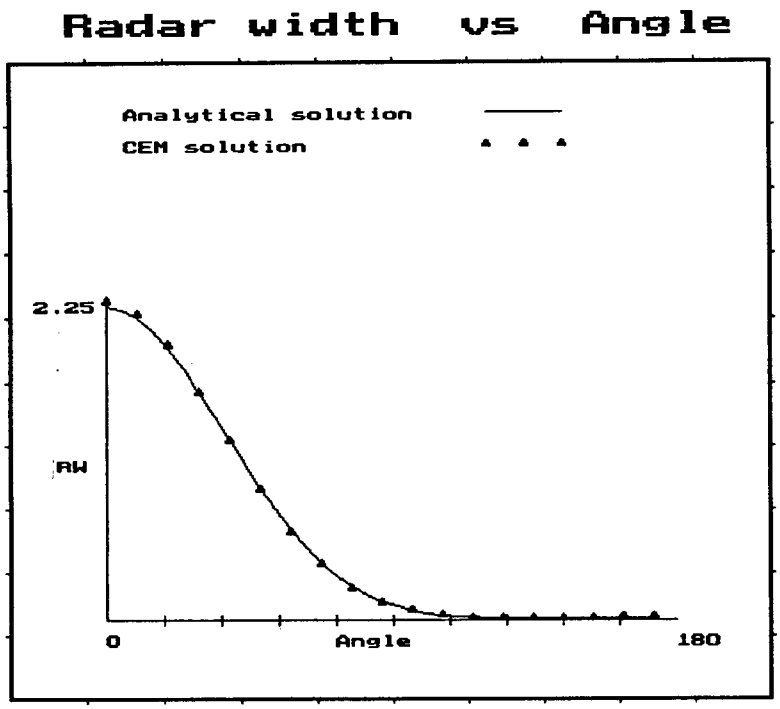

Analytical

	RW (m)	RW dB
0	2.22	3.46
180	0.02	-16.58

CEM

	RW (m)	RW dB
0	2.25	3.52
180	0.03	-15.46

Average normalized error
7.14%

4.8.6 Near fields

So far, only the far-fields due to scattering from an object were considered. The CEM also approximates the field values inside and around a scatterer. The electric field values for different coating materials (from left to right along the line in fig-4.3) are given in graph-4.5 and graph-4.6. These field values were calculated using the CEM and an analytical solution method (chapter 7).

Graph-4.5 Transverse electric field amplitude (FA) from left to right along the line in fig-4.3. The incident field is TE polarized with a frequency of 300 MHz. The material properties of the coated layer are $\epsilon_r = 3$ and $\mu_r = 1$.

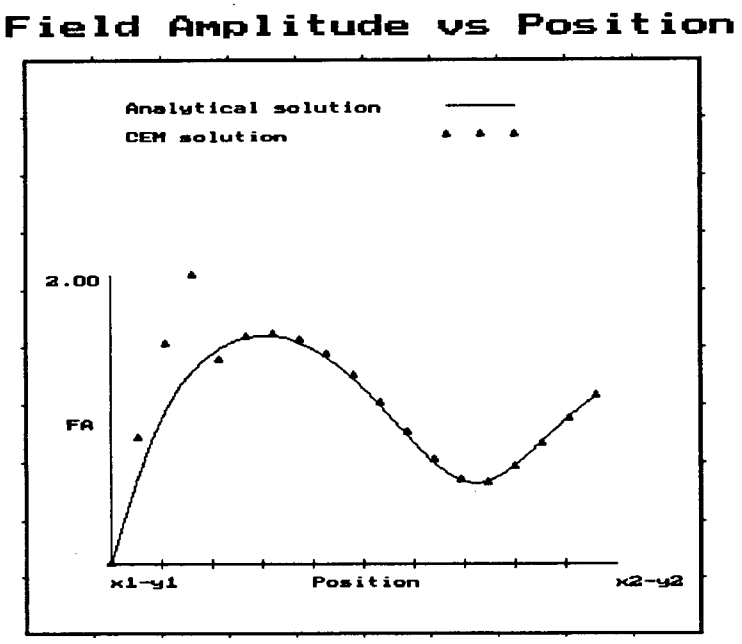

Graph-4.6 Transverse electric field amplitude (FA) from left to right along the line in fig-4.3. The incident field is TE polarized with a frequency of 100 MHz. The material properties of the coated layer are $\epsilon_r = 3 + j3$ and $\mu_r = 2 + j2$.

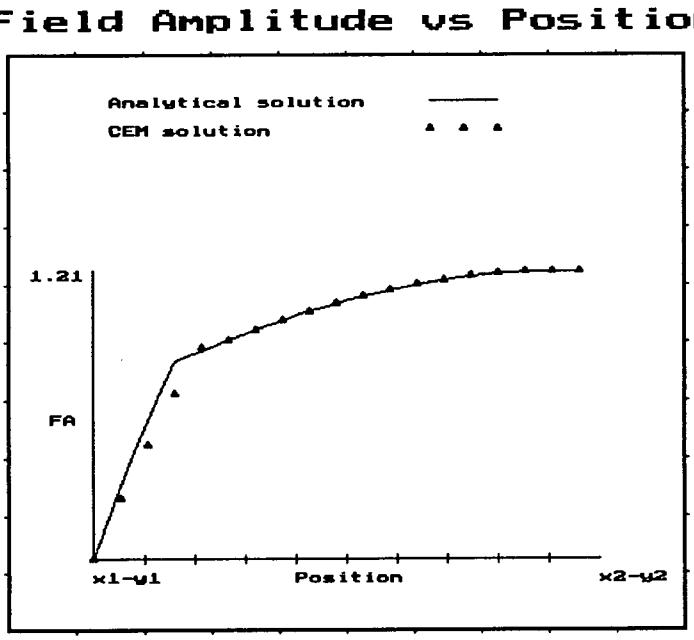

The transverse electric field values from left to right along the line in fig-4.4 are shown in graph-4.7. From graph-4.7 it can be seen that the near field approximations, in the finite element region, are not acceptably accurate. It can be expected that with higher order elements, the fields inside and near a scatterer, will be approximated more accurately. This, however, has not been validated.

Figure-4.4 Triangulation in and around the coating on a PC cylinder. The region has the same triangulation specifications as in fig-4.3. The line shown is 1 m long and 0.24m above the centre of the cylinder.

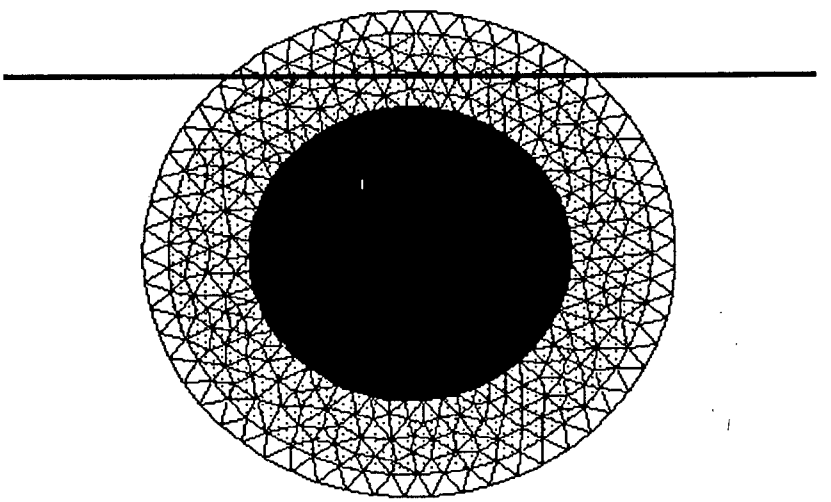

Graph-4.7 Electric field amplitude (FA) from left to right along the line in fig-4.4. The incident field is TE polarized with a frequency of 100 MHz. The material properties of the coated layer are $\epsilon_r = 3$ and $\mu_r = 1$.

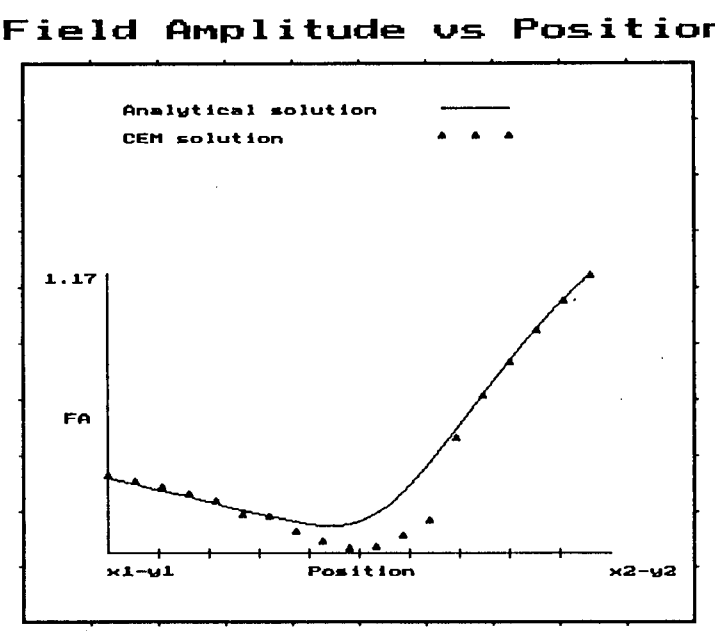

4.8.7 CEM vs. Transfinite Element Method (TEM)

Scattering from the dielectric half-shell shown in fig-4.5 was calculated using the CEM. The radar width was obtained and compared to a TEM solution. The TEM solution was obtained using the commercially available program RADAR [17]. In chapter 2, the TEM was mentioned but disregarded, due to its requirement of a circular boundary around the finite element region. The finite element region in and around the dielectric half-shell required for the TEM is shown in fig-4.6.

Figure-4.5 Triangulated region, in and around a dielectric half-shell. The inner radius of the shell is 0.75 m and the outer radius 0.9 m. The material properties of the dielectric shell are $\epsilon_r = 4$ and $\mu_r = 1$. The region consists of 88 total nodes, 37 boundary nodes and 137 finite elements.

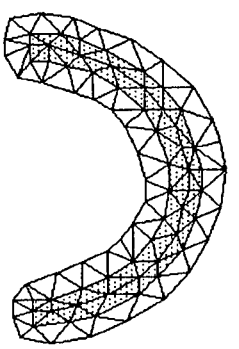

Figure-4.6 Triangulated region, in and around the same dielectric half-shell as in fig-4.5, but satisfying the circular boundary requirements for the TEM. The region consists of 245 total nodes, 48 boundary nodes and 146 triangles (second order elements).

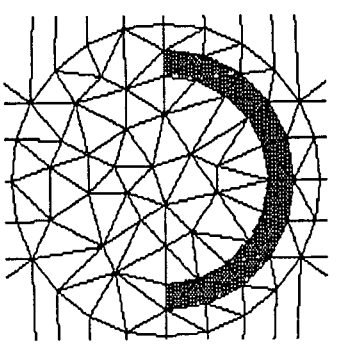

Both CEM and TEM solutions for TE polarization were compared to an integral eigenvalue (IE) solution [22,p56]. This comparison is shown in graph-4.8. Although more unknowns were used with the TEM, the CEM is much more accurate (in this case) than the TEM. Most of the finite elements of the TEM had to be used to fill the required circular region.

Graph-4.8 Normalized radar width of the dielectric half-shell of fig-4.5. The incident field is TE polarized with a frequency of 100 MHz. The CEM, TEM and IE solutions are shown. The TE field is incident from the left side of fig-4.5 with an incident angle of zero with respect to the horizontal.

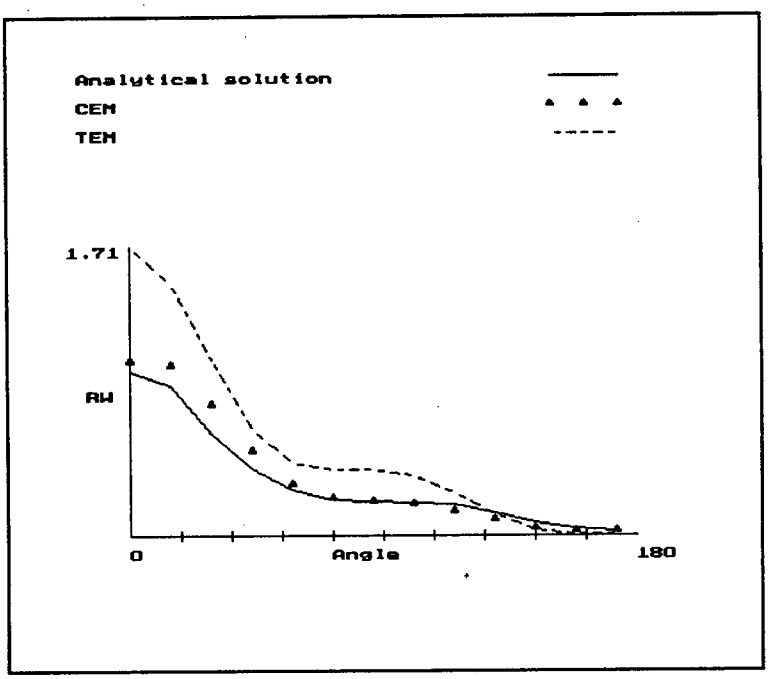

From this example, it is evident that the CEM is a better method to use for scattering from ill-shaped objects. It should, however, be noted that the TEM seems to be more accurate than the CEM when the scatterer is not ill-shaped (table-4.4). This is probably because an analytical solution for the far-field scattering is used with the TEM. The conclusion can, however, be made that the CEM is a better method than the TEM for solving general scattering problems.

Table-4.4 CEM vs. TEM back scattered radar width error at different frequencies of a round, coated PC cylinder with specifications as given in graph-4.3. Approximately the same number of unknowns were used in both methods. The incident field was TE polarized. The analytical back scattering values are given in table-4.2.

Frequency (MHz)	Normalized CEM error (%)	Normalized TEM error (%)
50	2.58	0.65
100	1.94	0.97
200	2.67	1.60
500	0.02	3.51
1000	23.81	7.14

4.8.8 Chiral media.

The CEM developed to handle chiral media requires the solution of an asymmetric matrix twice as large as that required for non-chiral media. This is due to the simultaneous solution of two Helmholtz equations (sec 4.7.3). It is expected that the manipulation of the matrix equations, in a similar manner as described in sec 5.3.1, might improve the efficiency of the solution. This has not been investigated. The number of unknowns that could be used with the developed code was very small because of the limited available memory. Results obtained for scattering from a homogeneous cylinder are compared to the analytical solutions in graph-4.9 (a) and (b). The numerical results seem to follow the expected tendency. Both the analytical and numerical results seem to compare reasonably well with results for the same scatterer found in the literature [23]. Another example of scattering from chiral object is shown in graph-4.10. Again only a few unknowns were used due to the large matrix equations originating. Again the results are satisfactory considering the limitations, but further validation of the method, using more unknowns, is definitely necessary.

Graph-4.9 (a) Radar width of a round, homogeneous ($\epsilon_r = 1.5, \quad \mu_r = 4, \quad \beta = 0$) **cylinder with radius 0.1 m at a frequency of 300 MHz. The incident field is TE polarized. The specifications for the numerical solution is: Total nodes: 78, boundary nodes: 22, triangular elements 138.**

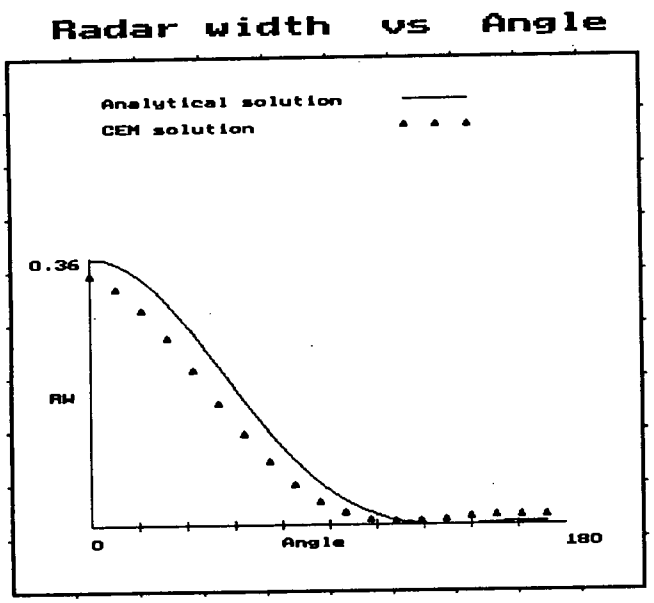

Analytical

	RW V/m	RW dB
0	0.36	-4.47
180	0.01	-22.72

CEM

	RW V/m	RW dB
0	0.33	-4.78
180	0.01	-19.55

Graph-4.9 (b) Radar width of the same round, homogeneous cylinder specified above, but with $\beta = 0.02$.

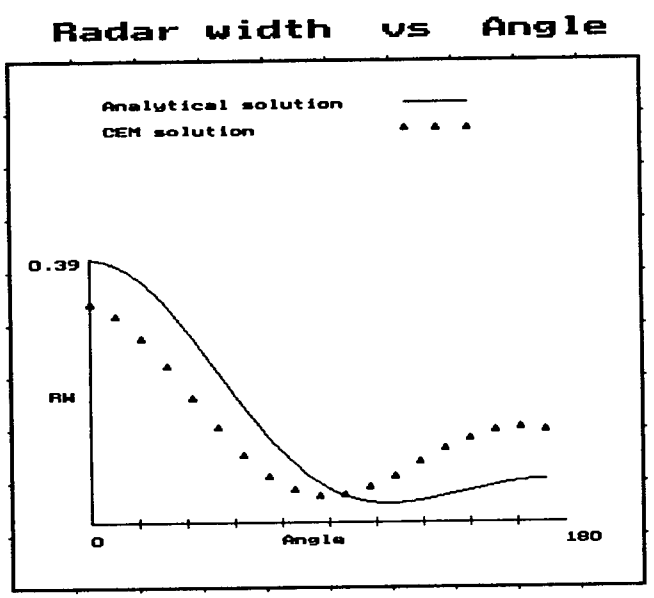

Analytical

	RW V/m	RW dB
0	0.39	-4.05
180	0.06	-11.93

CEM

	RW V/m	RW dB
0	0.33	-4.87
180	0.14	-8.63

Graph-4.10 Radar width of a round, coated PC cylinder. The results obtained for chiral and non-chiral coating are shown. The specifications is as follows: Frequency: 300 MHz, polarization: TM, PC radius: 0.1 m, Coating radius: 0.15 m, e_r: 1.5, μ_r: 4, β: 0 (non-chiral) and 0.1 (chiral), total nodes: 66, boundary nodes: 22 and triangles: 88.

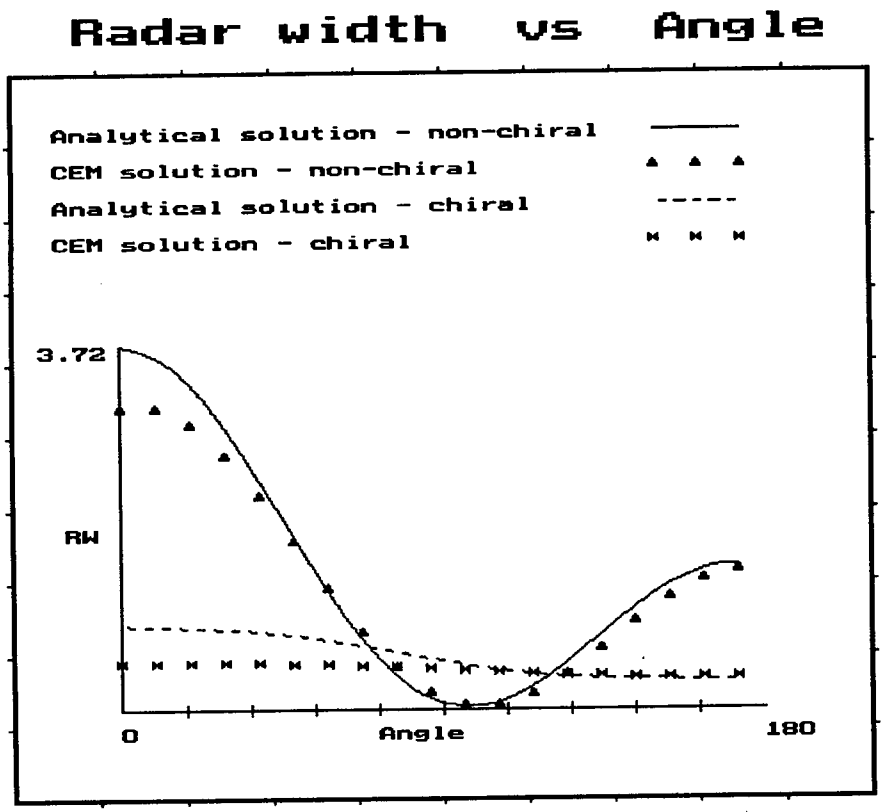

5 NUMERICAL IMPLEMENTATION METHODS

5.1 Introduction

The discussion on numerical methods for solving electromagnetic scattering problems in chapter 4 was mostly theoretical. The problem was reduced to such a stage that only a set of matrix equations had to be solved to obtain an approximated solution. For a practical implementation of these methods three stages can be defined. The first stage is pre-processing, consisting of the set-up of the problem. The second stage is the processing stage when the matrices are being solved. The final, post-processing stage, consists of manipulating the matrix solutions to obtain required results.

When developing code to implement these numerical methods, it is important that this code is as efficient as possible. Speed and memory are the most important aspects to be considered. The higher the accuracy one requires from these numerical methods the larger the matrices to be solved become. The time required to solve a matrix equation usually increases more than quadratically as the size of the matrix increases. The memory requirements also increase quadratically if no special methods are used for matrix storage.

For efficient code it is thus essential that the methods used in especially the processing stage, must be chosen and implemented correctly. In this chapter the methods used to implement all three stages will be discussed. It should be noted that more refined coding could increase the efficiency of the methods quite considerably, although the methods themselves are some of the most efficient methods in literature. All the methods described below were used to implement the CEM for electromagnetic scattering described theoretically in chapter 4.

5.2 Pre-processing

The first stage of the code written consists of the set-up of the specific problem. It is evident that this process should be a semi-automatic process because information in connection with the specific problem has to be provided by the user of the code. Information such as the frequency of the incident wave, shape and size of the scatterer and characteristics of the material the scatterer consists of, must be pro-

vided manually by the user. The next step of pre-processing is to generate nodes which will also be the joining points of the triangular finite elements and line boundary elements to be defined.

5.2.1 Node generation

To be able to create triangular elements that will not be too far from equilateral (this necessity will be discussed in sec 5.2.2), a proportional distribution of nodes is required. The density of node distribution must be specified by the user. Higher frequencies and materials with large relative permittivities or permeabilities result in shorter wavelengths. In these cases there is a necessity for more elements to approximate the fields. The node density should thus be chosen accordingly and might differ in separate sub-regions of the finite element region. A high spatial node density would be appropriate near a scatterer. A slow transition to lower densities is required when nodes further away from the scatterer is generated. The fields further away from the scatterer can usually be expected to become smoother.

5.2.1.1 Prescribed nodes

The geometry of the scatterer, and possibly different materials in it, have to be provided by the user. A boundary enclosing the total scatterer must also be specified. The first automatic step of the node generating procedure [13] is to replace the specified boundary and scatterer's geometry by polygons. These polygons must have all their corner nodes on the specified regions (see fig-5.1). The spatial density of the nodes on the polygons must be the same as the density specified for that specific region.

Figure-5.1 Nodes created on the corners of polygons representing the specified regions. The boundary region (outside circle of nodes) and a elliptical region (inside region of nodes) were specified.

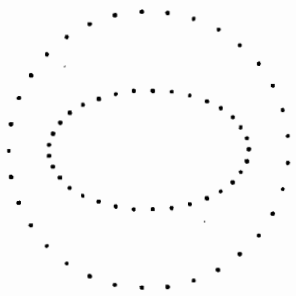

5.2.1.2 Randomly generated nodes

With the specified nodes already generated, the next step is to generate proportionally distributed nodes inside the finite element region. The whole region is divided into rectangles with sizes small enough to create the desired node density if each rectangle contains a node [13,683]. An attempt is now made to randomly generate a node in each small rectangle defined. The node is rejected if it lies closer than a specified distance from any other node already accepted. The specified distance is the size of the side of the rectangle under consideration. A few attempts are made to obtain an acceptable node before advancing to the next rectangle. This procedure ensures that a proportionally distributed node generation is performed.

5.2.2 Triangulation

With a region consisting of distributed nodes, triangulation can be performed. The triangular elements will be created in such a way as to avoid ill shaped triangles. It should be noted that ill shaped triangular elements will decrease the accuracy of the results obtained. The reason for this is twofold. Firstly, the elements of matrices [S] and [T] in (4.12) and (4.13) are dependent on the area size of the triangles. Ill-shaped triangles could have area sizes that are much smaller than the areas of other triangles. This could result in numerical instabilities. Secondly, the fields on the sides of each triangle are linearly approximated (higher orders will be discussed later). At least one of the sides of ill shaped triangles is much longer than the sides of equilateral triangles. A linear approximation of the fields over such a long side

would decrease accuracy. A procedure for triangulation will now be discussed [13,p684]. The boundary elements will be taken as the outmost side of the triangular elements created on the edge of the finite element region defined.

5.2.2.1 Choosing nodes that define the triangles

Two connected nodes (A and B) on the boundary are chosen as the side of the first triangle. A search is made for the closest five nodes ($C_1..C_5$) to the left of the two starting nodes. Closeness is defined as the distance between the first node and the node under consideration plus the second node and the node under consideration ($| AC_i | + | BC_i |$). Any of these five nodes are rejected as possibilities if the triangle ABC_i overlaps any existing triangles or contains any unused nodes. When deciding which of the remaining nodes should be used as the third node of the triangle, two factors have to be considered. Firstly, which node C_i would result in the triangle ABC_i which is the nearest to an equilateral triangle. Secondly, which triangle ABC_i's sides, used as bases in later stages of triangulation, would result in the least ill-shaped triangles. Combining these two considerations, the third node of the triangle is obtained [13,p686]. One of the sides of the triangle just created is now used as the base or starting point for creating the next triangle. This procedure is continued until the whole finite element region has been triangulated. It should be noted that the three node points defining each triangle should be stored in a spatially anti-clockwise order. This convention is necessary because the tabulated values of the sub-matrices described in sec 3.2.4.1 were calculated using this anti-clockwise configuration.

5.2.2.2 Smoothing the triangles created

The triangles created can be smoothed to create even more closely equilateral triangles [13,p687]. Each non-prescribed node will be shifted slightly to improve the triangulation. There is no reason why these nodes cannot be shifted slightly, remembering that they are not located at specific positions, but were randomly generated. Each node under consideration is connected through the triangular elements to a few other nodes surrounding it. These nodes form a polygon around the node under consideration (fig-5.2). The node is thus shifted to lie on the centroid of the polygon. This results in an average improvement of the equilaterality of the triangles connected to this node.

Figure-5.2 Shifting of an unspecified node to improve equilaterality.

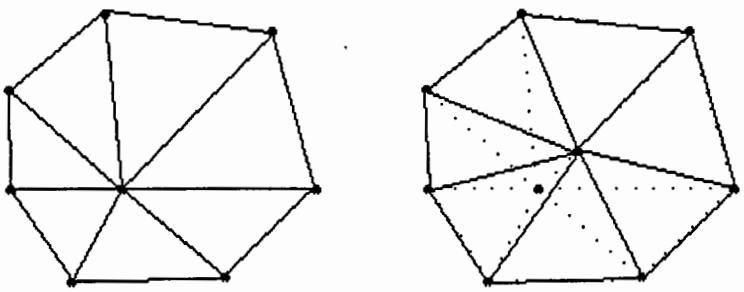

The centroid of a polygon in the x-y coordinate system is given mathematically by

$$(x_{centr}, y_{centr}) = \sum_{i=1}^{n} \frac{(x_i, y_i)}{n} \qquad (5.01)$$

[13,p687]. This smoothing procedure is repeated for all non-prescribed nodes. The whole process can also be repeated as many times as it is considered necessary.

5.2.3 Re-numbering

The [S] matrix of equation (4.12) is usually by far the largest matrix to be stored while solving scattering problems numerically. The [S] matrix is a square matrix of size n with n the number of unknowns or nodes in the finite element region. All other matrices in (4.12) and (4.35) are square matrices of size m, m being the number of boundary nodes. The number of boundary nodes is usually between 5 and 30 percent of the number of total nodes. Fortunately, [S] is a symmetric, sparse matrix due to the nature of the finite element method. The [S] matrix only has an entry in element position S_{ij} if i and j are nodes connected through a triangular element. Most nodes have only connections to a few other nodes, hence the sparseness of [S]. For every entry in S_{ij} a similar entry is made in S_{ji} hence the symmetry of [S]. The total [S] matrix would require a memory space of n^2 complex numbers. Because of the symmetry one only requires memory space for slightly more than $\frac{1}{2}n^2$ complex numbers. If the nodes are numbered correctly, the sparseness of [S] could result in

a narrow-banded matrix. A narrow-banded matrix requires much less memory space than $\frac{1}{2}n^2$. A technique for re-numbering the nodes, (after triangulation has been performed) resulting in a narrow-banded [S] matrix will now be discussed [6,p320].

5.2.3.1 Intuitive re-numbering technique

If one ensures that the nodes connected through the triangular elements to node number i, are all nodes with numbers as close as possible to i, a narrow-banded matrix would be obtained. If, on the other hand, node 1 is connected to node n, element S_{1n} will not have a value of zero and the matrix will have no bandedness. Using this knowledge, one starts by choosing the node with the fewest connections to any other nodes as node number 1. Define a level number 1 and place node 1 in level 1. All the nodes connected to node 1 are placed in level number 2. All nodes connected to any node in level 2 are placed in level 3 and so forth. Node number 2 will be the node in level 2 with the fewest connections to nodes in level 3, until all nodes in level 2 are numbered. This procedure is carried out on all levels until all nodes have been re-numbered. This is an intuitive method, attempting to keep the numbers of the connected nodes as close as possible to each other, resulting in a narrow banded-matrix. Fig-5.3 and fig-5.4 show how this re-numbering method converts an unbanded matrix to a banded matrix. No practical method ensuring an optimum banded matrix is available [6,p318].

Figure-5.3 Graphic representation of the population of the [S] matrix for a practical problem.

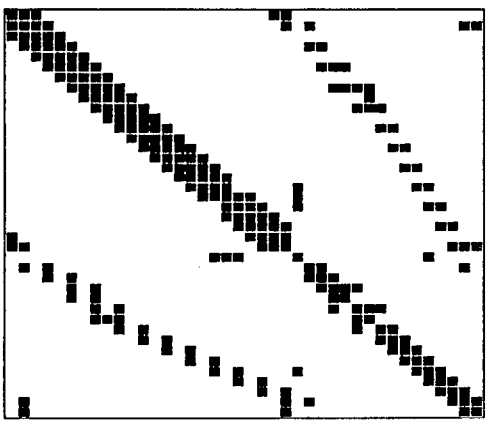

Figure-5.4 Graphic representation of the bandedness of the [S] matrix, after re-numbering was performed, for the same problem as in fig-5.3.

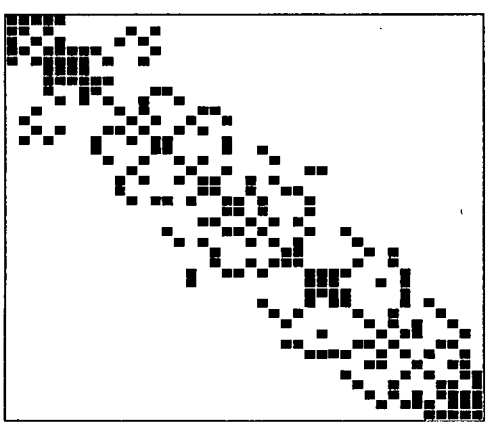

5.2.3.2 Storing of a banded matrix

The [S] matrix can be stored by only storing the lower, left-handed side of the symmetric matrix (losing no information). The half-bandwidth of the matrix can be calculated as

$$BW' = 1 + \max[i - p(i)] \qquad i = 1..n \tag{5.02}$$

[6,p318]. In (5.02), i is the index of a row in [S] and p(i) is the column in row i where the first non-zero element occurs. In each row, only the elements of BW' columns have to be stored. All other elements are known to be zero. The global position (in [S]) of the first element stored in each row is exactly BW' left of the diagonal, thus the position of each stored, non-zero element is also retained. The required storage space is thus reduced to nxBW'. Table-5.1 shows the half-bandwidth and the percentage storage of the total matrix size required, using the half-bandwidth storage method. From this table it is evident that the half-bandwidth storage method is very efficient in saving memory space especially when a large number of unknowns is used.

Table-5.1 Half-bandwidth and percentage storage necessary for a few practical examples.

Unknowns	$\frac{1}{2}$- bandwidth	$\frac{nxBW'}{nxn}$ (%)
39	13	33.3
59	16	27.11
88	18	20.45
121	22	18.18
152	27	17.76
207	34	16.42
293	35	11.94

5.3 Matrix solutions

All finite elements and boundary elements are created and defined in the pre-processing stage. A relative permittivity and permeability is associated with each finite element. At a specified frequency the matrices in equations (4.12) and (4.35) can be filled as described in chapter 4. These two equations both consist of two sets of unknowns. The two matrix equations can be connected through the boundary conditions specified in sec 4.5.1. Methods for solving these two matrix equations simultaneously will be described in this section.

5.3.1 Coupling the FEM and BEM matrix equations

The two matrix equations can be coupled in a number of ways. A straight forward coupling would result in the following matrix equation [3] (see appendix A5.1)

$$\begin{bmatrix} S_{rr} & S_{rb} & 0 \\ S_{br} & S_{bb} & T \\ 0 & H & -G \end{bmatrix} \begin{bmatrix} U_r \\ U_b \\ \frac{\delta U_b}{\delta n'} \end{bmatrix} = [F'] \qquad (5.03)$$

The subscript r is for fields inside the region and b for fields on the boundary. The matrix [F'] is a forcing matrix resulting because of the excitation by the incident field. The matrix on the left hand side of (5.03) is a non-symmetric, square matrix with size n+m (n - number of total nodes, m - number of boundary nodes). The main drawback in this kind of problem is that the computational time the actual numerical matrix solution takes, increases more than quadratically (almost to the power three, depending on the method used) as the size of the matrix increases. The necessity for the most economical matrix solution exists, especially when the number of unknowns becomes large. Combining the two matrix equations as done in appendix A5.2 reduces the problem to a situation where one can obtain a solution in a very economical way. The solution is divided into three steps. Firstly, the inverse of square, sparse matrix [S] is determined. The size of [S] is n. A set of matrix multiplications are secondly performed using the inverse of [S] to obtain a non-symmetric, square matrix [A] with size m and a single column, m row matrix [B]. The final step is obtaining the solution of the following matrix equation

$$[A]\begin{bmatrix} \frac{\delta U_b}{\delta n'} \end{bmatrix} = [B] \qquad (5.04)$$

5.3.2 Numerical solution of coupled matrix equations

Obtaining the inverse of [S] can be handled in a special way. The symmetry of [S] enables one to use the symmetric LU-decomposition algorithm [6,p309]. The matrix [S] is also a positive defined matrix [12,p344] because of the nature of the finite element method. This feature of [S] makes the use of pivoting, to avoid numerical instabilities occurring with large matrices, unnecessary [14,p67]. Because of the asymmetry of [A], the matrix equation (5.04) must be solved using normal LU-decomposition methods. This does not require too much computational time because the size of [A] is m, which becomes much less than n as the number of total unknowns

becomes larger (see table-5.2). From table-5.2 it is evident that the amount of computational work required to solve the asymmetric matrix equation of (5.04) becomes negligible in relation to the work required to obtain the inverse of [S] when the size of the problem increases.

Table-5.2 The number of boundary nodes as a percentage of the number of total nodes for a few practical examples.

Total number of nodes (n)	Number of boundary nodes (m)	$\frac{m}{n}$(%)
59	16	27.1
121	24	19.8
207	32	15.4
293	38	12.9

By solving (5.04), the normal derivatives of the fields on the boundary nodes are obtained. The field values can be obtained using

$$\begin{bmatrix} U \\ U_b \end{bmatrix} = [S]^{-1}[F] - [S]^{-1}\begin{bmatrix} 0 & 0 \\ 0 & T \end{bmatrix}\begin{bmatrix} 0 \\ \frac{\delta U_b}{\delta n'} \end{bmatrix} \qquad (5.05)$$

(appendix A5.1). With the inverse of [S] already known, and [F] a nx1 matrix, (5.05) can be solved by matrix multiplication. With [T] being a square matrix of size m, the computational time it takes to solve (5.05) is negligible. Table-5.3 shows the computational time of the matrix solution for a few practical problems performed on a 18 MHz 386 PC, with a numerical co-processor.

Table-5.3. Comparison of computational time for some practical problems. All the problems were solved using firstly a straight forward coupled method (5.03) and secondly, the three stage method discussed above.

Unknowns	Computational time (min:sec:fsec)	
	One stage solution	Three stage solution
39	00:04:95	00:05:21
59	00:12:53	00:10:16
88	00:43:39	00:25:09
121	01:15:25	00:34:27
152	02:25:61	00:56:08

Table-5.3 shows clearly that the tempo of increase in computational time (as a function of number of unknowns) is much lower when the three stage solution method is used. The reason for this is that one utilizes the symmetry and sparseness of the large matrix [S] with this method. The time saved by this method increases as the number of unknowns increases. The time consuming efficiency, especially for large problems, will thus be considerably increased by this three stage method.

5.4 Post-processing

After the two sets of matrix equations have been solved, it is possible to calculate the field values at any point in the interior finite element region as well as the exterior boundary element region (see sec.4.6). If the field at a point in the finite element region is required, a search algorithm is used to determine in which triangular element the point is situated. The element is defined by three nodal points at which the field values are now known. Equation (4.09) can thus be used to calculate the field value at the desired point. The field value at any point in the exterior region can be calculated using (4.28) with this point as the observation point. The integrals in (4.28) can be solved numerically in a similar manner as was done when determining the matrix elements of [H] and [G] (sec 4.4.3.1 and sec 4.4.3.2). There is, however, no need for avoiding singularities, because the observation point lies in the exterior region and never on any source point.

6 QUADRATIC ELEMENTS

6.1 Introduction

The theory discussed so far on the coupled element methods concerned linear approximation functions in each element. Higher order approximation functions have several advantages, with the its main disadvantage being complexity. In this chapter the extension from linear to quadratic (second order) approximation functions will be discussed. These second order elements contain six nodes on each triangle (fig-6.1) and three nodes on each boundary element.

Figure-6.1 Nodes on a quadratic (second order) finite element.

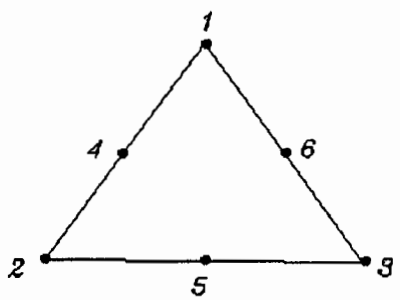

Compared to linear elements the number of triangles approximating a region can be much less, while the same number of nodes are created. Due to the curved nature of quadratic functions, the electromagnetic fields inside the finite element region can also be approximated more accurately than with linear elements. Because of the higher number of nodes per element, the triangular elements usually become bigger if the number of nodes is limited by memory capabilities. The elements must however be kept small enough to fit the geometry of the scatterer. For these reasons, higher order elements than quadratic ones were not investigated although they may prove to be even more accurate when enough memory is available. The basic FEM, BEM and implementation theories stay the same when the second order elements

are used. The alterations necessary will however be discussed. It should be noted that once the matrix equations have been obtained the combination of the two methods stays exactly the same as it was with linear elements.

6.2 Finite elements

6.2.1 Field approximation in triangular elements

The fields in the finite elements are again approximated using simplex coordinates. The three simplex coordinates are again given by (3.03), but the field approximating function in each triangle becomes

$$U = \sum_{i=1}^{6} \alpha_i u_i \qquad (6.01)$$

The six alfa functions in (6.01) are second order functions of the simplex coordinates (see appendix A6.1). The constant values, u_i are the field values at each node on the triangular element. The approximating alfa functions on one side of a triangular element are shown in fig-6.2. The fields on this side of the element will be approximated by the sum of these three functions. A typical approximation of the fields in an element is shown in fig-6.3.

Figure-6.2 Approximating functions on one side of a quadratic finite element.

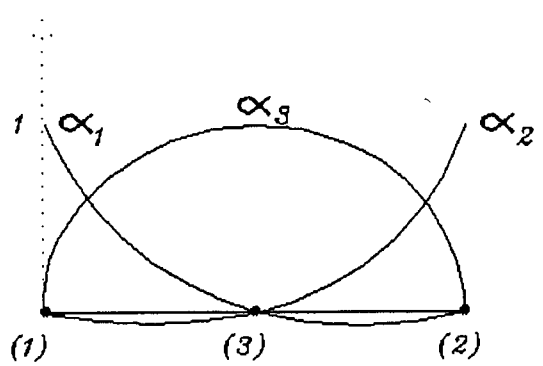

Figure-6.3 Typical field approximation in a quadratic finite element.

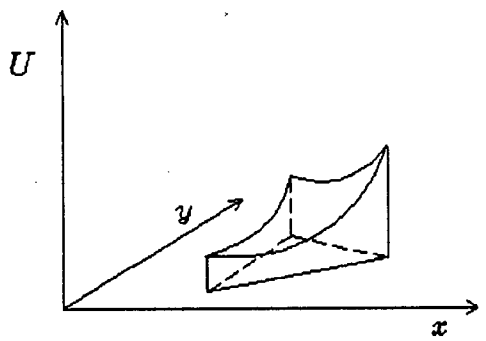

6.2.2 Matrix elements of [S] and [T]

The finite element matrix equation for second order elements can be derived in a similar manner as was done for first order elements (sec 4.3). The elements of [S] and [T] must however be calculated using second instead of first order approximation functions. The elements of the now 6x6 local matrices of each triangular elements are given by (TE-case)

$$S_e^{ij} = \frac{1}{\mu_{r_e}} \sum_{i=1}^{6} \sum_{k=1}^{6} \int_{\Omega_e} \nabla \alpha_i \cdot \nabla \alpha_j d\Omega_e - \epsilon_{r_e} k_o^2 \sum_{i=1}^{6} \sum_{k=1}^{6} \int_{\Omega_e} \alpha_i \alpha_j d\Omega_e \qquad (6.02)$$

These integrals can again be calculated and tabulated [6,p112]. The elements of the global [S] matrix are the sum of the elements of all local matrices whenever one of the nodes of these local matrices coincides with a node of the global matrix (sec 3.2.4.1). The elements of [T] can also be calculated using tabulated values [6,p118].

6.3 Boundary elements

6.3.1 Field approximation on line elements

The second order approximation functions on the boundary elements (fig-6.4) are given by

$$U = \sum_{i=1}^{3} \phi_i u_i \qquad (6.03)$$

In (6.03) the phi functions are given as [4,p62]

$$\phi_1 = \frac{1}{2}\xi(\xi - 1) \tag{6.04}$$

$$\phi_2 = \frac{1}{2}\xi(\xi + 1) \tag{6.05}$$

and

$$\phi_3 = (1 - \xi^2) \tag{6.06}$$

Figure-6.4 Nodes on a quadratic (second order) boundary element.

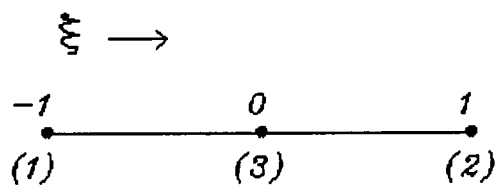

The form of these functions is the same as the alfa functions on the sides of the triangular elements (fig-6.2) and the equilibrium condition for compatibility between the FEM and BEM is thus satisfied.

6.3.2 Matrix elements of [H] and [G]

The elements the matrix [H] consists of, can be calculated using

$$H'^{j}_{i} = \int_{-1}^{1} \phi_k \frac{dW}{dn} J\, d\xi \qquad j = a, b, c \tag{6.07}$$

with everything staying the same as with linear elements except the second order phi functions. In (6.07) k=1 with j=a, k=2 with j=b and k=3 with j=c. The construction of the global matrix [H] using (6.07) is done in a similar manner as described

in sec 3.3.4.1. The matrix [G] is constructed in a similar manner as described in sec 3.3.4.2 using

$$G'^{j}_{i} = \int_{-1}^{1} \phi_k W J d\xi \qquad j = a, b, c \tag{6.08}$$

Both integrations in (6.07) and (6.08) can be calculated numerically using Gaussian integration. The singularity occurring in (6.08), when the observation point lies on the element integrated over, can again be avoided using an analytical integration solution (appendix A6.2).

6.4 Pre- and post-processing

6.4.1 Triangulation

The finite element region is divided into triangular elements as described in sec 5.2. With this method, every element is defined by the spatial positions of the three nodes on the corners of each triangle. With second order elements, three extra nodes are defined on each element as shown in fig-6.1. The spatial positions of these three nodes are exactly halfway between each of the corner nodes of the triangle. The nodes on each element must again be locally numbered in an anti-clockwise order to keep to the convention adopted when the tabulated values were calculated. The re-numbering and all other pre-processing procedures are similar to the procedures used with linear elements.

6.4.2 Determining field values with second order elements

The field at any point in the finite element region can be obtained after the matrix equations have been solved. Using (6.01), the field value at a point in a specific element can be calculated because the field values at the six nodal points are known. In the exterior region an equation similar to (4.28) can be used. The field is given by

$$U_{ex} = -\sum_{j=1}^{n} \int_{B_j} \frac{dW}{dn'} U_b \, dB_j + \sum_{j=1}^{n} \int_{B_j} \frac{dU_b}{dn'} W \, dB_j \tag{6.09}$$

In (6.09) the fields inside the integrals are the already calculated, approximated boundary fields. The integrals are calculated numerically in a similar manner as the elements of the [H] and [G] matrices (sec 6.3.2). The far-field scattering and radar width can thus be calculated as described in chapter 4, slight modifications being made when calculating the integrals over the second order boundary elements.

6.5 Numerical examples using quadratic elements

Code was developed to implement the CEM using quadratic elements. The greatest part of the code developed for first order elements was used with only slight modifications. The code has not yet been completed, and only the radar width and near fields in the exterior region can be obtained so far. The completion of the code should not take too long. A validation of the code will be performed in this section.

6.5.1 Quadratic vs. linear elements

Although the second order element theory for the CEM is slightly more complicated to implement, the computational advantages greatly outweigh the disadvantages of additional complexity. The results obtained with second order elements are almost always more accurate than those obtained with first order elements, as shown in table-6.1.

Table-6.1 Average normalized radar width errors (linear and quadratic elements) of a round, homogeneous dielectric ($\epsilon_r = 4$, $\mu_r = 1$) cylinder. The polarization of the incident field is TE and its frequency is 200 MHz. The radius of the cylinder is 0.25 m.

Linear elements			Quadratic elements		
Number of total nodes	Number of boundary nodes	Average normalized error (%)	Number of total nodes	Number of boundary nodes	Average normalized error (%)
61	17	23.64	64	18	19.23
111	22	22.40	97	24	18.46
178	34	14.57	167	32	15.06
203	40	8.97	200	42	7.94
246	45	11.39	247	44	7.71

It is evident from table-6.1 that the accuracy of the CEM is higher when quadratic elements are used. Apart from the higher accuracy obtained, the converging tendency, as the number of nodes increases, seems better than for linear elements. A comparison of the radar width for all angles between the linear element CEM and quadratic element CEM is shown in graph-6.1. The number of total unknowns used for the quadratic and linear element approximations is 247 and 246 respectively (see the last row in table-6.1).

Graph-6.1 Radar width of a round homogeneous cylinder. The linear and quadratic CEM is compared to the analytical solution. Frequency: 200 MHz, polarization: TE, ϵ_r: 4, μ_r: 1.

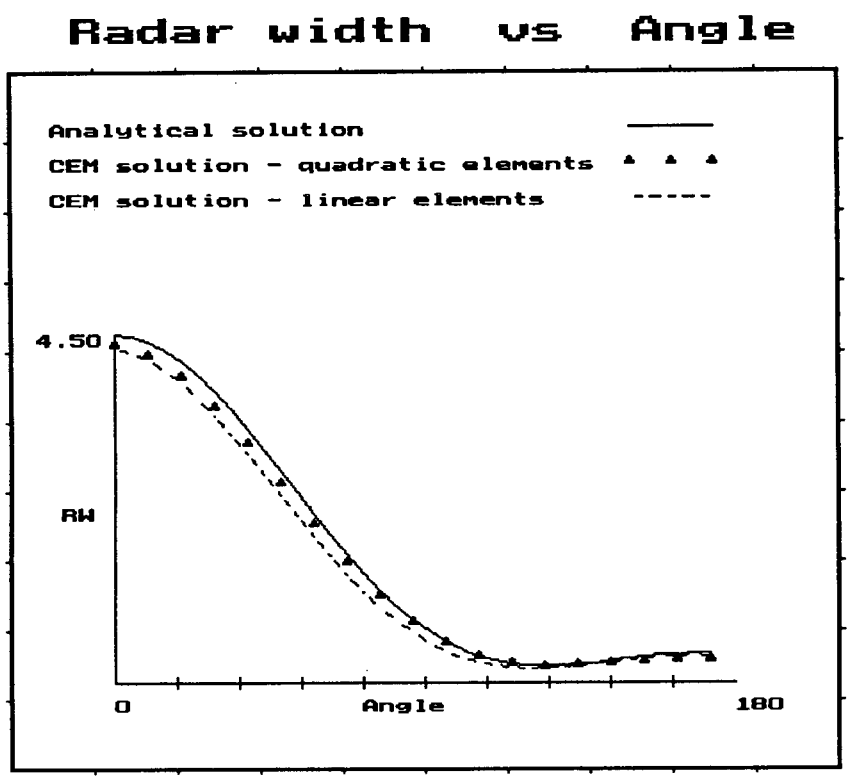

Although code implementing the near field computation for quadratic elements has not been developed, one can expect a much better approximation of these fields than

that experienced with first order elements. The curved nature of second order approximation functions should allow an accurate approximation of the curved fields near the scatterer. This, however, must still be validated.

6.5.2 Lossy, round homogeneous cylinder

The code developed implementing the quadratic element CEM can also handle lossy media. The imaginary parts of the complex relative permittivity and permeability must again be positive because of the time convention chosen. Fig-6.5 shows the triangulation of a round, homogeneous cylinder. Each triangular element now contains six nodes.

Figure-6.5 Triangulation of a round homogeneous cylinder for the quadratic element CEM. The radius of the homogeneous cylinder is 0.2 m. A total number of 161 quadratic elements was created resulting in 348 total nodes and 50 boundary nodes.

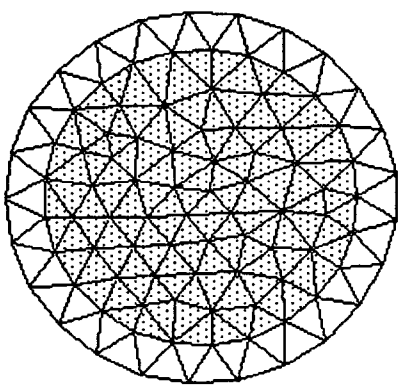

The radar width of a lossy, homogeneous cylinder using the triangulation of fig-6.5 is compared to the analytical solution (graph-6.2). The homogeneous cylinder in fig-6.5 is quite small compared to the free-space wavelength of the incident wave. The wavelength in the homogeneous cylinder is however much smaller than the

free-space wavelength due to the values chosen for the relative permittivity and permeability. It is evident that also the quadratic element CEM is acceptably accurate when scattering from lossy objects is approximated. The relatively high average normalized error is due to the very low back scattered radar width encountered at an angle of 180°.

Graph-6.2 Radar width of a round, lossy, homogeneous cylinder calculated using the quadratic element CEM and an analytical solution. Frequency: 200 MHz, polarization: TE, $\epsilon_r : 4 + j5$, $\mu_r : 2 + j4$.

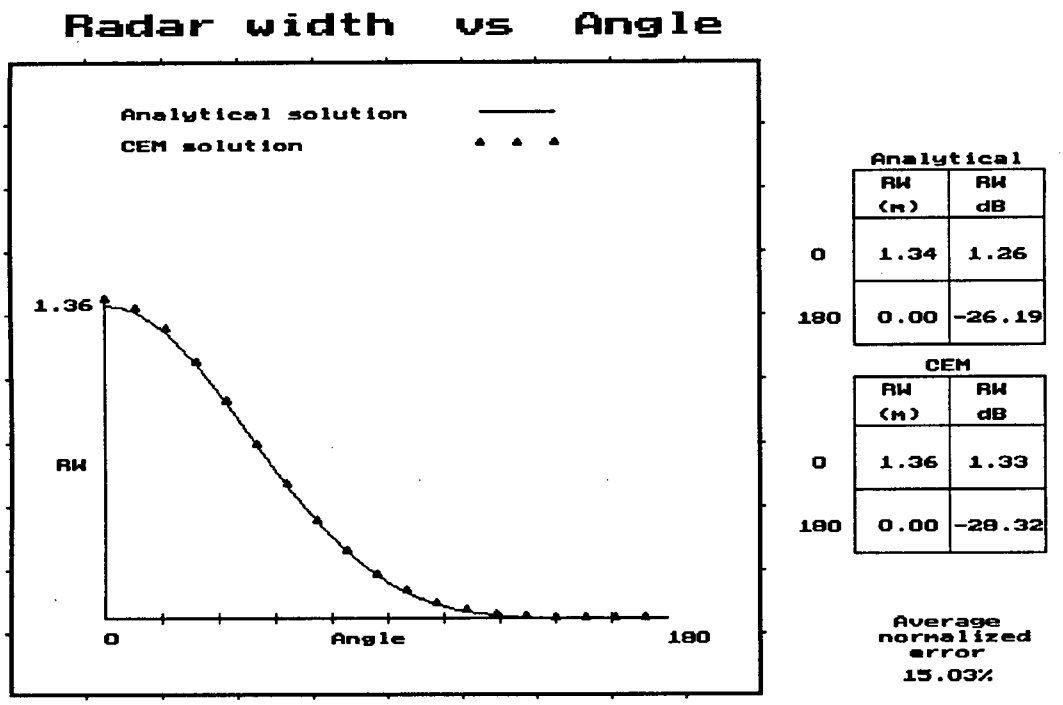

Analytical

	RW (m)	RW dB
0	1.34	1.26
180	0.00	-26.19

CEM

	RW (m)	RW dB
0	1.36	1.33
180	0.00	-28.32

Average normalized error 15.03%

7 ANALYTICAL SOLUTIONS FOR ROUND CYLINDERS

7.1 Introduction

The methods described so far enable one to obtain numerical approximations of the electromagnetic fields scattered by a possibly lossy, inhomogeneous object. The validation of the methods was checked by comparing approximated fields with exact analytically obtained fields. Scattering from round cylinders is one of the few problems for which an analytical solution can be obtained. Three round cylinder problems (two-dimensional) will be solved analytically in this chapter. Firstly, scattering from a round perfectly conducting (PC) cylinder of arbitrary radius (a). Secondly (see fig-7.1), scattering from a round PC cylinder (radius a) covered by a single, possibly lossy layer (outside radius b). Finally, scattering from a round, homogeneous, possibly lossy cylinder.

Figure-7.1 Round, coated PC cylinder. The radius of the PC cylinder is a, and the outer radius of the coated layer is b.

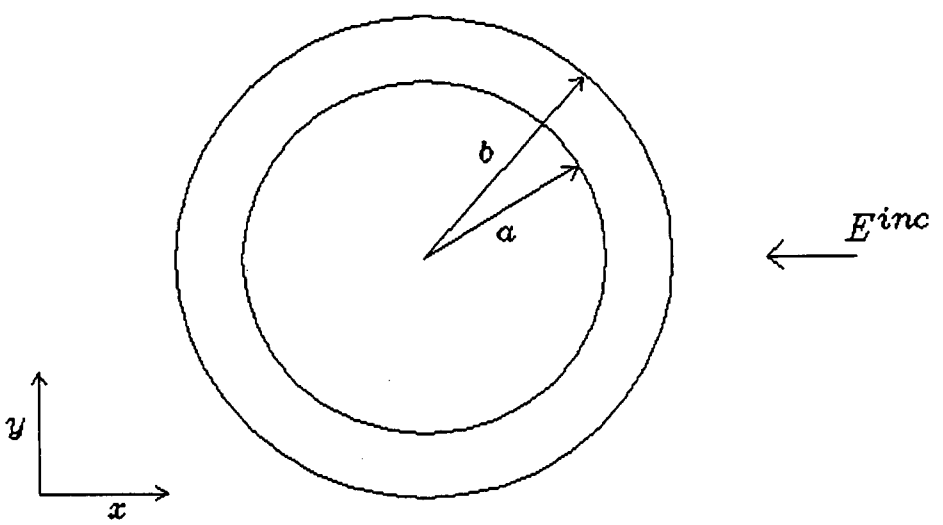

Comparing the solutions of these three kinds of problems to the approximated solutions using the CEM made it possible to evaluate the accuracy of the CEM. The Bessel function representation [9,p490], [11,p43] will be used to represent the electromagnetic fields in cylindrical coordinates.

It should be noted that a computer program implementing an analytical solution giving the back scattering radar width of the three kinds of scattering problems is available [15], but a need to compare the scattered fields in any direction made the development of this theory necessary. The material of which the homogeneous cylinder and layer covering the PC cylinder consists can have an arbitrary complex permeability, permittivity or chirality. The Bessel function representation consists of infinite summation series which fortunately converge quite rapidly if the size of the cylinder does not become too large compared to the wavelength of the incident field. The infinite series have to be approximated by finite series, but the errors are usually negligible because of the relatively rapid convergence.

7.2 Bessel function representation

Two different polarized incident waves can again be considered separately (TE and TM polarization). The incident as well as scattered fields (any polarization) in a region, can be written in terms of a superposition of cylindrical waves, satisfying the governing Helmholtz equations. This can be done using the so called wave transformation [9,p491]. These cylindrical waves are usually given in terms of the Bessel or Hankel functions. Only the TE-case will be considered in this chapter. The TM-case can be handled by using similar methods, with the TM cylindrical field representatives given in [11,p45]. It should be noted that the cylindrical waves, representing the fields, will be chosen to accommodate circular polarized waves that could arise from chiral media. The scattered fields as well as fields inside media, are thus represented by two components perpendicular to one another. A consequence of this is that the same field representatives can be used for both TE- and TM polarization [11,p46]. Only the incident fields will have different representatives for the two polarizations.

7.2.1 Incident field representation

Consider a transverse electric (TE) incident field

$$\overline{E}^{inc} = \hat{z} e^{jk_o x} \tag{7.01}$$

The direction of incidence is in the $\hat{x}$ direction. The incident electric and magnetic fields can be expressed in terms of cylindrical Bessel functions satisfying the Helmholtz equation [11,p43]

$$\overline{E}^{inc} = \sum_{n=-\infty}^{\infty} \left(\frac{j^n}{k_o} \right) \overline{N}_n^{(1)}(k_o r) \tag{7.02}$$

and

$$\overline{H}^{inc} = \left(\frac{k_o}{j\omega\mu_o} \right) \sum_{n=-\infty}^{\infty} \left(\frac{j^n}{k_o} \right) \overline{M}_n^{(1)}(k_o r) \tag{7.03}$$

The vector functions $\overline{N}_n$ and $\overline{M}_n$ are functions of the Bessel functions:

$$\overline{N}_n^{(1)}(k_o r) = \frac{1}{k_o} \nabla \times \nabla \times \{\hat{z} e^{jn\phi} J_n(k_o r)\} \tag{7.04}$$

$$\overline{M}_n^{(1)}(k_o r) = \nabla \times \{\hat{z} e^{jn\phi} J_n(k_o r)\} \tag{7.05}$$

J_n is the Bessel function of order n, and ϕ and r are cylindrical coordinates.

7.2.2 Scattered field representation

The scattered fields outside any scatterer can be written in terms of Hankel functions (outgoing waves) satisfying the Helmholtz wave equation [11,p44]:

$$\overline{E}^{sca} = -\sum_{n=-\infty}^{\infty} \left(\frac{j^n}{k_o} \right) \left\{ j c_n \overline{M}_n^{(3)}(k_o r) + b_n \overline{N}_n^{(3)}(k_o r) \right\} \tag{7.06}$$

and

$$\overline{H}^{sca} = \left(\frac{j k_o}{\omega\mu_o} \right) \sum_{n=-\infty}^{\infty} \left(\frac{j^n}{k_o} \right) \left\{ j c_n \overline{N}_n^{(3)}(k_o r) + b_n \overline{M}_n^{(3)}(k_o r) \right\} \tag{7.07}$$

with

$$N_n^{(3)}(k_o r) = \frac{1}{k_o} \nabla \times \nabla \times \{\hat{z} e^{jn\phi} H_n^{(1)}(k_o r)\} \tag{7.08}$$

and

$$M_n^{(3)}(k_o r) = \nabla \times \{\hat{z} e^{jn\phi} H_n^{(1)}(k_o r)\} \tag{7.09}$$

The unknown coefficients c_n and b_n have to be determined and $H_n^{(1)}$ are the Hankel function of the first kind order n.

7.2.3 Fields inside a medium

The fields inside a medium making up the scatterer or covering a PC cylinder can be represented using Bessel functions and Bohren's decomposition [11,p30]. The use of Bohren's decomposition is to represent the opposite circular polarized waves

present in a chiral medium. If the chirality factor β is zero, the usual TM or TE polarized waves are represented. With Bohren's decomposition, the electric field is given by

$$\overline{E}_{inside} = \overline{Q}_1 - j\sqrt{\frac{\mu}{\epsilon}}\overline{Q}_2 \tag{7.10}$$

and the magnetic field by

$$\overline{H}_{inside} = -j\sqrt{\frac{\epsilon}{\mu}}\overline{Q}_1 + \overline{Q}_2 \tag{7.11}$$

The vectors $\overline{Q}_1$ and $\overline{Q}_2$ can be represented by Bessel functions satisfying the Helmholtz equation inside the medium [11,p44],

$$\overline{Q}_1 = \sum_{n=-\infty}^{\infty}\left(\frac{j^n}{k_o}\right)g_n\left\{\overline{M}_n^{(1)}(\gamma_1 r) + \overline{N}_n^{(1)}(\gamma_1 r)\right\} \tag{7.12}$$

and

$$\overline{Q}_2 = \sum_{n=-\infty}^{\infty}\left(\frac{j^n}{k_o}\right)f_n\left\{\overline{M}_n^{(1)}(\gamma_2 r) - \overline{N}_n^{(1)}(\gamma_2 r)\right\} \tag{7.15}$$

The coefficients g_n and f_n have to be determined and γ_1 and γ_2 are the different wave numbers of the opposite circular polarized waves

$$\gamma_1 = \frac{k}{1 - k\beta} \tag{7.14}$$

and

$$\gamma_2 = \frac{k}{1 + k\beta} \tag{7.15}$$

with $k^2 = \epsilon_r \mu_r k_o^2$.

If a scatterer is present inside this medium (for instance a PC cylinder) there is also a scattering field in the medium. This scattered field can again be given using Bohren's decomposition together with a set of Hankel functions (outgoing waves) satisfying the Helmholtz equation

$$\overline{E}_{inside}^{sca} = -\overline{Q}_3 + j\sqrt{\frac{\mu}{\epsilon}}\overline{Q}_4 \tag{7.16}$$

and

$$\overline{H}_{inside}^{sca} = j\sqrt{\frac{\epsilon}{\mu}}\overline{Q}_3 - \overline{Q}_4 \tag{7.17}$$

with

$$\overline{Q}_3 = \sum_{n=-\infty}^{\infty} \left(\frac{j^n}{k_o}\right) o_n \left\{ \overline{M}_n^{(3)}(\gamma_1 r) + \overline{N}_n^{(3)}(\gamma_1 r) \right\} \tag{7.18}$$

and

$$\overline{Q}_4 = \sum_{n=-\infty}^{\infty} \left(\frac{j^n}{k_o}\right) p_n \left\{ \overline{M}_n^{(3)}(\gamma_2 r) - \overline{N}_n^{(3)}(\gamma_2 r) \right\} \tag{7.19}$$

7.3 Boundary conditions

The fields defined in sec 7.2 can be combined to give the total field in any region, inside or around a scatterer. The unknown coefficient values, necessary to obtain the field values, can be determined using the tangential boundary conditions.

7.3.1 Boundary conditions on a PC

The tangential boundary condition on a perfect conductor requires that the total tangential electric field on the conductor be zero [1,p146]. If the centre of a round PC cylinder is at the origin of the cylindrical coordinate system, and the PC cylinder has a radius a, the boundary conditions are met at r=a if

$$\overline{E}_{\tan}^{inc}(a) + \overline{E}_{\tan}^{sca}(a) = 0 \tag{7.20}$$

with $\overline{E}^{inc}$ given by (7.02) and $\overline{E}^{sca}$ given by (7.06).

7.3.2 Boundary conditions across different media

The boundary conditions across two mediums require that there be no discontinuities in the tangential electric and magnetic fields at the boundary of the two media. The boundary conditions at r=a, the radius of a round homogeneous cylinder, can thus be written as

$$\overline{E}_{inside_{\tan}}(a) = \overline{E}_{\tan}^{inc}(a) + \overline{E}_{\tan}^{sca}(a) \tag{7.21}$$

and

$$\overline{H}_{inside_{\tan}}(a) = \overline{H}_{\tan}^{inc}(a) + \overline{H}_{\tan}^{sca}(a) \tag{7.22}$$

The fields in (7.21) and (7.22) are again given by their representatives in sec 7.2. If a scatterer, consisting of a PC cylinder covered by a one layer medium (fig-7.1), is considered, two boundary conditions have to be met. On the PC cylinder with radius a, the total electric field must be zero at r=a

$$\overline{E}_{inside_{\tan}}(a) + \overline{E}^{sca}_{inside_{\tan}}(a) = 0 \qquad (7.23)$$

On the outer boundary of the one layer medium (r=b), there should be continuity of the electric and magnetic fields, thus

$$\overline{E}_{inside_{\tan}}(b) + \overline{E}^{sca}_{inside_{\tan}}(b) = \overline{E}^{inc}_{\tan}(b) + \overline{E}^{sca}_{\tan}(b) \qquad (7.24)$$

and

$$\overline{H}_{inside_{\tan}}(b) + \overline{H}^{sca}_{inside_{\tan\,\tan}}(b) = \overline{H}^{inc}_{\tan}(b) + \overline{H}^{sca}_{\tan}(b) \qquad (7.25)$$

7.4 Calculating the unknown coefficients

7.4.1 Homogeneous cylinder

By using the boundary conditions outlined in sec 7.3, the scattered fields as well as the fields inside a round homogeneous cylinder can be calculated. The scattered fields are given by (7.06) and the fields inside the cylinder by (7.10). The unknown coefficients c_n, b_n, f_n and g_n can be calculated using (7.21) and (7.22). In these equations, the radius is a given constant (a), and the only unknowns are the coefficients. The two boundary equations can be split into their $\hat{z}$, $\hat{\phi}$ and $\hat{r}$ components. This is done in appendix A7.1 (also done for the TM-case). This yields n sets of four independent equations which can be written in matrix form to solve and obtain the n sets of four unknown coefficients.

The matrix equations have to be solved for all values of n. The infinite series used to define the fields can however be approximated very accurately with a finite series. As $|n|$ increases, the Bessel and Hankel functions of order n tend to become negligibly small rather rapidly. This happens only if the arguments of the functions are not too large. The value of n, where the contribution of the Bessel and Hankel functions becomes negligibly small can be obtained by comparing their values to the values already calculated. It is thus only necessary to solve a finite number of matrix

equations to obtain a finite number of coefficients. These sets of four coefficients can then be substituted into (7.06) and (7.10), and the scattered as well as inside fields can be calculated using the approximated finite series.

7.4.2 Coated PC cylinder

Scattering from a round, PC is a special case of scattering from a round, coated PC cylinder with the coating being free-space. There will thus only be a discussion on obtaining the coefficients for a coated cylinder. The boundary conditions of sec 7.3 can again be used to obtain the unknown coefficients of (7.06), (7.10) and (7.16). The three boundary conditions equations (7.23), (7.24) and (7.25) are again split into their three components $\hat{z}$, $\hat{\phi}$ and $\hat{r}$ (appendix A7.2). This yields six linear independent equations which can be used in matrix form to obtain the unknown coefficients. With n, only a finite number, the fields can again be calculated very accurately. The fields inside the coating are calculated using the known coefficient values in (7.10) and (7.16). These fields are thus a superposition of the inside fields and the scattered, inside fields. The scattered fields outside the coated layer can be calculated using the finite set of coefficients in (7.06).

7.5 Radar width

With the coefficients calculated, the scattered fields of a homogeneous or coated PC cylinder can be obtained at any point outside the scatterer using (7.06). To obtain the radar width, the asymptotic expansions of the Hankel functions can be used. The definition of radar width is given in (4.31). By using the asymptotic expansion the radar width can be written as

$$\sigma(\phi) = \frac{4}{k_o}\left| \sum_{n=-\infty}^{\infty} e^{jn\phi}\{-c_n(\hat{x}\sin\phi - \hat{y}\cos\phi) + \hat{z}b_n\} \right|^2 \qquad (7.26)$$

(see appendix A7.3).

With the chirality factor zero, c_n will be zero and the scattered fields will thus be purely transverse electric.

7.6 Practical implementation

Computer code had to be developed to calculate the unknown coefficients, the values of the Bessel and Hankel functions as well as the final field values. Some of the algorithms used to implement the theory will now be discussed.

7.6.1 Matrix equation solution for obtaining the coefficients

The set of linear equations obtained through the boundary conditions (sec 7.4) can be written in matrix form (see appendix A7.1 and A7.2) as

$$\begin{bmatrix} A_{11}^n & A_{12}^n & A_{13}^n & A_{14}^n \\ A_{21}^n & A_{22}^n & A_{23}^n & A_{24}^n \\ A_{31}^n & A_{32}^n & A_{33}^n & A_{34}^n \\ A_{41}^n & A_{42}^n & A_{43}^n & A_{44}^n \end{bmatrix} \begin{bmatrix} c_n \\ b_n \\ g_n \\ f_n \end{bmatrix} = \begin{bmatrix} B_1^n \\ B_2^n \\ B_3^n \\ B_4^n \end{bmatrix} \tag{7.27}$$

for the homogeneous cylinder and

$$\begin{bmatrix} A_{11}^n & A_{12}^n & \cdot & \cdot & \cdot & A_{16}^n \\ A_{21}^n & A_{22}^n & \cdot & \cdot & \cdot & A_{26}^n \\ \cdot & \cdot & \cdot & \cdot & \cdot & \cdot \\ \cdot & \cdot & \cdot & \cdot & \cdot & \cdot \\ \cdot & \cdot & \cdot & \cdot & \cdot & \cdot \\ A_{61}^n & A_{62}^n & \cdot & \cdot & \cdot & A_{66}^n \end{bmatrix} \begin{bmatrix} c_n \\ b_n \\ g_n \\ f_n \\ o_n \\ p_n \end{bmatrix} = \begin{bmatrix} B_1^n \\ B_2^n \\ \cdot \\ \cdot \\ \cdot \\ B_6^n \end{bmatrix} \tag{7.28}$$

for the coated PC cylinder. These sets of matrix equations have to be solved for a finite number of n's. A LU-decomposition [6,p309] matrix solver is used and the coefficients obtained are stored in an array to be used later. Because the Bessel and Hankel functions have the characteristics that $J_n = -J_{-n}$ and $H_n^{(1)} = -H_{-n}^{(1)}$, it follows that $A_{ij}^n = -A_{ij}^{-n}$ and $B_i^n = -B_i^{-n}$ for all elements in (7.27) and (7.28). The reason for this is that every non-zero element is a function of either the Bessel or Hankel functions. This means that only the coefficients for $n \geq 0$ need to be calculated, because $c_n = c_{-n}$, $b_n = b_{-n}$. This is true for all coefficients.

7.6.2 Calculation of Bessel and Hankel function

Every element of (7.27) and (7.28) is calculated using either Bessel or Hankel functions. With the radius of a cylinder and frequency of the incident wave specified, the wave numbers and thus the arguments of the Bessel and Hankel functions are

known constants. The arguments can be complex if lossy media are considered. These functions are infinite series [10,137], but can be calculated accurately enough using finite series because of their convergence characteristics. For a specific argument value, a number of orders of the Bessel and Hankel functions are required. With two consecutive orders of the functions calculated (using the definition of the functions [10,p138]), the rest of the orders can be obtained by using the recurrence formulas which define a certain order functions in terms of the two orders just below (backward recurrence) or above (forward recurrence) [10,p137]. Backward recurrence should be performed when calculating the different orders of the imaginary parts of the Hankel functions to avoid numerical instabilities [16,p37].

7.6.3 Accuracy of code

Although the solutions of the scattering problems are analytical, the exact results are approximated due to the fact that for obvious practical reasons the infinite series encountered had to be approximated by finite series. With relatively small arguments used in the Bessel and Hankel functions, the series converge quite rapidly. The size of the cylinders compared to wavelength of the fields as well as the nature of the materials, determine the size of the arguments. The actual limits of argument size that would still ensure acceptable accuracies were not investigated. The calculated values for back scattering radar width at varies frequencies and for a number of materials were compared to the values obtained with an available package called Cylrad42 [15]. Table-7.1 and table-7.2 show some of the comparisons that were made. The results of the comparisons ensure that the code developed is very accurate in the scatterer size and frequency regions where the CEM code was validated. For improvement in convergence of the Bessel and Hankel functions, necessary with larger arguments, the Watson transformation method [9,p491] can be used.

Table-7.1 Back scattered radar width of a coated PC cylinder, calculated using the developed code and Cylrad42 code. The radius of the PC cylinder is 0.25 m and the coating thickness is 0.05 m. The material characteristics are $\epsilon_r = 2 + j2$ and $\mu_r = 3 + j2$.

Frequency (MHz)	Radar width TE polarization		Normalized difference (%)
	Developed code	Cylrad42	
100	0.5168	0.5161	0.136
200	0.2136	0.2134	0.094
500	0.0453	0.0452	0.221

Frequency (MHz)	Radar width TM polarization		Normalized difference (%)
	Developed code	Cylrad42	
100	0.5048	0.5051	0.059
200	0.1168	0.1161	0.602
500	0.0308	0.0307	0.325

Table-7.2 Back scattered radar width of a homogeneous cylinder, calculated using the developed code and Cylrad42 code. The radius of the cylinder is 0.25 m. The material characteristics are $\epsilon_r = 4$ and $\mu_r = 1$.

Frequency (MHz)	Radar width TE polarization		Normalized difference (%)
	Developed code	Cylrad42	
100	0.8375	0.8368	0.084
200	0.3927	0.3925	0.051
500	0.4527	0.4459	1.53

Frequency (MHz)	Radar width TM polarization		Normalized difference (%)
	Developed code	Cylrad42	
100	0.0982	0.0981	0.102
200	0.0223	0.0225	0.888
500	0.7542	0.7573	0.409

8 CONCLUSION

The CEM investigated and implemented in this thesis, enables one to obtain an approximated numerical solution for general (possibly lossy, inhomogeneous, arbitrarily shaped) two-dimensional electromagnetic scattering problems. The solutions were compared to analytical solutions for a few canonical problems. The far-field results obtained, indicate that the CEM is a reliable method for predicting scattering from general penetrable structures. The code developed can, however, not handle structures much larger than a wavelength. For larger structures, the results obtained are unacceptable. The main reason for this is the limited memory available on the personal computer used to run the code. The maximum number of unknowns was limited to approximately 350. Larger memory capabilities would enable one to create more triangular elements, resulting in acceptable accuracies when larger structures are considered. This would however lead to unacceptable computational times for solving the problems. The necessity will thus arise to use faster computers to avoid this problem. It should be noted that some of the pre-processing procedures also take on impractical computational time proportions as the number of unknowns increases. The use of parallel computing would enable one to overcome these difficulties to an extent. Parallel algorithms for some of the algorithms used in the code, have already been developed. With parallel CEM code one can expect to be able to handle structures of a few wavelengths long.

The near field results were less accurate than the far-field results, especially in the finite element regions. It seems that an even higher number of unknowns is required to approximate the near field values accurately. The development of a quadratic element code, approximating the fields in the finite element region, has not been completed. These second order finite elements would probably approximate the near fields more accurately. Their curved nature is much more suitable for approximating these electromagnetic fields. This must, however, still be validated.

The analytical solutions for scattering from round cylinders were developed mainly to validate the CEM. The code developed for the analytical solutions is limited to cylinders with radii of less than a wavelength. This limitation is due to the slower convergence of the Bessel and Hankel functions as their arguments increase. More refined coding and the use of existing methods to improve the convergence rates of these functions, would extend the limits on the size of the cylinders.

The development of the CEM for scattering from chiral materials was a natural extension of the CEM for non-chiral materials. The results obtained for scattering from chiral media, using the CEM, compared reasonably well with the analytical solutions obtained. Larger memory facilities need to be used to enable one to comment on the correctness, accuracy and efficiency of the CEM applied to chiral media scattering. Numerical solutions for scattering problems involving chiral media will however be investigated further.

The numerical methods discussed in this thesis concerns scattering from general two-dimensional structures. Real world problems are, however, three-dimensional. The two-dimensional solutions can, in some important special cases, be used to approximate three-dimensional solutions. This is not true for most problems, and many real world problems are still unsolved. The extension of the CEM, to handle three-dimensional problems, is theoretically possible. The complexity of the theory and its implementation can be expected to increase immensely. The memory and computational speed requirements would probably be very high due to huge matrix equations originating from a three-dimensional finite element region. The rapid improvement in computational hardware could result in the feasibility of the development of such code.

The field of computational electromagnetics is still growing rapidly, and the tools available are improving day by day. It has enabled the solution of a number of unsolved electromagnetic problems and will probably continue to do so in future.

REFERENCES

[1] S. Ramo, J.R. Whinnery, T. Van Duzer, **Field and Waves in Communication Electronics**, second edition. New York: John While & Sons, 1984.

[2] J. D'Angelo, "Finite element/Boundary element Analysis of Electromagnetic Fields," **AP-S Workshop on Differential Equation-Based Finite Methods**, IEEE AP-S Symposium, Syracuse, New-York, June 1988.

[3] K.L. Wu, G.Y. Delisle, D.G. Fang and M. Lecours, "Coupled Finite Element and Boundary Element Scattering," **Finite Element and Finite Difference Methods in Electromagnetic Scattering, PIER 2**, pp. 113-132. New York: Elsevier Science Publishing Co., 1990.

[4] C.A. Brebbia, S. Walker, **Boundary Element Techniques in Engineering**. London: Butterworth & Co. (Publishers) Ltd., 1980.

[5] C.A. Brebbia, **The Boundary Element Method for Engineers**. London: Pentech Press, 1980.

[6] P.P. Silvester, R.L. Ferrari, **Finite Elements for Electrical Engineers**, second edition. Cambridge: Cambridge University Press, 1990.

[7] O.C. Zienkiewicz, **The Finite Element Method**, third edition. London: McGraw-Hill, 1977.

[8] R.F. Harrington, **Field Computation by Moment Methods**. Malabar,FL: Robert E. Krieger Publishing Company, 1982.

[9] J.A. Kong, **Electromagnetic Wave Theory**. New York: John Wiley & sons, 1986.

[10] M.R. Spiegel, **Mathematical Handbook of Formulas and Tables**. New York: McGraw-Hill, 1968.

[11] A. Lakhtakia, V.K. Varadan, V.V. Varadan, "Time-Harmonic Electromagnetic Fields in Chiral Media," **Lecture Notes in Physics, 335**. Berlin: Springer-Verlag, 1989.

[12] E. Kreyszig, **Advanced Engineering Mathematics**, fifth edition. New York: John Wiley & Sons, 1983.

[13] J.C. Cavendish, "Automatic Triangulation of Arbitrary Planar Domains for the Finite Element Method," **International Journal for Numerical Methods in Engineering**, Vol. 8, pp. 679-696, 1974.

[14] W.E. Boyse, A.A. Seidl, "A Hybrid Finite Element Method for Conductors with Thin Dense Coatings," **Applied Computational Electromagnetics Society**, Vol. 4, No. 2, pp. 59-72, 1989.

[15] C.F du Toit, **Cylrad42 computer package**, 1988.

[16] C.F du Toit, **The Three-dimensional far-fields of antennas from probe corrected cylindrical near-field measurements**. Thesis for the degree M.Ing., University of Stellenbosch, 1986.

[17] G.M. Testa, **μ-Wave Radar User's Manual**, Version 3.0. ANSOFT Corporation, 1987.

[18] J.H. Cloete, C.F. du Toit, "Backscattering by an infinitely long cylinder with lossy multilayer coatings", paper presented at **SAIEE 2nd Joint AP-MTT Symposium**, Pretoria, August 1988, pp 22.1-22.13 of the proceedings.

[19] E.K. Miller, "A Selective Survey of Computational Electromagnetics," **IEEE Trans. Antennas Propagat.** Vol. 36, No. 9, pp. 1281-1305, 1988.

[20] J.F. Lee, Z.J. Cendes, "The Transfinite Element Method for Computing Electromagnetic Scattering from Arbitrary Lossy Cylinders," **IEEE Trans. Antennas Propagat.** Vol. AP30, No.5, pp. 99-102, 1987.

[21] S.K. Chang, K.K. Mei, "Application of the Unimoment Method to Electromagnetic Scattering of Dielectric Cylinders," **IEEE Trans. Antennas Propagat.** Vol. AP-24, pp. 35-42, January 1976.

[22] M.A. Morgan, "Principles of Finite Methods in Electromagnetic Scattering," **Finite Element and Finite Difference Methods in Electromagnetic Scattering, PIER 2**, pp. 1-68. New York: Elsevier Science Publishing Co., 1990.

[23] M.S. Kluskens, E.H. Newman, "Scattering by a Chiral Cylinder of Arbitry Cross Section," **IEEE Trans. Antennas Propagat.** Vol. 38, No. 9 pp. 1448-1455, 1990.

[24] D.B. Davidson, F.J.C. Meyer, "Finite element solutions of general two-dimensional electromagnetic scattering problems", paper presented at **SAIEE Joint AP-MTT Symposium**, Somerset West, August 1990, pp 267-274 of the proceedings.

APPENDIX A

Mathematical Deductions

Appendix A3
Coupled Element Method

A3.1 FEM matrix formulation

The discretised weak formulation

$$\sum_{j=1}^{o} \epsilon_j \int_{\Omega_{1j}} \nabla U \cdot \nabla W \, d\Omega_{1j} - \sum_{j=1}^{p} \epsilon_j \int_{B_j} W \frac{du}{dn} dB_j = 0 \qquad (A3.1.01)$$

can be written in matrix form using the approximation functions

$$U = \sum_{i=1}^{3} \xi_i u_i \qquad (A3.1.02)$$

$$W = \sum_{i=1}^{3} \xi_i \qquad (A3.1.03)$$

and

$$\frac{dU}{dn} = \sum_{i=1}^{2} \xi_i \frac{du_i}{dn} \qquad (A3.1.04)$$

Substituting these functions in (A3.1.01) yields

$$\sum_{j=1}^{o} \epsilon_j \int_{\Omega_{1j}} \left(\nabla \sum_{i=1}^{3} \xi_i u_i \right) \cdot \left(\nabla \sum_{k=1}^{3} \xi_k \right) d\Omega_{1j}$$

$$- \sum_{j=1}^{p} \epsilon_j \int_{B_j} \left(\sum_{i=1}^{2} \xi_i \right) \left(\sum_{k=1}^{2} \xi_k \frac{du_k}{dn} \right) dB_j = 0 \qquad (A3.1.05)$$

By extracting the summations out of the integrals (A3.1.05) becomes

$$\sum_{j=1}^{o} \epsilon_j \sum_{i=1}^{3} \sum_{k=1}^{3} \int_{\Omega_{1j}} (\nabla \xi_i \cdot \nabla \xi_k) u_i \, d\Omega_{1j}$$

$$- \sum_{j=1}^{p} \epsilon_j \sum_{i=1}^{2} \sum_{k=1}^{2} \int_{B_j} (\xi_i \xi_k) \frac{du_k}{dn} dB_j = 0 \qquad (A3.1.06)$$

With $[S_j]$ a 3x3 matrix

$$S_j^{ik} = \epsilon_j \sum_{i=1}^{3} \sum_{k=1}^{3} \int_{\Omega_{1j}} \nabla \xi_i . \nabla \xi_k \, d\Omega_{1j} \qquad (A3.1.07)$$

and $[T_j]$ a 2x2 matrix

$$T_j^{ik} = \epsilon_j \sum_{i=1}^{2} \sum_{k=1}^{2} \int_{B_j} \xi_i \xi_k \, dB_j \qquad (A3.1.08)$$

(A3.1.06) can be written as

$$\sum_{j=1}^{o} [S_j][u_j] - \sum_{j=1}^{p} [T_j]\left[\frac{du_j}{dn}\right] = 0 \qquad (A3.1.09)$$

In (A3.1.09)

$$[u_j] = \begin{bmatrix} u_1 \\ u_2 \\ u_3 \end{bmatrix} \qquad (A3.1.10)$$

and

$$\left[\frac{du_j}{dn}\right] = \begin{bmatrix} \frac{du_1}{dn} \\ \frac{du_2}{dn} \end{bmatrix} \qquad (A3.1.11)$$

(A 3.1.09) consists of a number of $[S_j]$ and $[T_j]$ matrices each associated with one specific element. Connecting these elements to form the global region corresponds to adding these matrices whenever their nodes coincide with each other [6,p31]. (A3.1.09) written in global form, after connecting all elements yields

$$[S][u] - [T]\left[\frac{du_b}{dn}\right] = 0 \qquad (A3.1.12)$$

A3.2 Integration over the delta function

Integration over the delta function has the following property:

$$\int_{\Omega} f \delta_o \, d\Omega = f_o \qquad (A3.2.01)$$

With (3.27) written as

$$\nabla^2 W = -\delta_o \qquad (A3.2.02)$$

and substituted into (3.26) yields

$$-\int_{\Omega_{ex}} \delta_o U \, d\Omega_{ex} - \int_B U \frac{dW}{dn} dB + \int_B \frac{dU}{dn} W \, dB = 0 \qquad (A3.2.03)$$

Using (A3.2.01), (A3.2.03) becomes

$$U_o = -\int_B U\frac{dW}{dn}dB + \int_B \frac{dU}{dn}W\,dB \qquad (A3.2.04)$$

A3.3 Observation point on boundary

The boundary equation (3.29) or (A3.2.04) is written in a form where the observation point o lies in the region under consideration. To be able to solve the boundary equation, this observation point must be taken to the boundary itself. This can be done by following the same procedure as was done for the three-dimensional case described in [4,p30]. The problem is, however, altered because the two-dimensional problem is considered.

Consider the observation point lying on a half-circle around a boundary point i (fig-A3.3.1).

Figure-A3.3.1 Taking the observation point to the boundary.

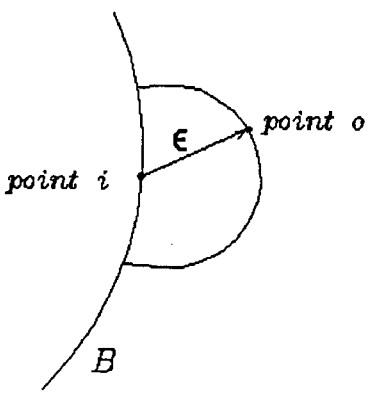

The radius of the half-circle is ϵ. Consider the first integral in (A3.2.04). The integral can be written as

$$\int_B u\frac{dW}{dn}dB = \int_{B-B_\epsilon} u\frac{dW}{dn}dB + \int_{B_\epsilon} u\frac{dW}{dn}dB \qquad (A3.3.01)$$

With

$$\frac{dW}{dr} = \frac{d}{dr}\left(\frac{1}{2\pi}\ln\left(\frac{1}{r}\right)\right)$$

$$= \frac{1}{2\pi}\ \frac{d}{dr}\left(\ln\left(\frac{1}{r}\right)\right)$$

$$= \frac{r}{2\pi}\ \frac{d}{dr}\left(\frac{1}{r}\right)$$

$$= \frac{r}{2\pi}\ \left(-\frac{1}{r^2}\right)$$

$$= -\frac{1}{2\pi r} \qquad (A3.3.02)$$

the integral over the B_ϵ

becomes

$$\int_{B_\epsilon} u\frac{dW}{dn}dB_\epsilon = \int_{B_\epsilon} u\left(-\frac{1}{2\pi\epsilon}\right)dB_\epsilon$$

$$= -\int_{B_\epsilon} u\left(\frac{1}{2\pi\epsilon}\right)dB_\epsilon \qquad (A3.3.03)$$

Taking the limit of $\epsilon \to 0$ and thus $u \to u_i$, and knowing the length of the half-circle ($\pi\epsilon$), (A3.3.03) can be written as

$$\lim_{\epsilon\to 0}\left(-\int_{B_\epsilon} u\frac{1}{2\pi\epsilon}dB_\epsilon\right) = \lim_{\epsilon\to 0}\left(-u\frac{1}{2\pi\epsilon}\int_{B_\epsilon} dB_\epsilon\right)$$

$$= \lim_{\epsilon\to 0}\left(-u\frac{1}{2\pi\epsilon}\pi\epsilon\right)$$

$$= \lim_{\epsilon\to 0}\left(-\frac{1}{2}u\right)$$

$$= \left(-\frac{1}{2}u_i\right) \qquad (A3.3.04)$$

Doing exactly the same with the second integral in (3.29) yields zero.
With $\epsilon \to 0$ and $B_\epsilon \to 0$,

$$\int_B u \frac{dW}{dn} dB$$

can thus be written as

$$\int_B u \frac{dW}{dn} dB - \frac{1}{2} u_i$$

when i lies on the boundary. Substituting this into (3.29) yields (3.30).

It should be noted that the boundary must be smooth around the point i to ensure that the part of a circle constructed around i becomes a half-circle in the limit. For accuracy the boundary elements should thus be constructed to create a boundary which is as smooth as possible.

A3.4 BEM matrix formulation

Substituting (3.19) into (3.31) gives

$$\frac{1}{2} U_o = -\sum_{j=1}^{n} \int_{B_j} \left(\sum_{i=1}^{2} \phi_i u_i \right) \frac{dW}{dn} dB_j + \sum_{j=1}^{n} \int_{B_j} \left(\sum_{i=1}^{2} \phi_i \frac{du_i}{dn} \right) W dB_j$$

$$= -\sum_{j=1}^{n} \sum_{i=1}^{2} \int_{B_j} \phi_i u_i \frac{dW}{dn} dB_j + \sum_{j=1}^{n} \sum_{i=1}^{2} \int_{B_j} \phi_i \frac{du_i}{dn} W dB_j \qquad (A3.4.01)$$

The matrix equation can be obtained by taking the observation point o to all the nodes on the boundary, thus

$$\frac{1}{2} U_o = -\sum_{j=1}^{n} \sum_{i=1}^{2} \int_{B_j} \phi_i u_i \frac{dW}{dn} dB_j + \sum_{j=1}^{n} \sum_{i=1}^{2} \int_{B_j} \phi_i \frac{du_i}{dn} W dB_j \qquad o = 1 \, to \, n$$

$$(A3.4.02)$$

This equation can be written in matrix form (3.32) with the right hand side incorporated into the global matrix [H] whenever o is equal to j (the diagonal of [H]).

A3.5 Transformation to homogeneous coordinates

Consider a specific boundary element in the global x-y coordinate system (fig-A3.5.1). It is evident that

$$dB_j = \sqrt{(dx_j)^2 + (dy_j)^2}$$

$$= \sqrt{\left(\frac{dx_j}{d\xi}\right)^2 + \left(\frac{dy_j}{d\xi}\right)^2}\, d\xi \qquad (A3.5.01)$$

Figure-A3.5.1 Coordinate transformation.

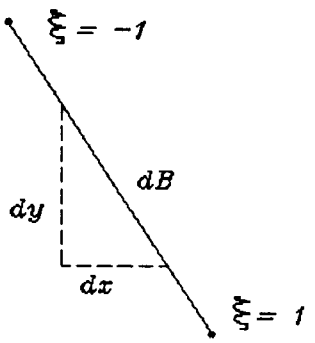

A transformation from the global x-y system to the local homogeneous coordinate system using (A3.5.01) gives the first integral in (3.31) with (3.19) substituted into it as

$$\sum_{i=1}^{2} \int_{B_j} \phi_i \frac{dW}{dn} dB_j = \sum_{i=1}^{2} \int_{-1}^{1} \phi_i \frac{dW}{dn} J\, d\xi \qquad (A3.5.02)$$

In this equation

$$J = \sqrt{\left(\frac{dx}{d\xi}\right)^2 + \left(\frac{dy}{d\xi}\right)^2} \qquad (A3.5.03)$$

Using (3.20),(3.21),(3.22) and (3.23) yields

$$\frac{dx}{d\xi} = \frac{d}{d\xi}(\phi_1 x_1 + \phi_2 x_2)$$

$$= \frac{d}{d\xi}\left(\frac{1}{2}(1-\xi)x_1 + \frac{1}{2}(1+\xi)x_2\right)$$

$$= -\frac{1}{2}x_1 + \frac{1}{2}x_2 \qquad (A3.5.04)$$

and in a similar manner $\frac{dy}{d\xi}$ can be derived as

$$\frac{dy}{d\xi} == -\frac{1}{2}y_1 + \frac{1}{2}y_2 \qquad (A3.5.05)$$

This means

$$J = \sqrt{\frac{1}{4}(x_2 - x_1)^2 + \frac{1}{4}(y_2 - y_1)^2} \qquad (A3.5.06)$$

A3.6 The normal derivative of Green's function

With

$$r = |\vec{r}_o - \vec{r}_s| \qquad (A3.6.01)$$

(3.28) becomes

$$W = \frac{1}{2\pi}\ln\left(\frac{1}{r}\right) \qquad (A3.6.02)$$

The derivative of W with respect to r are given by (A3.3.02) as

$$\frac{dW}{dr} = -\frac{1}{2\pi r} \qquad (A3.6.03)$$

The normal derivative, however, is the derivative in the direction of the normal on the boundary element under consideration. Therefore

$$\frac{dW}{dn} = \hat{r} \cdot \hat{n}\frac{dW}{dr}$$

$$= -\hat{r} \cdot \frac{\hat{n}}{2\pi r} \qquad (A3.6.04)$$

A3.7 Avoiding the singularity while determining the [G] matrix

When obtaining the elements of the [G] matrix in the BEM, the observation point might lie on the element to be integrated over. The argument of the natural logarithm can become zero, and a singularity occurs. This singularity can be avoided by logarithmic Gaussian integration (3.38), but the integral must be written in the correct form. Starting with (3.37) one would like to obtain the form of the left hand side of (3.38). By using (3.28), (3.37) becomes

$$G'^{j}_{i} = \int_{-1}^{1} \phi_j \frac{1}{2\pi} \ln\left(\frac{1}{r}\right) J\, d\xi \qquad (A3.7.01)$$

With the observation point on the one side of the boundary element and the source point somewhere on the same element, r is given by

$$r = \phi_2 R_{el} \qquad (A3.7.02)$$

with R_{el} the length of the boundary element. This means

$$\begin{aligned} G'^{j}_{i} &= \int_{-1}^{1} \phi_j \frac{1}{2\pi} \ln\left(\frac{1}{\phi_2 R_{el}}\right) J\, d\xi \\ &= \frac{J}{2\pi} \int_{-1}^{1} \phi_j \left\{ \ln\left(\frac{1}{\phi_2}\right) + \ln\left(\frac{1}{R_{el}}\right) \right\} d\xi \\ &= \frac{J}{2\pi} \left\{ \ln\left(\frac{1}{R_{el}}\right) \int_{-1}^{1} \phi_j d\xi + \int_{-1}^{1} \phi_j \ln\left(\frac{1}{\phi_2}\right) d\xi \right\} \end{aligned} \qquad (A3.7.03)$$

Consider only the second integral. Set

$$\begin{aligned} \eta &= \phi_2 \\ &= \frac{1}{2}(1 + \xi) \end{aligned} \qquad (A3.7.04)$$

which gives

$$\xi = 2\eta - 1 \qquad (A3.7.05)$$

and

$$\frac{d\xi}{d\eta} = 2 \qquad (A3.7.06)$$

Substituting the previous three equations into the second integral of (A3.7.03) gives

$$\int_{-1}^{1} \phi_j(\xi) \ln\left(\frac{1}{\phi_2}\right) d\xi = 2 \int_{0}^{1} \ln\left(\frac{1}{\eta}\right) \phi_j(\eta) d\eta \qquad (A3.7.07)$$

with

$$\phi_j(\eta) = \frac{1}{2}\{1 + (-1)^j(2\eta - 1)\} \qquad (A3.7.08)$$

Using (A3.7.07), (A3.7.03) can be written as

$$G'^{j}_{i} = \frac{J}{2\pi}\left\{ \ln\left(\frac{1}{R_{el}}\right) \int_{-1}^{1} \phi_j d\xi + 2 \int_{0}^{1} \phi_j(\eta) \ln\left(\frac{1}{\eta}\right) d\eta \right\} \qquad (A3.7.09)$$

The first integral can be calculated using normal four point Gaussian integration while the second integral has the form of (3.38) and this logarithmic integration formula can thus be used.

A3.8 Potential between parallel plates

Obtaining the analytical solution of the potential between two parallel plates requires the solution of Laplace's equation in one dimension. Consider two perfectly conducting parallel plates a certain distance, a, apart. The potential at the top plate (y=a) is set to 1 Volt. The potential at the bottom plate (y=0) is 0 Volt. The one-dimensional, homogeneous Laplace equation

$$\frac{d^2\Phi}{dy^2} = 0 \qquad (A3.8.01)$$

governs between the plates, because there is no variation in the x or z directions. Integration on both sides yields

$$\frac{d\Phi}{dy} = C_1 \qquad (A3.8.02)$$

Integrating again gives

$$\Phi = C_1 y + C_2 \qquad (A3.8.03)$$

With $\Phi = 0$ at y=0, $C_2 = 0$ and with $\Phi = 1$ at y=a gives $C_1 = \frac{1}{a}$.

Thus

$$\Phi = \frac{1}{a} y \qquad (A3.8.04)$$

which is the analytical solution of the potential between the two parallel plates. It should be noted that fringing was neglected.

Appendix A4
Helmholtz equation solution

A4.1 Inhomogeneous Helmholtz equation

Maxwell's source-free equations in phasor form is [9,p60]

$$\nabla \times \overline{E} = j\omega\mu\overline{H} \qquad (A4.1.1)$$

and

$$\nabla \times \overline{H} = -j\omega\epsilon\overline{E} \qquad (A4.1.2)$$

(a time convention of $e^{-j\omega t}$ is used). Combining the (A4.1.1) and (A4.1.2) yields

$$\nabla \times \frac{1}{j\omega\mu}\nabla \times \overline{E} + j\omega\epsilon\overline{E} = 0 \qquad (A4.1.3)$$

or

$$\nabla \times \frac{1}{j\omega\epsilon}\nabla \times \overline{H} + j\omega\mu\overline{H} = 0 \qquad (A4.1.4)$$

Consider (A4.1.3). If the vector $\overline{E}$ has only a z-component in the cartesian coordinate system, (A4.1.3) can be written as

$$\nabla \times \frac{1}{j\omega\mu}\left(\hat{x}\frac{\delta E_z}{\delta y} - \hat{y}\frac{\delta E_z}{\delta x}\right) + j\omega\epsilon E_z = 0 \qquad (A4.1.5)$$

using the definition of the curl of a vector ($\nabla \times \overline{E}$) given by [10,p120] with no variation in the z direction. Defining

$$U'_x = \frac{1}{j\omega\mu}\frac{\delta E_z}{\delta y} \qquad (A4.1.6)$$

and

$$U'_y = -\frac{1}{j\omega\mu}\frac{\delta E_z}{\delta x} \qquad (A4.1.7)$$

(A4.1.5) becomes

$$\nabla \times (\hat{x}U'_x + \hat{y}U'_y + j\omega\epsilon E_z = 0 \qquad (A4.1.8)$$

Using the curl definition again yields

$$\hat{z}\left(-\frac{\delta U'_x}{\delta y} + \frac{\delta U'_y}{\delta_x}\right) + \hat{z}j\omega\epsilon E_z = 0 \qquad (A4.1.9)$$

Substituting (A4.1.6) and (A4.1.7) back into (A4.1.9) gives

$$\hat{z}\left(-\frac{\delta}{\delta y}\frac{1}{j\omega\mu}\frac{\delta E_z}{\delta y}-\frac{\delta}{\delta x}\frac{1}{j\omega\mu}\frac{\delta E_z}{\delta x}\right)+j\omega\epsilon\hat{z}E_z=0 \qquad (A4.1.10)$$

or

$$-\nabla\frac{1}{j\omega\mu}\nabla E_z+j\omega\epsilon E_z=0 \qquad (A4.1.11)$$

with the gradient ($\nabla\overline{E}$) of a vector defined in [10,p119] and no variation in the z direction. By multiplying all terms with the constant term $j\omega\mu_o$, (A4.1.11) becomes

$$\nabla\frac{1}{\mu_r}\nabla E_z+k_o^2\epsilon_r E_z=0 \qquad (A4.1.12)$$

the so-called scalar Helmholtz equation for TE polarization. The constant k_0 is the free-space wave number ($k_o^2=\epsilon_o\mu_o\omega^2$). The scalar Helmholtz equation for TM polarization can be obtained in a similar manner starting with (A4.1.4) giving

$$\nabla\frac{1}{\epsilon_r}\nabla H_z+k_o^2\mu_r H_z=0 \qquad (A4.1.13)$$

A4.2 Normal derivative of incident field

The incident field is given as [9,p490]

$$U_{inc}=U_o e^{-jk(r\hat{r}\cdot\hat{n}_{inc})} \qquad (A4.2.1)$$

The normal derivative is equal to the derivative with respect to the cylindrical coordinate r but in the direction of the normal. Mathematically this is given by

$$\frac{\delta U^{inc}}{\delta n'}=\frac{\delta U^{inc}}{\delta r}\hat{r}\cdot\hat{n}'$$

$$=\frac{\delta}{\delta r}\left(U_o e^{-jk_o(r\hat{r}\cdot\hat{n}_{inc})}\right)\hat{r}\cdot\hat{n}'$$

$$=-jk_o\hat{r}\cdot\hat{r}\cdot\hat{n}'\cdot\hat{n}_{inc}U_o e^{-jk_o(r\hat{r}\cdot\hat{n}_{inc})}$$

$$=-jk_o\hat{n}'\cdot\hat{n}_{inc}U_{inc} \qquad (A4.2.2)$$

with $\hat{n}'$ the unit vector in the direction of the normal on the boundary (B).

A4.3 Integration by parts

Consider the integral over a domain Ω_{in}

$$\int_{\Omega_{in}} \nabla p(x,y) \nabla U_z W \, d\Omega_{in} \qquad (A4.3.1)$$

or

$$\int_{\Omega_{in}} \left(\frac{\delta}{\delta x} p(x,y) \frac{\delta U_z}{\delta x} + \frac{\delta}{\delta y} p(x,y) \frac{\delta U_z}{\delta y} \right) W \, d\Omega_{in} \qquad (A4.3.2)$$

This integral can be integrated by parts using the following equation [7,p766],[6,p335]

$$\int_{\Omega_{in}} \left(\frac{\delta^2 U_z}{\delta x^2} + \frac{\delta^2 U_z}{\delta y^2} \right) W \, d\Omega_{in}$$

$$= - \int_{\Omega_{in}} \left(\frac{\delta W}{\delta x} \frac{\delta U_z}{\delta x} + \frac{\delta W}{\delta y} \frac{\delta U_z}{\delta y} \right) d\Omega_{in} + \int_B W \frac{dU_z}{dn} dB \qquad (A4.3.3)$$

This, applied to (A4.3.2) yields

$$\int_{\Omega_{in}} \left(\frac{\delta}{\delta x} p(x,y) \frac{\delta U_z}{\delta x} + \frac{\delta}{\delta y} p(x,y) \frac{\delta U_z}{\delta y} \right) W \, d\Omega_{in}$$

$$= - \int_{\Omega_{in}} \left(\frac{\delta W}{\delta x} p(x,y) \frac{\delta U_z}{\delta x} + \frac{\delta W}{\delta y} p(x,y) \frac{\delta U_z}{\delta y} \right) d\Omega_{in}$$

$$+ \int_B W \, p(x,y) \frac{dU_z}{dn} dB \qquad (A4.3.4)$$

or

$$\int_{\Omega_{in}} \nabla p(x,y) \nabla U_z \, d\Omega_{in}$$

$$= - \int_{\Omega_{in}} \nabla W \, p(x,y) \nabla U_z \, d\Omega_{in} + \int_B W \, p(x,y) \frac{\delta U_z}{\delta n} dB \qquad (A4.3.5)$$

A4.4 Normal derivative of Helmholtz Green's function

The normal derivative of (4.21) is equal to the derivative with respect to r (variable of the cylindrical coordinate system) in the direction of the normal on the boundary (B)

$$\frac{\delta W}{\delta n'} = \frac{\delta W}{\delta r}\hat{r}\cdot\hat{n}'$$

$$= \frac{\delta}{\delta r}\left(\frac{j}{4}H_0^{(1)}(k_o r)\right)\hat{r}\cdot\hat{n}' \qquad (A4.4.1)$$

The derivative of the zeroth order Hankel function can be obtained using

$$\frac{\delta}{\delta r}(J_0(r)) = -J_1(r) \qquad (A4.4.2)$$

and

$$\frac{\delta}{\delta r}(Y_0(r)) = -Y_1(r) \qquad (A4.4.3)$$

[10,p137] where J_0 and J_1 are Bessel functions of the first kind and zeroth and first order, and Yo and Y1 are Bessel functions of the second kind, zeroth and first order. With

$$H_n^{(1)}(r) = J_n(r) + jY_n(r) \qquad (A4.4.4)$$

[10,p138] and using (A4.4.2) and (A4.4.3),

$$\frac{\delta W}{\delta n'} = \frac{-jk_o}{4}H_0^{(1)}(k_o r)\hat{r}\cdot\hat{n}' \qquad (A4.4.5)$$

A4.5 Analytical integration avoiding singularity in Hankel function

Consider the following integral that has to be determined,

$$G'^{i} = \sum_{i=1}^{2}\int_{-1}^{1}\phi_i W J\, d\xi \qquad (A4.5.1)$$

The integral consists of J, a constant with a value as given in (3.34) and

$$W = \frac{j}{4} H_o^{(1)}(k_o |\vec{r}_o - \vec{r}_s|)$$

$$= \frac{j}{4} H_o^{(1)}(k_o r) \qquad (A4.5.2)$$

with r_0 the observation point and r_s the source point on the boundary element. The functions approximating the fields are

$$\phi_1 = \frac{1}{2}(1 - \xi) \qquad (A4.5.3)$$

$$\phi_2 = \frac{1}{2}(\xi + 1) \qquad (A4.5.4)$$

(A4.5.1) consists of a singularity if the observation point lies on the element to be integrated over. The variable r in (A4.5.2) can then be written in terms of ξ as

$$r = R_{el}\frac{1}{2}(1 + \xi) \qquad (A4.5.5)$$

with R_{el} the length of the element. It can be seen from (A4.5.5) that r becomes zero when $\xi = -1$ (the side of the element where the observation point (r_0) lies). The argument of the Hankel function thus becomes zero causing the singularity. The integral can, however, be solved analytically as follows:

$$G'^{i} = \sum_{i=1}^{2} \int_{-1}^{1} \phi_i W J d\xi$$

$$= \sum_{i=1}^{2} J \int_{-1}^{1} \phi_i \frac{j}{4} H_o^{(1)}(k_o r) d\xi$$

$$= \sum_{i=1}^{2} \frac{jJ}{4} \int_{-1}^{1} \phi_i \{J_o(k_o r) + jY_o(k_o r)\} d\xi$$

$$= \sum_{i=1}^{2} \frac{jJ}{4} \left\{ \int_{-1}^{1} \phi_i J_o(k_o r) d\xi + j \int_{-1}^{1} \phi_i Y_o(k_o r) d\xi \right\} \qquad (A4.5.6)$$

The second integral on the right hand side (RHS) of (A4.5.6) contains the singularity. Consider only this integral and use the definition of the Bessel function of the second kind [10,p137]

$$\int_{-1}^{1} \phi_i Y_o(k_o r)d\xi = \int_{-1}^{1} \phi_i \frac{2}{\pi}\ln\left(\frac{k_o r}{2}\right)J_o(k_o r)d\xi + \int_{-1}^{1} \phi_i \frac{2\gamma}{\pi}J_o(k_o r)d\xi$$

$$+ \int_{-1}^{1} \phi_i \frac{2}{\pi}\sum_{k=0}^{\infty}(-1)^{k+1}\left\{\frac{\left(\frac{k_o r}{2}\right)^{2k}}{(k!)^2}\right\}\sum_{p=1}^{k}\left(\frac{1}{p}\right)d\xi \qquad (A4.5.7)$$

where $\gamma = 0.5772156...$ is Euler's constant. The first integral on the RHS of (A4.5.7) contains the singularity and both other integrals can be calculated numerically without any problems. Consider only the integral with the singularity and define

$$x = \frac{1}{2}(1 + \xi)$$

$$\therefore \frac{dx}{d\xi} = \frac{1}{2}$$

$$\xi = 2x - 1$$

and

$$d\xi = 2dx$$

Thus $r = R_{el}x$ which yields

$$\int_{-1}^{1} \phi_i \ln\left(\frac{k_o r}{2}\right)J_o(k_o r)d\xi$$

$$= \int_{-1}^{1} \phi_i \ln\left(\frac{k_o R_{el} x}{2}\right)J_o(k_o r)d\xi$$

$$= \int_{-1}^{1} \phi_i \left\{\ln\left(\frac{k_o R_{el}}{2}\right) + \ln(x)\right\}J_o(k_o r)d\xi$$

$$= \int_{-1}^{1} \phi_i \ln\left(\frac{k_o R_{el}}{2}\right)J_o(k_o r)d\xi + 2\int_{0}^{1} \phi_i \ln(x)J_o(k_o R_{el}x)dx$$

$$(A4.5.8)$$

Again only the second integral on the RHS contains the singularity.

Consider the following integral of which the second integral on the RHS of (A4.5.8) is a type

$$\int_0^1 x^P \ln(x) J_o(k_o R_{el} x) dx$$

It can be solved analytically:

$$\int_0^1 x^P \ln(x) J_o(k_o R_{el} x) dx$$

$$= \int_0^1 x^P \ln(x) \sum_{k=0}^{\infty} \frac{(-1)^k \left(\frac{k_o R_{el} x}{2}\right)^{2k}}{(k!)^2} dx$$

$$= \int_0^1 \ln(x) x^P \sum_{k=0}^{\infty} \frac{(-1)^k \left(\frac{k_o R_{el}}{2}\right)^{2k}}{(k!)^2} x^{2k} dx$$

$$= \sum_{k=0}^{\infty} \frac{(-1)^k \left(\frac{k_o R_{el}}{2}\right)^{2k}}{(k!)^2} \int_0^1 \ln(x) x^{2k+P} dx \qquad (A4.5.9)$$

with

$$\int_0^1 \ln(x) x^{2k+P} dx = \frac{(-1)}{(2k+p)^2} \qquad (A4.5.10)$$

[10,p99]. Define a function

$$f'(arg, p) = \sum_{k=0}^{\infty} \frac{(-1)^k \left(\frac{arg}{2}\right)^{2k}}{(k!)^2} \left\{ \frac{(-1)}{(2k+p)^2} \right\} \qquad (A4.5.11)$$

Using (A4.5.9), (A4.5.10) and (A4.5.11) one kan write

$$\int_0^1 x^P \ln(x) J_o(k_o R_{el} x) dx = f'(k_o R_{el}, p) \qquad (A4.5.12)$$

Consider $i = 1$ and $i = 2$ separately in the second integral on the RHS of (A4.5.8)

$i = 1$:

$$\phi_1(\xi) = \frac{1}{2}(1 - \xi)$$

$$\therefore \phi_1(x) = \frac{1}{2}(1 - 2x + 1)$$

$$= -x + 1$$

thus

$$\int_0^1 (-x + 1)\ln(x) J_o(k_o R_{el} x)dx$$

$$= -f'(k_o R_{el}, 1) + f'(k_o R_{el}, 0) \qquad (A4.5.13)$$

$i = 2$:

$$\phi_1(\xi) = \frac{1}{2}(\xi + 1)$$

$$\therefore \phi_1(x) = \frac{1}{2}(2x + 1 + 1)$$

$$= x + 1$$

thus

$$\int_0^1 (x + 1)\ln(x) J_o(k_o R_{el} x)dx$$

$$= f'(k_o R_{el}, 1) + f'(k_o R_{el}, 0) \qquad (A4.5.14)$$

By back substituting every integral that was considered separately, the total integral can be written as

$$G'^{,i} = \sum_{i=1}^{2} \frac{jJ}{4}\{\int_{-1}^{1} \phi_i J_o(k_o r)d\xi + \frac{j2}{\pi}[\gamma \int_{-1}^{1} \phi_i J_o(k_o r)d\xi$$

$$+ \int_{-1}^{1} \phi_i \sum_{k=0}^{\infty} (-1)^{k+1} \left(\frac{\left(\frac{k_o r}{2}\right)^{2k}}{(k!)^2} \right) \sum_{p=1}^{k} \left(\frac{1}{p} \right) d\xi + \ln\left(\frac{k_o R_{el}}{2} \right) \int_{-1}^{1} \phi_i J_o(k_o r)d\xi$$

$$+2\{A_i f'(k_o R_{el}, 1) + B_i f'(k_o R_{el}, 0)\}]\} \qquad (A4.5.15)$$

with $A_1 = -1$, $A_2 = 1$ and $B_1 = 1$, $B_2 = 1$. All remaining integrals can be calculated numerically using Gaussian integration. The function f' consists of an infinite series which converges and can thus be approximated by a finite series. The infinite series in the third integral in (A4.5.15) also converges and can also be approximated by a finite series.

A4.6 Far-field approximations

Consider fig-A4.6.1. If the point p is a large distance from the origin of the coordinate system and the scatterer close to the origin, the function W can be approximated by using the asymptotic expansion functions of the Hankel functions [1,p369] which gives

$$H_o^{(1)}(k_o r) = \sqrt{\frac{2}{\pi k_o r}} e^{j\left(k_o r - \frac{\pi}{4}\right)} \qquad (A4.6.1)$$

Applying the far-field assumptions [1,p587], (A4.6.1) can be approximated as

Figure-A4.6.1 Far-field approximations [1,p587].

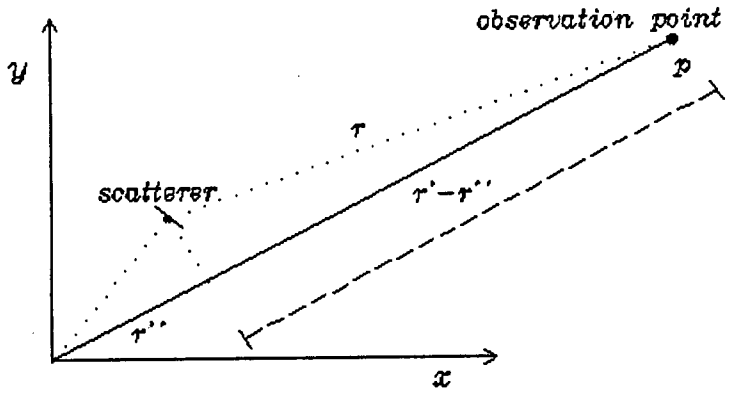

$$H_o^{(1)}(k_o r) \approx \sqrt{\frac{2}{\pi k_o r}} e^{j\left(k_o r' - \frac{\pi}{4}\right)} \qquad (A4.6.2)$$

When calculating the radar width of a scatterer one is only interested in the absolute value of the scattered field. The relative phase is thus sufficient and r' can be replaced by r". This yields

$$H_o^{(1)}(k_o r) \approx \sqrt{\frac{2}{\pi k_o r}} e^{j(k_o r'')} \qquad (A4.6.3)$$

and W can thus be approximated (with relative phase) as

$$W = \frac{j}{4} H_o^{(1)}(k_o r)$$

$$\approx \frac{j}{4}\sqrt{\frac{2}{\pi k_o r}} e^{j k_o r''} \qquad (A4.6.4)$$

The normal derivative of W can be calculated by first calculating the derivative of the asymptotic form of $H_o^{(1)}(k_o r)$ with respect to r giving

$$\frac{\delta}{\delta r}\{H_0^{(1)}(k_o r)\} = \frac{\delta}{\delta r}\left(\sqrt{\frac{2}{\pi k_o r}}e^{j\left(k_o r-\frac{\pi}{4}\right)}\right)$$

$$= \frac{\delta}{\delta r}\left(\sqrt{\frac{2}{\pi k_o r}}\right).e^{j\left(k_o r-\frac{\pi}{4}\right)} + \sqrt{\frac{2}{\pi k_o r}}\frac{\delta}{\delta r}\left(e^{j\left(k_o r-\frac{\pi}{4}\right)}\right)$$

$$= -\sqrt{\frac{1}{\pi k_o r}})\left(\frac{1}{r}\right).e^{j\left(k_o r-\frac{\pi}{4}\right)} + jk_o\sqrt{\frac{2}{\pi k_o r}}e^{j\left(k_o r-\frac{\pi}{4}\right)}$$

(A4.6.5)

The amplitude term $\frac{1}{r^{3/2}}$ is negligible in comparison with the $\frac{1}{r^{1/2}}$ term because of the far-field approximations. This yields

$$\frac{\delta}{\delta r}\{H_0^{(1)}(k_o r)\} = jk_o\sqrt{\frac{2}{\pi k_o r}}e^{j\left(k_o r-\frac{\pi}{4}\right)} \qquad (A4.6.6)$$

and using the same far-field assumptions as were used with W, gives

$$\frac{\delta}{\delta r}\{H_0^{(1)}(k_o r)\} = jk_o\sqrt{\frac{2}{\pi k_o r}}e^{j(k_o r'')} \qquad (A4.6.7)$$

with relative phase shift. The derivative of W with respect to r is thus

$$\frac{\delta W}{\delta r} = -\frac{k_o}{4}\sqrt{\frac{2}{\pi k_o r}}e^{j(k_o r'')} \qquad (A4.6.8)$$

and in the normal direction

$$\frac{\delta W}{\delta n} = \hat{n}' \cdot \hat{r}\,\delta\frac{W}{\delta r}$$

$$= -\hat{n}' \cdot \hat{r}\frac{k_o}{4}\sqrt{\frac{2}{\pi k_o r}}e^{j(k_o r'')} \qquad (A4.6.9)$$

A4.7 A chiral Helmholtz equation

A Helmholtz type equation incorporating chirality can be derived using the newly defined constitutive relations (4.34) and (4.35) together with Maxwell's equations [9,p60]. Substituting Maxwell's equations

$$\nabla \times \overline{E} = j\omega\overline{B} \qquad (A4.7.1)$$

and

$$\nabla \times \overline{H} = -j\omega\overline{D} \qquad (A4.7.2)$$

into (4.34) and (4.35) yields

$$\overline{D} = \epsilon\overline{E} + j\omega\epsilon\beta\overline{B} \qquad (A4.7.3)$$

and

$$\overline{B} = \mu\overline{H} - j\omega\mu\beta\overline{D} \qquad (A4.7.4)$$

Substituting (A4.7.4) into (A4.7.3) gives

$$\overline{D} = \epsilon\overline{E} + j\omega\epsilon\beta(\mu\overline{H} - j\omega\mu\beta\overline{D})$$

$$\therefore \overline{D} = \epsilon\overline{E} + j\omega\epsilon\mu\beta\overline{H} + \omega^2\epsilon\mu\beta^2\overline{D}$$

$$\therefore \overline{D} - \omega^2\epsilon\mu\beta^2\overline{D} = \epsilon\overline{E} + j\omega\epsilon\mu\beta\overline{H}$$

$$\therefore (1 - \omega^2\epsilon\mu\beta^2)\overline{D} = \epsilon\overline{E} + j\omega\epsilon\mu\beta\overline{H}$$

$$\therefore \overline{D} = \frac{\epsilon}{(1 - \omega^2\epsilon\mu\beta^2)}\overline{E} + \frac{j\omega\epsilon\mu\beta}{(1 - \omega^2\epsilon\mu\beta^2)}\overline{H}$$

$$\therefore \overline{D} = \frac{\epsilon}{\tau_1}\overline{E} + \frac{j\omega\epsilon\mu\beta}{\tau_1}\overline{H} \qquad (A4.7.5)$$

with

$$\tau_1 = 1 - \epsilon\mu\omega^2\beta^2$$

$$= 1 - \epsilon_r\mu_r k_o^2\beta^2 \qquad (A4.7.6)$$

In (A4.7.6) k_o is the free-space wave constant. By substituting (A4.7.3) into (A4.7.4) and manipulating in a similar manner as in (A4.7.5) one obtains

$$\overline{B} = \frac{\mu}{(1 - \epsilon\mu\omega^2\beta^2)}\overline{H} - \frac{j\epsilon\mu\omega\beta}{(1 - \epsilon\mu\omega^2\beta^2)}\overline{E}$$

$$\therefore \overline{B} = \frac{\mu}{\tau_1}\overline{H} - \frac{j\epsilon\mu\omega\beta}{\tau_1}\overline{E} \qquad (A4.7.7)$$

Using (A4.7.7) and (A4.7.5) in (A4.7.1) and (A4.7.2) respectively gives

$$\nabla \times \overline{E} = j\omega\left(\frac{\mu}{\tau_1}\overline{H} - \frac{j\epsilon\mu\omega\beta}{\tau_1}\overline{E}\right)$$

$$\therefore \nabla \times \overline{E} = \frac{j\omega\mu}{\tau_1}\overline{H} + \frac{\epsilon\mu\omega^2\beta}{\tau_1}\overline{E} \qquad (A4.7.8)$$

and

$$\nabla \times \overline{H} = -j\omega\left(\frac{\epsilon}{\tau_1}\overline{E} + \frac{j\epsilon\mu\omega\beta}{\tau_1}\overline{H}\right)$$

$$\therefore \nabla \times \overline{H} = -\frac{j\omega\epsilon}{\tau_1}\overline{E} + \frac{\epsilon\mu\omega^2\beta}{\tau_1}\overline{H} \qquad (A4.7.9)$$

Two scalar chiral Helmholtz equations can be derived. Firstly the Helmholtz equation is developed where the Laplacian of the electric field E_Z is given in terms of E_Z and H_Z. From (A4.7.8) it follows that

$$\overline{H} = \frac{\nabla \times \overline{E} - \frac{\epsilon\mu\omega^2\beta}{\tau_1}\overline{E}}{\frac{j\omega\mu}{\tau_1}}$$

$$\therefore \overline{H} = \tau_1 \frac{\nabla \times \overline{E}}{j\omega\mu} - \frac{\epsilon\mu\omega^2\beta}{j\omega\mu}\overline{E} \qquad (A4.7.10)$$

Substituting (A4.7.10) in the left hand side of (A4.7.9) yields

$$\nabla \times \left(\tau_1 \frac{\nabla \times \overline{E}}{j\omega\mu} - \frac{\epsilon\mu\omega^2\beta}{j\omega\mu}\overline{E}\right) = -\frac{j\omega\epsilon}{\tau_1}\overline{E} + \frac{\epsilon\mu\omega^2\beta}{\tau_1}\overline{H}$$

$$\therefore \nabla \times \left(\tau_1 \frac{\nabla \times \overline{E}}{j\omega\mu}\right) - \nabla \times \left(\frac{\epsilon\mu\omega^2\beta}{j\omega\mu}\overline{E}\right) = -\frac{j\omega\epsilon}{\tau_1}\overline{E} + \frac{\epsilon\mu\omega^2\beta}{\tau_1}\overline{H} \qquad (A4.7.11)$$

Multiplying with the constant value $j\omega\mu_o$ on both sides of (A4.7.11) gives

$$\nabla \times \left(\tau_1 \frac{\nabla \times \overline{E}}{\mu_r}\right) - \nabla \times \left(\frac{\epsilon\mu\omega^2\beta}{\mu_r}\overline{E}\right) = \frac{\epsilon_r k_o^2}{\tau_1}\overline{E} + \frac{j\epsilon_r k_o^2 \mu\omega\beta}{\tau_1}\overline{H}$$

$$\therefore \nabla \times \left(\tau_1 \frac{\nabla \times \overline{E}}{\mu_r}\right) - \nabla \times \left(\frac{\epsilon\mu\omega^2\beta}{\mu_r}\overline{E}\right) - \frac{\epsilon_r k_o^2}{\tau_1}\overline{E} - \frac{j\epsilon_r k_o^2 \mu\omega\beta}{\tau_1}\overline{H} = 0 \qquad (A4.7.12)$$

With the assumption made that there will be no spatial variation in ϵ_r, μ_r and β in any triangular element of the global region, (A4.7.12) becomes

$$\nabla \times \left(\tau_1 \frac{\nabla \times \overline{E}}{\mu_r}\right) - \frac{\epsilon\mu\omega^2\beta}{\mu_r}\nabla \times \overline{E} - \frac{\epsilon_r k_o^2}{\tau_1}\overline{E} - \frac{j\epsilon_r k_o^2 \mu\omega\beta}{\tau_1}\overline{H} = 0 \qquad (A4.7.13)$$

Substituting (A4.7.8) in the second term of (A4.7.13) gives

$$\nabla\times\left(\tau_1\frac{\nabla\times\overline{E}}{\mu_r}\right)-\frac{\epsilon\mu\omega^2\beta}{\mu_r}\left(\frac{j\omega\mu}{\tau_1}\overline{H}+\frac{\epsilon\mu\omega^2\beta}{\tau_1}\overline{E}\right)-\frac{\epsilon_r k_o^2}{\tau_1}\overline{E}-\frac{j\epsilon_r k_o^2\mu\omega\beta}{\tau_1}\overline{H}=0$$

$$\therefore\nabla\times\left(\tau_1\frac{\nabla\times\overline{E}}{\mu_r}\right)-\frac{j\omega\epsilon\mu^2\omega^2\beta}{\tau_1\mu_r}\overline{H}-\frac{(\epsilon\mu\omega^2\beta)^2}{\tau_1\mu_r}\overline{E}-\frac{\epsilon_r k_o^2}{\tau_1}\overline{E}-\frac{j\epsilon_r k_o^2\mu\omega\beta}{\tau_1}\overline{H}=0$$

$$\therefore\nabla\times\left(\tau_1\frac{\nabla\times\overline{E}}{\mu_r}\right)-\left\{\frac{(\epsilon_r\mu_r k_o^2\beta)^2+\epsilon_r\mu_r k_o^2}{\tau_1\mu_r}\right\}\overline{E}-\frac{2j\epsilon_r\mu_r k_o^2\mu\omega\beta}{\tau_1\mu_r}\overline{H}=0$$

$$\therefore\nabla\times\left(\tau_1\frac{\nabla\times\overline{E}}{\mu_r}\right)-\tau_2\overline{E}-\tau_3\overline{H}=0 \qquad (A4.7.14)$$

with

$$\tau_2=\left\{\frac{(\epsilon_r\mu_r k_o^2\beta)^2+\epsilon_r\mu_r k_o^2}{\tau_1\mu_r}\right\}$$

$$=\epsilon_r k_o^2\frac{(1+\epsilon_r\mu_r k_o^2\beta^2)}{((1-\epsilon_r\mu_r k_o^2\beta^2)} \qquad (A4.7.15)$$

and

$$\tau_3=\frac{2j\epsilon_r\mu_r k_o^2\mu\omega\beta}{\tau_1\mu_r}$$

$$=\frac{2j\epsilon_r k_o^2\mu\omega\beta}{(1-\epsilon_r\mu_r k_o^2\beta^2)} \qquad (A4.7.16)$$

Consider only the first term in (A4.7.14). The field vector $\overline{E}$ in the chiral medium can have the following components

$$\overline{E}=\hat{z}E_z+\hat{y}E_y+\hat{x}E_x \qquad (A4.7.17)$$

The cross-product [10,p120] of the field vector, with no variation in the z-direction (2-dimensional problem), is

$$\nabla\times\overline{E}=\hat{x}\frac{\delta E_z}{\delta y}+\hat{y}\left(-\frac{\delta E_z}{\delta x}\right)+\hat{z}\left(\frac{\delta E_y}{\delta x}-\frac{\delta E_x}{\delta y}\right) \qquad (A4.7.18)$$

The first term in (A4.7.14) thus becomes

$$\nabla\times\left\{\tau_1\frac{\nabla\times\overline{E}}{\mu_r}\right\}$$

$$=\nabla\times\left\{\frac{\tau_1}{\mu_r}\hat{x}\frac{\delta E_z}{\delta y}+\frac{\tau_1}{\mu_r}\hat{y}\left(-\frac{\delta E_z}{\delta x}\right)+\frac{\tau_1}{\mu_r}\hat{z}\left(\frac{\delta E_y}{\delta x}-\frac{\delta E_x}{\delta y}\right)\right\}$$

$$=\hat{x}\frac{\delta}{\delta y}\left\{\frac{\tau_1}{\mu_r}\left(\frac{\delta E_y}{\delta x}-\frac{\delta E_x}{\delta y}\right)\right\}-\hat{y}\frac{\delta}{\delta x}\left\{\frac{\tau_1}{\mu_r}\left(\frac{\delta E_y}{\delta x}-\frac{\delta E_x}{\delta y}\right)\right\}$$

$$+\hat{z}\frac{\delta}{\delta x}\left\{\frac{\tau_1}{\mu_r}\left(-\frac{\delta E_z}{\delta x}\right)\right\}-\hat{z}\frac{\delta}{\delta y}\left\{\frac{\tau_1}{\mu_r}\left(\frac{\delta E_z}{\delta y}\right)\right\} \qquad (A4.7.19)$$

The $\hat{z}$ component of (A4.7.19) can be written as

$$\hat{z}\frac{\delta}{\delta x}\left\{\frac{\tau_1}{\mu_r}\left(-\frac{\delta E_z}{\delta x}\right)\right\}-\hat{z}\frac{\delta}{\delta y}\left\{\frac{\tau_1}{\mu_r}\left(\frac{\delta E_z}{\delta y}\right)\right\}=-\nabla\frac{\tau_1}{\mu_r}\nabla E_z \qquad (A4.7.20)$$

This follows from the definition of the ∇ operator [10,p119]. Considering only the $\hat{z}$ components of equation (A4.7.14), thus substituting (A4.7.20) in the first term of (A4.7.14), the scalar Helmholtz equation can be obtained as

$$\nabla\left(\frac{\tau_1}{\mu_r}\nabla E_z\right)+\tau_2 E_z+\tau_3 H_z=0 \qquad (A4.7.21)$$

The second scalar chiral Helmholtz equation is obtained in a similar manner but it gives the Laplacian of the magnetic field H_z in terms of H_z and E_z. From (A4.7.9) it follows that

$$\overline{E}=\frac{-\nabla\times\overline{H}+\frac{\epsilon\mu\omega^2\beta}{\tau_1}\overline{H}}{\frac{j\omega\epsilon}{\tau_1}}$$

$$\therefore\overline{E}=-\tau_1\frac{\nabla\times\overline{H}}{j\omega\epsilon}+\frac{\epsilon\mu\omega^2\beta}{j\omega\epsilon}\overline{H} \qquad (A4.7.22)$$

Substituting (A4.7.22) in the left hand side of (A4.7.8) yields

$$\nabla\times\left(-\tau_1\frac{\nabla\times\overline{H}}{j\omega\epsilon}+\frac{\epsilon\mu\omega^2\beta}{j\omega\epsilon}\overline{H}\right)=\frac{j\omega\mu}{\tau_1}\overline{H}+\frac{\epsilon\mu\omega^2\beta}{\tau_1}\overline{E}$$

$$\therefore-\nabla\times\left(\tau_1\frac{\nabla\times\overline{H}}{j\omega\epsilon}\right)+\nabla\times\left(\frac{\epsilon\mu\omega^2\beta}{j\omega\epsilon}\overline{H}\right)=\frac{j\omega\mu}{\tau_1}\overline{H}+\frac{\epsilon\mu\omega^2\beta}{\tau_1}\overline{E} \qquad (A4.7.23)$$

Multiplying with the constant $j\omega\epsilon_o$ on both sides of (A4.7.23) gives

$$-\nabla\times\left(\tau_1\frac{\nabla\times\overline{H}}{\epsilon_r}\right)+\nabla\times\left(\frac{\epsilon\mu\omega^2\beta}{\epsilon_r}\overline{H}\right)=-\frac{\mu_r k_o^2}{\tau_1}\overline{H}+\frac{j\mu_r k_o^2\epsilon\omega\beta}{\tau_1}\overline{E}$$

$$\therefore -\nabla\times\left(\tau_1\frac{\nabla\times\overline{H}}{\epsilon_r}\right)+\nabla\times\left(\frac{\epsilon\mu\omega^2\beta}{\epsilon_r}\overline{H}\right)+\frac{\mu_r k_o^2}{\tau_1}\overline{H}-\frac{j\mu_r k_o^2\epsilon\omega\beta}{\tau_1}\overline{E}=0$$

(A4.7.24)

With the same assumption made that there will be no spatial variation in ϵ_r, μ_r and β in any triangular element of the global region, (A4.7.24) becomes

$$-\nabla\times\left(\tau_1\frac{\nabla\times\overline{H}}{\epsilon_r}\right)+\frac{\epsilon\mu\omega^2\beta}{\epsilon_r}\nabla\times\overline{H}+\frac{\mu_r k_o^2}{\tau_1}\overline{H}-\frac{j\mu_r k_o^2\epsilon\omega\beta}{\tau_1}\overline{E}=0 \quad (A4.7.25)$$

Substituting the (A4.7.9) in the second term of (A4.7.25) gives

$$-\nabla\times\left(\tau_1\frac{\nabla\times\overline{H}}{\epsilon_r}\right)+\frac{\epsilon\mu\omega^2\beta}{\epsilon_r}\left(-\frac{j\omega\epsilon}{\tau_1}\overline{E}+\frac{\epsilon\mu\omega^2\beta}{\tau_1}\overline{H}\right)+\frac{\mu_r k_o^2}{\tau_1}\overline{H}-\frac{j\mu_r k_o^2\epsilon\omega\beta}{\tau_1}\overline{E}=0$$

$$\therefore -\nabla\times\left(\tau_1\frac{\nabla\times\overline{H}}{\epsilon_r}\right)-\frac{j\omega\mu\epsilon^2\omega^2\beta}{\tau_1\epsilon_r}\overline{E}+\frac{(\epsilon\mu\omega^2\beta)^2}{\tau_1\epsilon_r}\overline{H}+\frac{\mu_r k_o^2}{\tau_1}\overline{H}-\frac{j\mu_r k_o^2\epsilon\omega\beta}{\tau_1}\overline{E}=0$$

$$\therefore -\nabla\times\left(\tau_1\frac{\nabla\times\overline{H}}{\epsilon_r}\right)+\left\{\frac{(\epsilon_r\mu_r k_o^2\beta)^2+\epsilon_r\mu_r k_o^2}{\tau_1\epsilon_r}\right\}\overline{H}-\frac{2j\epsilon_r\mu_r k_o^2\epsilon\omega\beta}{\tau_1\epsilon_r}\overline{E}=0$$

$$\therefore -\nabla\times\left(\tau_1\frac{\nabla\times\overline{H}}{\epsilon_r}\right)+\tau'_2\overline{H}-\tau'_3\overline{E}=0 \quad (A4.7.26)$$

with

$$\tau'_2=\left\{\frac{(\epsilon_r\mu_r k_o^2\beta)^2+\epsilon_r\mu_r k_o^2}{\tau_1\epsilon_r}\right\}$$

$$=\mu_r k_o^2\frac{(1+\epsilon_r\mu_r k_o^2\beta^2)}{(1-\epsilon_r\mu_r k_o^2\beta^2)} \quad (A4.7.27)$$

and

$$\tau'_3=\frac{2j\epsilon_r\mu_r k_o^2\epsilon\omega\beta}{\tau_1\epsilon_r}$$

$$=\frac{2j\mu_r k_o^2\epsilon\omega\beta}{(1-\epsilon_r\mu_r k_o^2\beta^2)} \quad (A4.7.28)$$

The scalar form of (A4.7.26) can be obtained by following the same procedures used to obtain the scalar form of (A4.7.14). Only the $\hat{z}$ components of (A4.7.26) are thus used to obtain the following scalar chiral Helmholtz equation

$$\nabla\left(\frac{\tau_1}{\epsilon_r}\nabla H_z\right)+\tau'_2 H_z-\tau'_3 E_z=0 \qquad (A4.7.29)$$

A4.8 Matrix form of chiral Helmholtz equation

The two chiral Helmholtz equations in appendix A4.7, (A4.7.21) and (A4.7.29) can be used as the governing equations in a region consisting of chiral media. The field values E_z and H_z can be approximated linearly in the region by E'_z and H'_z giving

$$\nabla\frac{\tau_1}{\mu_r}\nabla E'_z+\tau_2 E'_z+\tau_3 H'_z\neq 0=error \qquad (A4.8.1)$$

and

$$\nabla\frac{\tau_1}{\epsilon_r}\nabla H'_z+\tau'_2 H'_z-\tau'_3 E'_z\neq 0=error \qquad (A4.8.2)$$

These errors can be distributed and minimized in an average sense by weighting it over the region and setting this weighted approximation equal to zero giving

$$\int_{\Omega_{in}}\left(\nabla\frac{\tau_1}{\mu_r}\nabla E'_z+\tau_2 E'_z+\tau_3 H'_z\right)W\,d\Omega_{in}=0 \qquad (A4.8.3)$$

and

$$\int_{\Omega_{in}}\left(\nabla\frac{\tau_1}{\epsilon_r}\nabla H'_z+\tau'_2 H'_z-\tau'_3 E'_z\right)W\,d\Omega_{in}=0 \qquad (A4.8.4)$$

Integrating only the terms on the extreme left in the two integrals by parts following the same procedures as in appendix A4.3 gives

$$\int_{\Omega_{in}}\nabla W\frac{\tau_1}{\mu_r}\nabla E'_z\,d\Omega_{in}-\int_{\Omega_{in}}\tau_2 W E'_z\,d\Omega_{in}$$

$$-\int_{\Omega_{in}}\tau_3 W H'_z\,d\Omega_{in}-\int_B W\frac{\tau_1}{\mu_r}\frac{\delta E'_{z_b}}{\delta n}dB=0 \qquad (A4.8.5)$$

and

$$\int_{\Omega_{in}} \nabla W \frac{\tau_1}{\epsilon_r} \nabla H_z' d\Omega_{in} - \int_{\Omega_{in}} \tau_2 W H_z' d\Omega_{in}$$

$$+ \int_{\Omega_{in}} \tau_3 W E_z' d\Omega_{in} - \int_B W \frac{\tau_1}{\epsilon_r} \frac{\delta H_{z_b}'}{\delta n} dB = 0 \qquad (A4.8.6)$$

Every one of the integrals in the above two equations can be discretised [3] and written in matrix formulation

$$[S][E_z'] - [R][H_z'] - [T]\left[\frac{\delta E_{z_b}'}{\delta n}\right] = 0 \qquad (A4.8.7)$$

and

$$[S'][H_z'] + [R'][E_z'] - [T']\left[\frac{\delta H_{z_b}'}{\delta n}\right] = 0 \qquad (A4.8.8)$$

The elements of the matrices can be obtained in a similar manner as described in sec 4.3.4.

Appendix A5
Numerical implementation methods

A5.1 Combining of FEM and BEM matrix equations

The matrix equations of (4.12) and (4.25) or (4.13) and (4.26) can be combined using the boundary conditions (4.29) and (4.30). The field value U will be used, representing either the TE field E_z or the TM field H_z. The combined matrix has the same form irrespective of the polarization of the field. The finite element matrix equation

$$[S][U]-[T]\left[\frac{\delta U_b}{\delta n}\right]=0 \qquad (A5.1.1)$$

can be written as

$$\begin{bmatrix} S_{rr} & S_{rb} & \cdot \\ S_{br} & S_{bb} & -T \\ \cdot & \cdot & \cdot \end{bmatrix}\begin{bmatrix} U_r^{FEM} \\ U_b^{FEM} \\ \left\{\frac{\delta U_b^{FEM}}{\delta n}\right\} \end{bmatrix}=0 \qquad (A5.1.2)$$

with the subscript r for fields inside the finite element region and b for fields on the boundary. The boundary element matrix equation can be written as

$$[H][U_b^{BEM}]-[G]\left[\frac{\delta U_b^{BEM}}{\delta n'}\right]=0 \qquad (A5.1.3)$$

or

$$\begin{bmatrix} \cdot & \cdot & \cdot \\ \cdot & \cdot & \cdot \\ \cdot & H & -G \end{bmatrix}\begin{bmatrix} U_r^{BEM} \\ U_b^{BEM} \\ \left\{\frac{\delta U_b^{BEM}}{\delta n'}\right\} \end{bmatrix}=0 \qquad (A5.1.4)$$

Using

$$U^{FEM}=U^{BEM}+U^{inc} \qquad (A5.1.5)$$

and

$$\frac{dU_b^{FEM}}{dn}=-\frac{dU_b^{BEM}}{dn'}-\frac{dU_b^{inc}}{dn'} \qquad (A5.1.6)$$

following out of the boundary conditions (sec 4.5.1), in (A5.1.2) yields

$$\begin{bmatrix} S_{rr} & S_{rb} & \cdot \\ S_{br} & S_{bb} & -T \\ \cdot & \cdot & \cdot \end{bmatrix} \begin{bmatrix} U_r^{FEM} \\ \{U_b^{BEM} + U_b^{inc}\} \\ \left\{ -\frac{\delta U_b^{BEM}}{\delta n'} - \frac{\delta U_b^{inc}}{\delta n'} \right\} \end{bmatrix} = 0 \qquad (A5.1.7)$$

The incident fields and their normal derivatives on the boundary are known values. By multiplying them with the [S] and [T] matrices and taking the product to the right hand side one obtains

$$\begin{bmatrix} S_{rr} & S_{rb} & \cdot \\ S_{br} & S_{bb} & -T \\ \cdot & \cdot & \cdot \end{bmatrix} \begin{bmatrix} U_r^{FEM} \\ U_b^{BEM} \\ \left\{ -\frac{\delta U_b^{BEM}}{\delta n'} \right\} \end{bmatrix} = \begin{bmatrix} -S_{rb} U_b^{inc} \\ \left\{ -S_{bb} U_b^{inc} - T \frac{\delta U_b^{inc}}{\delta n'} \right\} \\ \cdot \end{bmatrix} \qquad (A5.1.8)$$

Substituting (A5.1.4) into (A5.1.8) yields

$$\begin{bmatrix} S_{rr} & S_{rb} & \cdot \\ S_{br} & S_{bb} & T \\ \cdot & H & -G \end{bmatrix} \begin{bmatrix} U_r^{FEM} \\ U_b^{BEM} \\ \left\{ \frac{\delta U_b^{BEM}}{\delta n'} \right\} \end{bmatrix} = \begin{bmatrix} -S_{rb} U_b^{inc} \\ \left\{ -S_{bb} U_b^{inc} - T \frac{\delta U_b^{inc}}{\delta n'} \right\} \\ \cdot \end{bmatrix} \qquad (A5.1.9)$$

A5.2 Indirect combination of FEM and BEM matrix equations

The two matrix equations (A5.1.1) and (A5.1.3) can be coupled to make a more economical solution possible. (A5.1.1) can be written as

$$\begin{bmatrix} S_{rr} & S_{rb} \\ S_{br} & S_{bb} \end{bmatrix} \begin{bmatrix} U_r^{FEM} \\ U_b^{FEM} \end{bmatrix} - \begin{bmatrix} \cdot & \cdot \\ \cdot & T \end{bmatrix} \begin{bmatrix} \cdot \\ \left\{ \frac{\delta U_b^{FEM}}{\delta n} \right\} \end{bmatrix} = 0 \qquad (A5.2.1)$$

Substituting (A5.1.5) and (A5.1.6) into (A5.2.1) yields

$$\begin{bmatrix} S_{rr} & S_{rb} \\ S_{br} & S_{bb} \end{bmatrix} \begin{bmatrix} U_r^{FEM} \\ \{U_b^{BEM} + U_b^{inc}\} \end{bmatrix} - \begin{bmatrix} \cdot & \cdot \\ \cdot & T \end{bmatrix} \begin{bmatrix} \cdot \\ \left\{ -\frac{\delta U_b^{BEM}}{\delta n'} - \frac{\delta U_b^{inc}}{\delta n'} \right\} \end{bmatrix} = 0 \qquad (A5.2.2)$$

Multiplying [S] and [T] with the incident fields and taking the products to the right hand side gives

$$\begin{bmatrix} S_{rr} & S_{rb} \\ S_{br} & S_{bb} \end{bmatrix}\begin{bmatrix} U_r^{FEM} \\ U_b^{BEM} \end{bmatrix}+\begin{bmatrix} \cdot & \cdot \\ \cdot & T \end{bmatrix}\begin{bmatrix} \cdot \\ \left\{\frac{\delta U_b^{BEM}}{\delta n'}\right\} \end{bmatrix}$$

$$=\begin{bmatrix} -S_{rb}U_b^{inc} \\ \left\{-S_{bb}U_b^{inc}-T\frac{\delta U_b^{inc}}{\delta n'}\right\} \end{bmatrix} \qquad (A5.2.3)$$

Define a matrix [F] as

$$F=\begin{bmatrix} -S_{rb}U_b^{inc} \\ \left\{-S_{bb}U_b^{inc}-T\frac{\delta U_b^{inc}}{\delta n'}\right\} \end{bmatrix} \qquad (A5.2.4)$$

By using (A5.2.4), (A5.2.3) can be written as

$$\begin{bmatrix} U_r^{FEM} \\ U_b^{BEM} \end{bmatrix}=[S]^{-1}[F]-[S]^{-1}\begin{bmatrix} \cdot & \cdot \\ \cdot & T \end{bmatrix}\begin{bmatrix} \cdot \\ \left\{\frac{\delta U_b^{BEM}}{\delta n'}\right\} \end{bmatrix} \qquad (A5.2.5)$$

The boundary element equation (A5.1.3) can be written as

$$\begin{bmatrix} \cdot & \cdot \\ \cdot & H \end{bmatrix}\begin{bmatrix} \cdot \\ U_b^{BEM} \end{bmatrix}-\begin{bmatrix} \cdot & \cdot \\ \cdot & G \end{bmatrix}\begin{bmatrix} \cdot \\ \frac{\delta U_b^{BEM}}{\delta n'} \end{bmatrix}=0 \qquad (A5.2.6)$$

Substituting (A5.2.5) into (A5.2.6) yields

$$\begin{bmatrix} \cdot & \cdot \\ \cdot & H \end{bmatrix}[S]^{-1}[F]-\begin{bmatrix} \cdot & \cdot \\ \cdot & H \end{bmatrix}[S]^{-1}\begin{bmatrix} \cdot & \cdot \\ \cdot & T \end{bmatrix}\begin{bmatrix} \cdot \\ \left\{\frac{\delta U_b^{BEM}}{\delta n'}\right\} \end{bmatrix}$$

$$-\begin{bmatrix} \cdot & \cdot \\ \cdot & G \end{bmatrix}\begin{bmatrix} \cdot \\ \left\{\frac{\delta U_b^{BEM}}{\delta n'}\right\} \end{bmatrix}=0 \qquad (A5.2.7)$$

or

$$\left(-\begin{bmatrix} \cdot & \cdot \\ \cdot & H \end{bmatrix}[S]^{-1}\begin{bmatrix} \cdot & \cdot \\ \cdot & T \end{bmatrix}-\begin{bmatrix} \cdot & \cdot \\ \cdot & G \end{bmatrix}\right)\begin{bmatrix} \cdot \\ \left\{\frac{\delta U_b^{BEM}}{\delta n'}\right\} \end{bmatrix}$$

$$=-\begin{bmatrix} \cdot & \cdot \\ \cdot & H \end{bmatrix}[S]^{-1}[F] \qquad (A5.2.8)$$

Defining

$$[A] = \left(-\begin{bmatrix} \cdot & \cdot \\ \cdot & H \end{bmatrix} [S]^{-1} \begin{bmatrix} \cdot & \cdot \\ \cdot & T \end{bmatrix} - \begin{bmatrix} \cdot & \cdot \\ \cdot & G \end{bmatrix} \right) \qquad (A5.2.9)$$

and

$$[B] = -\begin{bmatrix} \cdot & \cdot \\ \cdot & H \end{bmatrix} [S]^{-1} [F] \qquad (A5.2.10)$$

Equation (A5.2.8) can thus be written as

$$[A] \left[\frac{\delta U_b^{BEM}}{\delta n'} \right] = [B] \qquad (A5.2.11)$$

The first step in determining the unknowns is to obtain $[S]^{-1}$. With some matrix multiplication [A] and [B], can be obtained using $[S]^{-1}$. Solving the relatively small matrix equation (A5.2.11), one obtains the normal field derivatives on the boundary. Equation (A5.2.5) can now be used to calculate all the unknown field values.

Appendix A6
Second order elements

A6.1 Second order simplex functions

The second order approximation functions are given by

$$\alpha_{ijk} = R_i(2,\xi_1)R_j(2,\xi_2)R_k(2,\xi_3) \qquad (A6.1.1)$$

[[6],p107] with $0 \geq i, j, k \leq 2$ and i+j+k = 2 a requirement. In (A6.1.1) the R functions are [[6],p105]

$$R_o(2,\xi_p) = 1 \qquad (A6.1.2)$$

$$R_1(2,\xi_p) = 2\xi_p \qquad (A6.1.3)$$

and

$$R_2(2,\xi_p) = 2\xi_p^2 - \xi_p \qquad (A6.1.4)$$

By calculating (A6.1.1) for different values of i, j and k the following six approximating functions are obtained.

$$\alpha_{200} = \alpha_1 = \xi_1(2\xi_1 - 1) \qquad (A6.1.5)$$

$$\alpha_{020} = \alpha_2 = \xi_2(2\xi_2 - 1) \qquad (A6.1.6)$$

$$\alpha_{002} = \alpha_3 = \xi_3(2\xi_3 - 1) \qquad (A6.1.7)$$

$$\alpha_{110} = \alpha_4 = 4\xi_1\xi_2 \qquad (A6.1.8)$$

$$\alpha_{011} = \alpha_5 = 4\xi_2\xi_3 \qquad (A6.1.9)$$

and

$$\alpha_{101} = \alpha_6 = 4\xi_1\xi_3 \qquad (A6.1.10)$$

A6.2 Analytical integration to avoid singularities for quadratic elements

A very similar procedure is performed as was done in appendix A4.5. The whole integration method stays the same but the approximating functions ϕ_1, ϕ_2 and ϕ_3 are quadratic.

It is necessary to write these functions in terms of a variable x defined in appendix A4.5 as $\xi = 2x - 1$. Using this together with the (6.04), (6.05) and (6.06) yields

$$\phi_1(x) = 2x^2 - 3x + 1 \qquad (A6.2.1)$$

$$\phi_2(x) = 2x^2 - x \qquad (A6.2.2)$$

and

$$\phi_3(x) = -4x^2 + 4x$$

These functions used as the approximation functions and integrating in exactly the same way as in appendix A4.5 result in an integral solution

$$G'^{,i} = \sum_{i=1}^{3} \frac{jJ}{4}\{\int_{-1}^{1} \phi_i J_o(k_o r)d\xi + \frac{j2}{\pi}[\gamma \int_{-1}^{1} \phi_i J_o(k_o r)d\xi$$

$$+ \int_{-1}^{1} \phi_i \sum_{k=0}^{\infty} (-1)^{k+1} \left(\frac{\left(\frac{k_o r}{2}\right)^{2k}}{(k!)^2} \right) \sum_{p=1}^{k} \left(\frac{1}{p} \right) d\xi + \ln\left(\frac{k_o R_{el}}{2} \right) \int_{-1}^{1} \phi_i J_o(k_o r)d\xi$$

$$+ 2\{A_i f'(k_o R_{el}, 2) + B_i f'(k_o R_{el}, 1) + C_i f'(k_o R_{el}, 0)\}]\} \qquad (A6.2.4)$$

with

$A_1 = 2$, $A_2 = 2$ and $A_3 = -4$

$B_1 = -3$, $B_2 = -1$ and $B_3 = 4$

$C_1 = 1$, $C_2 = 0$ and $C_3 = 0$.

Equation (A6.2.4) can be used whenever the observation point is on one of the nodes lying on the edges of the boundary element, as was the case with linear elements. When the observation point, however, lies on the node in the middle of the boundary element, the integral must be altered a bit. Solving the integral when the observation point lies on the centre node stays the same as in appendix A4.5 up to equation (A4.5.7). The first integral on the right hand side contains a singularity. With the observation point on the centre node the variable r in (A4.5.7) is given by

$$r = R_{el} \left| \frac{1}{2} \xi \right| \qquad (A6.2.5)$$

The integral in (A4.5.7) containing the singularity can thus be written as

$$\int_{-1}^{1} \phi_i \frac{2}{\pi} \ln\left(\frac{k_o r}{2}\right) J_o(k_o r)\, d\xi$$

$$= \int_{-1}^{1} \phi_i \frac{2}{\pi} \ln\left(\frac{k_o R_{el} \frac{1}{2} |\xi|}{2}\right) J_o(k_o r)\, d\xi$$

$$= \int_{-1}^{1} \phi_i \frac{2}{\pi} \ln\left(\frac{k_o R_{el} \frac{1}{2}}{2}\right) J_o(k_o r)\, d\xi + \int_{-1}^{1} \phi_i \frac{2}{\pi} \ln(|\xi|) J_o(k_o r)\, d\xi$$

(A6.2.6)

The first term on the RHS of (A6.2.6) can be calculated numerically without any problems, but the second term still contains a singularity. Consider this second term:

$$\int_{-1}^{1} \phi_i \frac{2}{\pi} \ln(|\xi|) J_o(k_o r)\, d\xi$$

$$= \int_{-1}^{0} \phi_i \frac{2}{\pi} \ln(-\xi) J_o\left(k_o R_{el}\left(-\frac{1}{2}\xi\right)\right) d\xi + \int_{0}^{1} \phi_i \frac{2}{\pi} \ln(\xi) J_o\left(k_o R_{el}\left(\frac{1}{2}\xi\right)\right) d\xi$$

$$= -\int_{0}^{1} \phi_i(-\xi) \frac{2}{\pi} \ln(\xi) J_o\left(k_o R_{el}\left(\frac{1}{2}\xi\right)\right) d\xi + \int_{0}^{1} \phi_i \frac{2}{\pi} \ln(\xi) J_o\left(k_o R_{el}\left(\frac{1}{2}\xi\right)\right) d\xi$$

(A6.2.7)

Both integrals in (A6.2.7) are of the form defined in (A4.5.12). These integrals can thus be solved for the three different approximation functions. Consider them separately

$i = 1$:

$$\phi_1 = \frac{1}{2}\xi^2 - \frac{1}{2}\xi \qquad (A6.2.8)$$

and

$$\phi_1(-\xi) = \frac{1}{2}\xi^2 + \frac{1}{2}\xi \qquad (A6.2.9)$$

$i = 2$:

$$\phi_2 = \frac{1}{2}\xi^2 + \frac{1}{2}\xi \qquad (A6.2.10)$$

and

$$\phi_2(-\xi) = \frac{1}{2}\xi^2 - \frac{1}{2}\xi \qquad (A6.2.11)$$

$i = 3$:

$$\phi_3 = -\xi^2 + 1 \qquad (A6.2.12)$$

and

$$\phi_3(-\xi) = -\xi^2 + 1 \qquad (A6.2.13)$$

From these approximation functions one can write

$$\phi_i = A_i\xi^2 + B_i\xi + C_i \qquad (A6.2.14)$$

with

$A_1 = \frac{1}{2}$, $A_2 = \frac{1}{2}$ and $A_3 = -1$

$B_1 = -\frac{1}{2}$, $B_2 = \frac{1}{2}$ and $B_3 = 0$

$C_1 = 0$, $C_2 = 0$ and $C_3 = 1$.

It is evident that

$$\phi_i(-\xi) = A_i\xi^2 - B_i\xi + C_i \qquad (A6.2.15)$$

Substituting these approximation functions in (A6.2.7) and using (A4.5.12) to solve the integrals, yield

$$-\int_0^1 \phi_i(-\xi)\frac{2}{\pi}\ln(\xi)J_o\left(k_oR_{el}\left(\frac{1}{2}\xi\right)\right)d\xi+\int_0^1 \phi_i\frac{2}{\pi}\ln(\xi)J_o\left(k_oR_{el}\left(\frac{1}{2}\xi\right)\right)d\xi$$

$$=-\int_0^1 (A_i\xi^2-B_i\xi+C_i)\frac{2}{\pi}\ln(\xi)J_o\left(k_oR_{el}\left(\frac{1}{2}\xi\right)\right)d\xi$$

$$+\int_0^1 (A_i\xi^2+B_i\xi+C_i)\frac{2}{\pi}\ln(\xi)J_o\left(k_oR_{el}\left(\frac{1}{2}\xi\right)\right)d\xi$$

$$=2\int_0^1 (B_i\xi)\frac{2}{\pi}\ln(\xi)J_o\left(k_oR_{el}\left(\frac{1}{2}\xi\right)\right)d\xi$$

$$=2B_if'\left(\frac{1}{2}k_oR_{el},1\right) \qquad (A6.2.16)$$

Back substituting these equations into the original starting equation gives the solution when the observation point lies on the centre node of a second order element as

$$G'^{,i}=\sum_{i=1}^{3}\frac{jJ}{4}\{\int_{-1}^{1}\phi_iJ_o(k_or)d\xi+\frac{j2}{\pi}[\gamma\int_{-1}^{1}\phi_iJ_o(k_or)d\xi$$

$$+\int_{-1}^{1}\phi_i\sum_{k=0}^{\infty}(-1)^{k+1}\left(\frac{\left(\frac{k_or}{2}\right)^{2k}}{(k!)^2}\right)\sum_{p=1}^{k}\left(\frac{1}{p}\right)d\xi+\ln\left(\frac{k_oR_{el}}{2}\right)\int_{-1}^{1}\phi_iJ_o(k_or)d\xi$$

$$+2\left\{B_if'\left(\frac{1}{2}k_oR_{el},1\right)\right\}]\} \qquad (A6.2.17)$$

Appendix A7
Analytical solutions of round cylinders

A7.1 Matrix form of boundary conditions equations for analytical solution of homogeneous cylinder

Equation (7.21) can be written as

$$\overline{E}_{inside_{tan}}(a) - \overline{E}^{inc}_{tan}(a) - \overline{E}^{sca}_{tan}(a) = 0 \qquad (A7.1.1)$$

By substituted (7.02), (7.06) and (7.10) into (7.21) one obtains

$$\sum_{n=-\infty}^{\infty}\left(\frac{j^n}{k_o}\right)g_n\left\{\overline{M}_n^{(1)}(\gamma_1 a)+\overline{N}_n^{(1)}(\gamma_1 a)\right\}$$

$$-j\sqrt{\frac{\mu}{\epsilon}}\sum_{n=-\infty}^{\infty}\left(\frac{j^n}{k_o}\right)f_n\left\{\overline{M}_n^{(1)}(\gamma_2 a)-\overline{N}_n^{(1)}(\gamma_2 a)\right\}$$

$$-\sum_{n=-\infty}^{\infty}\left(\frac{j^n}{k_o}\right)\overline{N}_n^{(1)}(k_o a)+\sum_{n=-\infty}^{\infty}\left(\frac{j^n}{k_o}\right)\left\{jc_n\overline{M}_n^{(3)}(k_o a)+b_n\overline{N}_n^{(3)}(k_o a)\right\}=0$$

$$(A7.1.2)$$

From here on, only the tangential components of the vectors must be used. Equation (A7.1.2) can be written for each value of n as

$$\left(\frac{j^n}{k_o}\right)g_n\left\{\overline{M}_n^{(1)}(\gamma_1 a)+\overline{N}_n^{(1)}(\gamma_1 a)\right\}$$

$$-j\sqrt{\frac{\mu}{\epsilon}}\left(\frac{j^n}{k_o}\right)f_n\left\{\overline{M}_n^{(1)}(\gamma_2 a)-\overline{N}_n^{(1)}(\gamma_2 a)\right\}$$

$$-\left(\frac{j^n}{k_o}\right)\overline{N}_n^{(1)}(k_o a)+\left(\frac{j^n}{k_o}\right)\left\{jc_n\overline{M}_n^{(3)}(k_o a)+b_n\overline{N}_n^{(3)}(k_o a)\right\}=0 \qquad (A7.1.3)$$

Dividing every term with $\frac{j^n}{k_o}$ yields

$$g_n\left\{\overline{M}_n^{(1)}(\gamma_1 a)+\overline{N}_n^{(1)}(\gamma_1 a)\right\}-j\sqrt{\frac{\mu}{\epsilon}}f_n\left\{\overline{M}_n^{(1)}(\gamma_2 a)-\overline{N}_n^{(1)}(\gamma_1 a)\right\}$$

$$-\overline{N}_n^{(1)}(k_o a)+\left\{jc_n\overline{M}_n^{(3)}(k_o a)+b_n\overline{N}_n^{(3)}(k_o a)\right\}=0 \qquad (A7.1.4)$$

Define a vector $\overline{A}$ with only a component in the z direction

$$\overline{A} = \hat{z} A_z \qquad (A7.1.5)$$

By using the definition of the Curl of a vector (cylindrical coordinates) [[1],inner front page] and remembering that there is no z direction variation one can write

$$\nabla \times \overline{A} = \nabla \times \hat{z} A_z$$

$$= \hat{r} \frac{1}{r} \frac{\delta A_z}{\delta \phi} - \hat{\phi} \frac{\delta A_z}{\delta r} \qquad (A7.1.6)$$

and

$$\nabla \times \nabla \times \overline{A} = \nabla \times \left(\hat{r} \frac{1}{r} \frac{\delta A_z}{\delta \phi} - \hat{\phi} \frac{\delta A_z}{\delta r} \right)$$

$$= -\hat{z} \frac{1}{r} \frac{\delta}{\delta \phi} \frac{1}{r} \frac{\delta A_z}{\delta \phi} - \hat{z} \frac{1}{r} \frac{\delta}{\delta r} r \frac{\delta A_z}{\delta r}$$

$$= -\nabla^2 A_z \qquad (A7.1.7)$$

The vectors $M_n^{(1)}$ and $N_n^{(1)}$ were defined in sec 7.2. By using (A7.1.6) and (A7.1.7), $M_n^{(1)}$ and $N_n^{(1)}$ can be written as

$$\overline{M}_n^{(1)}(k_o r) = \nabla \times \{(\hat{z} e^{jn\phi} J_n(k_o r)\}$$

$$= \hat{r} \frac{1}{r} \frac{\delta}{\delta \phi} \{e^{jn\phi} J_n(k_o r)\} - \hat{\phi} \frac{\delta}{\delta r} \{e^{jn\phi} J_n(k_o r)\}$$

$$= \hat{r} \frac{1}{r} jn e^{jn\phi} J_n(k_o r) - \hat{\phi} e^{jn\phi} k_o J_n'(k_o r)$$

$$(A7.1.8)$$

and

$$\overline{N}_n^{(1)}(k_o r) = \frac{1}{k_o}\nabla \times \nabla \times \{\hat{z} e^{jn\phi} J_n(k_o r)\}$$

$$= -\frac{1}{k_o}\nabla^2 \{\hat{z} e^{jn\phi} J_n(k_o r)\}$$

$$= -\hat{z}\frac{1}{k_o}\left(\frac{1}{r^2}\frac{\delta^2}{\delta\phi^2}\{e^{jn\phi} J_n(k_o r)\} + \frac{1}{r}\frac{\delta}{\delta r}\left(r\frac{\delta}{\delta r}\{e^{jn\phi} J_n(k_o r)\}\right)\right)$$

$$= -\hat{z}\frac{1}{k_o}\left(\frac{1}{r^2}\frac{\delta}{\delta\phi}\{jne^{jn\phi} J_n(k_o r)\} + \frac{1}{r}\frac{\delta}{\delta r}\{re^{jn\phi} k_o J_n'(k_o r)\}\right)$$

$$= -\hat{z}\frac{1}{k_o}\left(\frac{1}{r^2}(jn)^2 e^{jn\phi} J_n(k_o r) + e^{jn\phi}\frac{k_o}{r}\{J_n'(k_o r) + r k_o J_n''(k_o r)\}\right)$$

$$= -\hat{z}\frac{1}{k_o} e^{jn\phi}\left\{-\frac{n^2}{r^2} J_n(k_o r) + \frac{k_o}{r} J_n'(k_o r) + k_o^2 J_n''(k_o r)\right\}$$

(A7.1.9)

One can write

$$\frac{n^2}{r^2} J_n(k_o r) = k_o^2\left\{\frac{1}{4} J_{n+2}(k_o r) + \frac{1}{2} J_n(k_o r) + \frac{1}{4} J_{n-2}(k_o r)\right\} \qquad (A7.1.10)$$

$$J_n''(k_o r) = \frac{1}{4} J_{n+2}(k_o r) - \frac{1}{2} J_n(k_o r) + \frac{1}{4} J_{n-2}(k_o r) \qquad (A7.1.11)$$

and

$$J_n'(k_o r) = \frac{1}{2} J_{n-1}(k_o r) - \frac{1}{2} J_{n+1}(k_o r) \qquad (A7.1.12)$$

(see [[10],p137]).

By substituting (A7.1.10 - A7.1.12) into (A7.1.9) one obtains

$$\overline{N}_n^{(1)}(k_o r) = \frac{k_o}{2r}\{J_{n-1}(k_o r) - J_{n+1}(k_o r)\} - k_o^2 J_n(k_n(k_o r) \qquad (A7.1.13)$$

The first term on the right hand side of (A7.1.13) becomes zero when it is used in an infinite series $\sum_{n=-\infty}^{\infty}$. In the equations above,

$$J_n'(k_o) = \frac{\delta}{\delta r}\{J_n(k_o r)\}$$

In a similar manner, $M_n^{(3)}$ and $N_n^{(3)}$ can be developed to give

$$\overline{M}_n^{(3)}(k_o r) = \hat{r}\frac{1}{r} jn e^{jn\phi} H_n(k_o r) - \hat{\phi} e^{jn\phi} k_o H_n'(k_o r) \qquad (A7.1.14)$$

and

$$\overline{N}_n^{(3)}(k_o r) = -\hat{z} k_o e^{jn\phi} k_o H_n(k_o r) \qquad (A7.1.15)$$

It should be noted that only the ϕ component in (A7.1.8) and (A7.1.14) is tangential. Substituting the tangential components of (A7.1.8), (A7.1.13), (A7.1.14) and (A7.1.15) into (A7.1.4) gives

$$\begin{aligned} & g_n\{-\hat{\phi} e^{jn\phi}\gamma_1 J_n'(\gamma_1 a) - \hat{z} e^{jn\phi}\gamma_1 J_n(\gamma_1 a)\} \\ & - j\sqrt{\frac{\mu}{\epsilon}} f_n\{-\hat{\phi} e^{jn\phi}\gamma_2 J_n'(\gamma_2 a) + \hat{z} e^{jn\phi}\gamma_2 J_n(\gamma_2 a)\} \\ & + \hat{z} e^{jn\phi} k_o J_n(k_o a) + \{-\hat{\phi} j c_n e^{jn\phi} k_o H_n'(k_o a) \\ & - \hat{z} b_n e^{jn\phi}\gamma_1 H_n(k_o a)\} = 0 \end{aligned} \qquad (A7.1.16)$$

This equation can be split into its two tangential components $\hat{z}$ and $\hat{\phi}$ and the common term $e^{jn\phi}$ can be cancelled out giving

$$\begin{aligned} & -\{\gamma_1 J_n(\gamma_1 a)\} g_n - \left\{ j\sqrt{\frac{\mu}{\epsilon}}\gamma_2 J_n(\gamma_2 a)\right\} f_n \\ & + \{k_o H_n(k_o a)\} b_n = -k_o J_n(k_o a) \end{aligned} \qquad (A7.1.17)$$

and

$$\begin{aligned} & -\{\gamma_1 J_n'(\gamma_1 a)\} g_n + \left\{ j\sqrt{\frac{\mu}{\epsilon}}\gamma_2 J_n'(\gamma_2 a)\right\} f_n \\ & - \{j k_o H_n'(k_o a)\} c_n = 0 \end{aligned} \qquad (A7.1.18)$$

Equation (7.22) together with (7.03), (7.07) and (7.11) can be used to obtain another two linear independent equations with the required coefficients as unknowns. By following similar steps as described above, the third and forth linear equations can be obtained as

$$\begin{aligned} & \left\{ j\sqrt{\frac{\epsilon}{\mu}}\gamma_1 J_n(\gamma_1 a)\right\} g_n + \{\gamma_2 J_n(\gamma_2 a)\} f_n \\ & - \left\{ j\left(\frac{k_o}{j\omega\mu_o}\right) k_o H_n(k_o a)\right\} c_n = 0 \end{aligned} \qquad (A7.1.19)$$

and

$$\left\{ j\sqrt{\frac{\epsilon}{\mu}}\gamma_1 J_n'(\gamma_1 a)\right\} g_n - \{\gamma_2 J_n'(\gamma_2 a)\} f_n$$

$$-\left\{\left(\frac{k_o}{j\omega\mu_o}\right) k_o H_n'(k_o a)\right\} b_n = -\left(\frac{k_o}{j\omega\mu_o}\right) k_o J_n'(k_o a) \qquad (A7.1.20)$$

Equations (A7.1.17) to (A7.1.20) can be joined in matrix equation form resulting in

$$\begin{bmatrix} 0 & \{k_o H_n(k_o a)\} & -\{\gamma_1 J_n(\gamma_1 a)\} & -\left\{ j\sqrt{\frac{\mu}{\epsilon}}\gamma_2 J_n(\gamma_2 a)\right\} \\ -\{jk_o H_n'(k_o a)\} & 0 & -\{\gamma_1 J_n'(\gamma_1 a)\} & \left\{ j\sqrt{\frac{\mu}{\epsilon}}\gamma_2 J_n'(\gamma_2 a)\right\} \\ -\left\{ j\left(\frac{k_o}{j\omega\mu_o}\right) k_o H_n(k_o a)\right\} & 0 & \left\{ +j\sqrt{\frac{\epsilon}{\mu}}\gamma_1 J_n(\gamma_1 a)\right\} & \{\gamma_2 J_n(\gamma_2 a)\} \\ 0 & -\left\{\left(\frac{k_o}{j\omega\mu_o}\right) k_o H_n'(k_o a)\right\} & \left\{ j\sqrt{\frac{\epsilon}{\mu}}\gamma_1 J_n'(\gamma_1 a)\right\} & -\{\gamma_2 J_n'(\gamma_2 a)\} \end{bmatrix} \begin{bmatrix} c_n \\ b_n \\ g_n \\ f_n \end{bmatrix} = \begin{bmatrix} -k_o J_n(k_o a) \\ 0 \\ 0 \\ -\left(\frac{k_o}{j\omega\mu_o}\right) k_o J_n'(k_o a) \end{bmatrix}$$

$$(A7.1.21)$$

For TM polarization the fields given in [[11],p45] can be used together with the boundary conditions described in sec 7.3 to give, in a similar manner as above, the following matrix equation:

$$\begin{bmatrix} 0 & \{k_o H_n(k_o a)\} & -\{\gamma_1 J_n(\gamma_1 a)\} & -\left\{ j\sqrt{\frac{\mu}{\epsilon}}\gamma_2 J_n(\gamma_2 a)\right\} \\ -\{jk_o H_n'(k_o a)\} & 0 & -\{\gamma_1 J_n'(\gamma_1 a)\} & \left\{ j\sqrt{\frac{\mu}{\epsilon}}\gamma_2 J_n'(\gamma_2 a)\right\} \\ -\left\{ j\left(\frac{k_o}{j\omega\mu_o}\right) k_o H_n(k_o a)\right\} & 0 & \left\{ +j\sqrt{\frac{\epsilon}{\mu}}\gamma_1 J_n(\gamma_1 a)\right\} & \{\gamma_2 J_n(\gamma_2 a)\} \\ 0 & -\left\{\left(\frac{k_o}{j\omega\mu_o}\right) k_o H_n'(k_o a)\right\} & \left\{ j\sqrt{\frac{\epsilon}{\mu}}\gamma_1 J_n'(\gamma_1 a)\right\} & -\{\gamma_2 J_n'(\gamma_2 a)\} \end{bmatrix} \begin{bmatrix} a_n \\ d_n \\ g_n \\ f_n \end{bmatrix} = \begin{bmatrix} 0 \\ -jk_o J_n'(k_o a) \\ j\left(\frac{k_o}{j\omega\mu_o}\right) k_o J_n(k_o a) \\ 0 \end{bmatrix}$$

$$(A7.1.22)$$

It is evident that only the matrix on the right hand side differs from its corresponding matrix in (A7.1.22). The reason is that only the incident fields differ with different polarizations. The formulation for representing the scattered and inside fields as given in sec 7.2 is applicable to both polarizations.

A7.2 Matrix form of boundary conditions equations for analytical solution of PC, coated cylinder

Two different kinds of boundary conditions have to be satisfied with a PC coated cylinder. The first kind is on the boundary of the PC cylinder (r=a) and given by (7.23). Substituting (7.10), (7.16) into (7.23) yields

$$\sum_{n=-\infty}^{\infty}\left(\frac{j^n}{k_o}\right)g_n\left\{\overline{M}_n^{(1)}(\gamma_1 a)+\overline{N}_n^{(1)}(\gamma_1 a)\right\}$$

$$-j\sqrt{\frac{\mu}{\epsilon}}\sum_{n=-\infty}^{\infty}\left(\frac{j^n}{k_o}\right)f_n\left\{\overline{M}_n^{(1)}(\gamma_2 a)-\overline{N}_n^{(1)}(\gamma_2 a)\right\}$$

$$-\sum_{n=-\infty}^{\infty}\left(\frac{j^n}{k_o}\right)o_n\left\{\overline{M}_n^{(3)}(\gamma_1 a)+\overline{N}_n^{(3)}(\gamma_1 a)\right\}$$

$$+j\sqrt{\frac{\mu}{\epsilon}}\sum_{n=-\infty}^{\infty}\left(\frac{j^n}{k_o}\right)p_n\left\{\overline{M}_n^{(3)}(\gamma_2 a)-\overline{N}_n^{(3)}(\gamma_2 a)\right\}=0$$

(A7.2.1)

Only the tangential components of the vectors must be used. Written for any value of n and dividing every term by $\frac{j^n}{k_o}$ gives

$$g_n\left\{\overline{M}_n^{(1)}(\gamma_1 a)+\overline{N}_n^{(1)}(\gamma_1 a)\right\}-j\sqrt{\frac{\mu}{\epsilon}}f_n\left\{\overline{M}_n^{(1)}(\gamma_2 a)-\overline{N}_n^{(1)}(\gamma_2 a)\right\}$$

$$-o_n\left\{\overline{M}_n^{(3)}(\gamma_1 a)+\overline{N}_n^{(3)}(\gamma_1 a)\right\}+j\sqrt{\frac{\mu}{\epsilon}}p_n\left\{\overline{M}_n^{(3)}(\gamma_2 a)-\overline{N}_n^{(3)}(\gamma_2 a)\right\}=0$$

(A7.2.2)

Substituting the tangential vector values, as given in appendix A7.1 into (A7.2.2) and splitting the equation into its two tangential components give

$$-\{\gamma_1 J_n(\gamma_1 a)\}g_n-\left\{j\sqrt{\frac{\mu}{\epsilon}}\gamma_2 J_n(\gamma_2 a)\right\}f_n$$

$$+\{\gamma_1 H_n(\gamma_1 a)\}o_n+\left\{j\sqrt{\frac{\mu}{\epsilon}}\gamma_2 H_n(\gamma_2 a)\right\}p_n=0$$

(A7.2.3)

and

$$-\{\gamma_1 J_n'(\gamma_1 a)\}g_n + \left\{ j\sqrt{\frac{\mu}{\epsilon}}\gamma_2 J_n'(\gamma_2 a)\right\} f_n$$

$$+\{\gamma_1 H_n'(\gamma_1 a)\}g_n - \left\{ j\sqrt{\frac{\mu}{\epsilon}}\gamma_2 H_n'(\gamma_2 a)\right\} f_n = 0$$

(A7.2.4)

These are the first two linear independent equations required to solve the unknown coefficients.

The second kind of boundary conditions equations have to be satisfied at the outer radius of the coating (r=b). A very similar procedure as in appendix A7.1 will be followed to obtain the last four equations required to solve the unknown coefficients. Equation (7.24) can be written as

$$\overline{E}_{inside_{\tan}}(b) + \overline{E}^{sca}_{inside_{\tan}}(b) - \overline{E}^{inc}_{\tan}(b) - \overline{E}^{sca}_{\tan}(b) = 0 \qquad (A7.2.5)$$

By substituting (7.02), (7.06),(7.10) and (7.16) into (A7.2.5) one obtains

$$\sum_{n=-\infty}^{\infty}\left(\frac{j^n}{k_o}\right) g_n\left\{\overline{M}_n^{(1)}(\gamma_1 b) + \overline{N}_n^{(1)}(\gamma_1 b)\right\}$$

$$- j\sqrt{\frac{\mu}{\epsilon}}\sum_{n=-\infty}^{\infty}\left(\frac{j^n}{k_o}\right) f_n\left\{\overline{M}_n^{(1)}(\gamma_2 b) - \overline{N}_n^{(1)}(\gamma_2 b)\right\}$$

$$- \sum_{n=-\infty}^{\infty}\left(\frac{j^n}{k_o}\right) o_n\left\{\overline{M}_n^{(3)}(\gamma_1 b) + \overline{N}_n^{(3)}(\gamma_1 b)\right\}$$

$$+ j\sqrt{\frac{\mu}{\epsilon}}\sum_{n=-\infty}^{\infty}\left(\frac{j^n}{k_o}\right) p_n\left\{\overline{M}_n^{(3)}(\gamma_2 b) - \overline{N}_n^{(3)}(\gamma_2 b)\right\}$$

$$- \sum_{n=-\infty}^{\infty}\left(\frac{j^n}{k_o}\right)\overline{N}_n^{(1)}(k_o b) + \sum_{n=-\infty}^{\infty}\left(\frac{j^n}{k_o}\right)\left\{ j c_n \overline{M}_n^{(3)}(k_o b) + b_n \overline{N}_n^{(3)}(k_o b)\right\} = 0$$

(A7.2.6)

From here on, as in appendix A7.1, only the tangential components of the vectors must be used. Equation (A7.2.6) can be written for any value of n, and the common factor $\frac{j^n}{k_o}$ can be cancelled out to yield

$$g_n\left\{\overline{M}_n^{(1)}(\gamma_1 b)+\overline{N}_n^{(1)}(\gamma_1 b)\right\}-j\sqrt{\frac{\mu}{\epsilon}}f_n\left\{\overline{M}_n^{(1)}(\gamma_2 b)-\overline{N}_n^{(1)}(\gamma_2 b)\right\}$$

$$-o_n\left\{\overline{M}_n^{(3)}(\gamma_1 b)+\overline{N}_n^{(3)}(\gamma_1 b)\right\}+j\sqrt{\frac{\mu}{\epsilon}}p_n\left\{\overline{M}_n^{(3)}(\gamma_2 b)-\overline{N}_n^{(3)}(\gamma_2 b)\right\}$$

$$-\overline{N}_n^{(1)}(k_o b)+\left\{jc_n\overline{M}_n^{(3)}(k_o b)+b_n\overline{N}_n^{(3)}(k_o b)\right\}=0 \qquad (A7.2.7)$$

By using exactly the same method described in appendix A7.1, (A7.2.7) can be split into its two different tangential components yielding two linear independent equations. Satisfying the magnetic field boundary conditions, (7.25) using (7.03), (7.07),(7.11) and (7.17) can, in a similar manner as described above, be used to obtain the last two linear independent equations. This together with (A7.2.3), (A7.2.4) and (A7.2.7) yields the matrix equation

$$\begin{bmatrix}
0 & 0 & -(\gamma_1 J_n(\gamma_1 a)) & -\left(j\sqrt{\frac{\mu}{\epsilon}}\gamma_2 J_n(\gamma_2 a)\right) & (\gamma_1 H_n(\gamma_1 a)) & \left(j\sqrt{\frac{\mu}{\epsilon}}\gamma_2 H_n(\gamma_2 a)\right) \\
0 & 0 & -(\gamma_1 J_n'(\gamma_1 a)) & \left(j\sqrt{\frac{\mu}{\epsilon}}\gamma_2 J_n'(\gamma_2 a)\right) & (\gamma_1 H_n'(\gamma_1 a)) & -\left(j\sqrt{\frac{\mu}{\epsilon}}\gamma_2 H_n'(\gamma_2 a)\right) \\
0 & (k_1 H_n(k_1 a)) & -(\gamma_1 J_n(\gamma_1 a)) & -\left(j\sqrt{\frac{\mu}{\epsilon}}\gamma_2 J_n(\gamma_2 a)\right) & (\gamma_1 H_n(\gamma_1 a)) & \left(j\sqrt{\frac{\mu}{\epsilon}}\gamma_2 H_n(\gamma_2 a)\right) \\
-(jk_1 H_n'(k_1 b)) & 0 & -(\gamma_1 J_n'(\gamma_1 b)) & \left(j\sqrt{\frac{\mu}{\epsilon}}\gamma_2 J_n'(\gamma_2 b)\right) & (\gamma_1 H_n'(\gamma_1 b)) & -\left(j\sqrt{\frac{\mu}{\epsilon}}\gamma_2 H_n'(\gamma_2 b)\right) \\
-\left(j\left(\frac{k_1}{j\omega\mu_1}\right)k_1 H_n(k_1 b)\right) & 0 & \left(-j\sqrt{\frac{\epsilon}{\mu}}\gamma_1 J_n(\gamma_1 b)\right) & (\gamma_2 J_n(\gamma_2 b)) & \left(-j\sqrt{\frac{\epsilon}{\mu}}\gamma_1 H_n(\gamma_1 b)\right) & -(\gamma_2 H_n(\gamma_2 b)) \\
0 & -\left(\left(\frac{k_1}{j\omega\mu_1}\right)k_1 H_n'(k_1 b)\right) & \left(j\sqrt{\frac{\epsilon}{\mu}}\gamma_1 J_n'(\gamma_1 b)\right) & -(\gamma_2 J_n'(\gamma_2 b)) & \left(-j\sqrt{\frac{\epsilon}{\mu}}\gamma_1 H_n'(\gamma_1 b)\right) & (\gamma_2 H_n'(\gamma_2 b))
\end{bmatrix}
\begin{bmatrix} c_n \\ b_n \\ g_n \\ f_n \\ o_n \\ p_n \end{bmatrix}
=
\begin{bmatrix} 0 \\ 0 \\ -k_1 J_n(k_1 b) \\ 0 \\ 0 \\ -\left(\frac{k_1}{j\omega\mu_1}\right)k_1 J_n'(k_1 b) \end{bmatrix}$$

(A7.2.8)

For TM polarization the same procedures can be followed as described above. As was the case with a homogeneous cylinder in appendix A7.1, the only difference between the TM and TE polarization occurs with the incident wave. The following matrix equation can thus be used for TM polarization:

$$\begin{bmatrix}
0 & 0 & -(\gamma_1 J_n(\gamma_1 a)) & -\left(j\sqrt{\frac{\mu}{\epsilon}}\gamma_2 J_n(\gamma_2 a)\right) & (\gamma_1 H_n(\gamma_1 a)) & \left(j\sqrt{\frac{\mu}{\epsilon}}\gamma_2 H_n(\gamma_2 a)\right) \\
0 & 0 & -(\gamma_1 J_n'(\gamma_1 a)) & \left(j\sqrt{\frac{\mu}{\epsilon}}\gamma_2 J_n'(\gamma_2 a)\right) & (\gamma_1 H_n'(\gamma_1 a)) & -\left(j\sqrt{\frac{\mu}{\epsilon}}\gamma_2 H_n'(\gamma_2 a)\right) \\
0 & (k_1 H_n(k_1 a)) & -(\gamma_1 J_n(\gamma_1 a)) & -\left(j\sqrt{\frac{\mu}{\epsilon}}\gamma_2 J_n(\gamma_2 a)\right) & (\gamma_1 H_n(\gamma_1 a)) & \left(j\sqrt{\frac{\mu}{\epsilon}}\gamma_2 H_n(\gamma_2 a)\right) \\
-(jk_1 H_n'(k_1 b)) & 0 & -(\gamma_1 J_n'(\gamma_1 b)) & \left(j\sqrt{\frac{\mu}{\epsilon}}\gamma_2 J_n'(\gamma_2 b)\right) & (\gamma_1 H_n'(\gamma_1 b)) & -\left(j\sqrt{\frac{\mu}{\epsilon}}\gamma_2 H_n'(\gamma_2 b)\right) \\
-\left(j\left(\frac{k_1}{j\omega\mu_1}\right)k_1 H_n(k_1 b)\right) & 0 & \left(-j\sqrt{\frac{\epsilon}{\mu}}\gamma_1 J_n(\gamma_1 b)\right) & (\gamma_2 J_n(\gamma_2 b)) & \left(-j\sqrt{\frac{\epsilon}{\mu}}\gamma_1 H_n(\gamma_1 b)\right) & -(\gamma_2 H_n(\gamma_2 b)) \\
0 & -\left(\left(\frac{k_1}{j\omega\mu_1}\right)k_1 H_n'(k_1 b)\right) & \left(j\sqrt{\frac{\epsilon}{\mu}}\gamma_1 J_n'(\gamma_1 b)\right) & -(\gamma_2 J_n'(\gamma_2 b)) & \left(-j\sqrt{\frac{\epsilon}{\mu}}\gamma_1 H_n'(\gamma_1 b)\right) & (\gamma_2 H_n'(\gamma_2 b))
\end{bmatrix}
\begin{bmatrix} a_n \\ d_n \\ g_n \\ f_n \\ o_n \\ p_n \end{bmatrix}
=
\begin{bmatrix} 0 \\ 0 \\ 0 \\ -jk_1 J_n'(k_1 b) \\ j\left(\frac{k_1}{j\omega\mu_1}\right)k_1 J_n(k_1 b) \\ 0 \end{bmatrix}$$

(A7.2.9)

As expected, the only difference between (A7.2.9) and (A7.2.8) is the right hand side matrix representing the incident fields.

A7.3 Asymptotic representation of far-field scattering

The scattered field of (7.06) is written in terms of Hankel functions. For far-field scattering, the asymptotic expansions of the Hankel functions can be used [[1],p369]. The functions in (7.06) ($\overline{M}_n^{(3)}$ and $\overline{N}_n^{(3)}$) can be written as (see appendix A7.1)

$$\overline{M}_n^{(3)}(k_o r) = e^{jn\phi} H_n^{'(1)}(k_o r)\left\{\frac{\delta r}{\delta y}\hat{x} - \frac{\delta r}{\delta x}\hat{y}\right\} \qquad (A7.3.1)$$

and

$$\overline{N}_n^{(3)}(k_o r) = -\left(\frac{1}{k_o}\right) e^{jn\phi} H_n^{''(1)}(k_o r) \qquad (A7.3.2)$$

with $H_n^{'(1)}$ and $H_n^{''(1)}$ the first and second derivative of the Hankel function with respect to r. The asymptotic expansions of these Hankel functions are:

$$H_n^{(1)}(k_o r) = \sqrt{\frac{2}{\pi k_o r}} e^{jk_o r} e^{-\frac{j\pi}{4}} e^{-\frac{jn\pi}{2}} \qquad (A7.3.3)$$

$$H_n^{'(1)}(k_o r) = jk_o H_n^{(1)}(k_o r) \qquad (A7.3.4)$$

and

$$H_n^{''(1)}(k_o r) = -k_o^2 H_n^{(1)}(k_o r) \qquad (A7.3.5)$$

Using these asymptotic expansions, (A7.3.1) and (A7.3.2) can be written as

$$\overline{M}_n^{(3)}(k_o r) = e^{jn\phi} jk_o \sqrt{\frac{2}{\pi k_o r}} e^{jk_o r} e^{-\frac{j\pi}{4}} e^{-\frac{jn\pi}{2}} \left\{\frac{\delta r}{\delta y}\hat{x} - \frac{\delta r}{\delta x}\hat{y}\right\} \qquad (A7.3.6)$$

and

$$\overline{N}_n^{(3)}(k_o r) = e^{jn\phi} k_o \sqrt{\frac{2}{\pi k_o r}} e^{jk_o r} e^{-\frac{j\pi}{4}} e^{-\frac{jn\pi}{2}} \qquad (A7.3.7)$$

With

$$e^{-\frac{jn\pi}{2}} = \cos\left(\frac{n\pi}{2}\right) - j\sin\left(n\frac{\pi}{2}\right)$$

$$= j^{-n} \quad , \qquad (A7.3.8)$$

$$\frac{y}{r} = \sin\phi \qquad (A7.3.9)$$

and

$$\frac{x}{r} = \cos\phi \qquad (A7.3.10)$$

and using (7.3.6) and (7.3.7) the scattered field in (7.06) can be written as

$$\overline{E}^{sca}(\phi) = -\sum_{n=-\infty}^{\infty}\left(\frac{j^n}{k_o}\right)\{jc_n e^{jn\phi} jk_o\sqrt{\frac{2}{\pi k_o r}}e^{jk_o r}e^{-\frac{j\pi}{4}}(j^{-n})[\hat{x}\sin\phi - \hat{y}\cos\phi]$$

$$+ b_n k_o e^{jn\phi}\sqrt{\frac{2}{\pi k_o r}}e^{jk_o r}e^{-\frac{j\pi}{4}}(j^{-n})\hat{z}\} \qquad (A7.3.11)$$

Equation (A7.3.11) can be simplified yielding

$$\overline{E}^{sca}(\phi) = -\sqrt{\frac{2}{\pi k_o r}}e^{jk_o r}e^{-\frac{j\pi}{4}}\sum_{n=-\infty}^{\infty}e^{jn\phi}\{-c_n[\hat{x}\sin\phi - \hat{y}\cos\phi] + b_n\hat{z}\} \qquad (A7.3.12)$$

With the incident field given by (7.01) one can write

$$\left|\frac{\overline{E}^{sca}(\phi)}{\overline{E}^{inc}}\right| = \left|\sqrt{\frac{2}{\pi k_o r}}\sum_{n=-\infty}^{\infty}e^{jn\phi}\{-c_n[\hat{x}\sin\phi - \hat{y}\cos\phi] + b_n\hat{z}\}\right| \qquad (A7.3.13)$$

Using (4.31) the radar width can be written as

$$\sigma(\phi) = (2\pi r)\frac{2}{\pi k_o r}\left|\sum_{n=-\infty}^{\infty}e^{jn\phi}\{-c_n[\hat{x}\sin\phi - \hat{y}\cos\phi] + b_n\hat{z}\}\right|^2$$

$$= \frac{4}{k_o}\left|\sum_{n=-\infty}^{\infty}e^{jn\phi}\{-c_n[\hat{x}\sin\phi - \hat{y}\cos\phi] + b_n\hat{z}\}\right|^2 \qquad (A7.3.14)$$